UNIVERSITY OF SÃO PAULO
ENERGY GRADUATION PROGRAM
INSTITUTE OF ENERGY AND ENVIRONMENT

MICHELE DE NAZARÉ NOVAES SANTOS

ANALYSIS OF MEASURED LIGHTNING-INDUCED VOLTAGES ON A MATCHED EXPERIMENTAL OVERHEAD LINE

SÃO PAULO
2022

MICHELE DE NAZARÉ NOVAES SANTOS

ANALYSIS OF MEASURED LIGHTNING-INDUCED VOLTAGES ON A MATCHED EXPERIMENTAL OVERHEAD LINE

Ph.D. Dissertation presented at the Energy Graduation Program of the Institute of Energy and Environment of the University of São Paulo to obtain the Doctorate degree in Science.

Supervisor: Prof. Dr. Alexandre Piantini

Corrected Version

SÃO PAULO
2022

PUBLISHER'S CATALOGING-IN-PUBLICATION DATA

Santos, Michele de Nazaré Novaes
Analysis of measured lightning-induced-voltages on a matched experimental overhead line. /Michele de Nazaré Novaes Santos; supervisor: Alexandre Piantini – São Paulo, 2022.
107 p.: il; 30 cm.

Ph.D. Dissertation (Doctorate degree in Science) – Energy Graduation Program – Institute of Energy and Environment of the University of São Paulo.

1. Electrical power systems. 2. Lightning. 3. Lightning-induced voltages. I. Title.

Prepared by Maria Penha da Silva Oliveira CRB-8/6961

Name: Michele de Nazaré Novaes Santos
Title: Analysis of measured lightning-induced voltages on a matched experimental overhead line

Ph.D. Dissertation presented at the Energy Graduation Program of the Institute of Energy and Environment of the University of São Paulo to obtain the Doctorate degree in Science.

Supervisor: Prof. Dr. Alexandre Piantini

Approved in: March 31st, 2022

Examination Committee:

Prof. Dr. Ruy Alberto Corrêa Altafim	Institution: EESC/USP Decision: Approved
Prof. Dr. Arnaldo Gakiya Kanashiro	Institution: IEE/USP Decision: Approved
Prof. Dr. Vilson Luiz Coelho	Institution: UNISACT Decision: Approved
Prof. Dr. Signie Laureano França Santos	Institution: Institutos Lactec Decision: Approved
Dr. Acácio Silva Neto	Institution: IEE/USP Decision: Approved

To my dear mother, Rosemeire,
who has always been dedicated
to her children.

ACKNOWLEDGEMENTS

First, I thank God for health and the gift of life.

I would like to thank my advisor Prof. Dr. Alexandre Piantini for trusting me and allowing me to develop this work. I am grateful for the understanding and support that was given to me with great generosity whenever I needed it throughout this work journey.

I would like to thank the Universidade Federal do Amapá (Unifap) for the opportunity granted to qualify for a doctorate and to fully withdraw from the position of professor, as well as to all of the Electrical Engineering collegiate who supported me, especially Prof. Alaan Ubaiara and Prof. Kellen Gomes.

I thank my family for always being present in my life, my parents, Pedro Paulo and Rosemeire, for the education given to me, and immense gratitude to Aline Thiele who knew how to be a great companion when I could not be there and who gave me the strength to stay focused.

I would like to thank my great friend Hellen Paiva for her help in developing the LabVIEW program, which was used as a tool for the development of this Ph.D. Dissertation, without her contribution it would not have the same level of quality.

I would like to thank the CENDAT Group, Engineers Acácio Neto and Milton Shigihara who welcomed me on my admission, explaining the experimental system, clearing up my doubts whenever they arose. And Prof. Dr. Arnaldo G. Kanashiro for encouraging my studies, and I also thank Diana for everything I learned with her help and friendship.

Finally, I would like to thank the Institute of Energy and the Environment of the University of São Paulo, which provided the conditions for the development of this work, the Financier of Studies and Projects (FINEP), Companhia Paulista de Força e Luz (CPFL) and Rio Grande Energia (RGE), who provided financial support for the development of the two experimental systems (USP/SP System: CPFL Support and URI system: RGE, CPFL and FINEP support).

“If you don’t know, the thing to do is
not to get scared, but to learn.”

Ayn Rand

ABSTRACT

SANTOS, M. N. N. **Analysis of measured lightning-induced voltages on a matched experimental overhead line.** 2022. 107 p. Ph.D. Dissertation – Graduate Program on Energy, University of São Paulo, São Paulo. 2022.

This Ph.D. dissertation presents an analysis of 64 lightning-induced voltages recorded on a 2.7 km long, 10 m high, matched, non-energized experimental line located on the University of São Paulo campus. The recorded voltages were classified into four categories and the parameters that characterize each type, as well as their statistical distributions, are presented and discussed. About 67% of the voltages were classified as unipolar (Type I) and, except for one case, all of them had positive polarity. About 20% of the voltages were classified as Type II, whose waveshape is composed of two semi-cycles, the first one of positive polarity. About 10% of the recorded voltages were classified as Type III, whose waveshape is also composed of two semi-cycles, but the first one which a much shorter duration and lower magnitude. Only 3% were classified as Type IV, whose waveshape has three semi-cycles and the maximum voltage value occurs in the third one, which has negative polarity and the longest duration. The maximum absolute voltage values of the recorded voltages varied widely, from about 2 kV to 69 kV. Since the stroke locations and the characteristics of the lightning channels and stroke currents were not known, a quantitative comparison between measured and calculated voltages is not possible. However, a qualitative analysis was made, and the comparisons between measured and calculated results shown that the main features of the recorded voltages can be well reproduced by simulations considering typical conditions. It is clearly demonstrated that lightning-induced voltages may present oscillations even in the case of a matched line without surge arresters, shield wire, or neutral conductor, which is certainly not an obvious result. The measured lightning-induced voltages, even the unipolar ones, differed significantly from the standard lightning impulse voltage (1.2/50 μs). The study allowed a better understanding of the features of the lightning-induced voltages on a simple, matched line. The characterization of such surges is an important step for a more accurate estimation of the lightning performance of overhead distribution lines, as well as for the selection of the more efficient protection methods.

Keywords: Electromagnetic transients. Lightning. Lightning-induced voltages. Overvoltages.

RESUMO

SANTOS, M. N. N. **Análise de tensões induzidas por descargas atmosféricas medidas em uma linha experimental aérea casada**. 2022. 104 p. Tese de Doutorado – Programa de Pós-Graduação em Energia, Universidade de São Paulo, São Paulo. 2022.

Este trabalho apresenta uma análise de 64 tensões induzidas por descargas atmosféricas registradas em uma linha experimental não energizada de 2,7 km de comprimento, 10 m de altura, casada, localizada no campus da Universidade de São Paulo. As tensões registradas foram classificadas em quatro categorias e os parâmetros que caracterizam cada tipo, bem como suas distribuições estatísticas, são apresentados e discutidos. Cerca de 67% das tensões foram classificadas como unipolares (Tipo I) e, com exceção de um caso, todas apresentaram polaridade positiva. Cerca de 20% das tensões foram classificadas como Tipo II, cuja forma de onda é composta por dois semiciclos, sendo o primeiro de polaridade positiva. Cerca de 10% das tensões foram classificadas como Tipo III, cuja forma de onda também é composta por dois semiciclos, mas o primeiro com duração e magnitude muito menores. Apenas 3% foram classificadas como Tipo IV, cuja forma de onda possui três semiciclos e o valor de pico ocorre no terceiro, que possui polaridade negativa e maior duração. Os valores absolutos de pico das tensões registradas variaram amplamente, de cerca de 2 kV a 69 kV. Uma vez que as localizações dos pontos de incidência e as características dos canais e das correntes das descargas não eram conhecidas, uma comparação quantitativa entre as tensões medidas e calculadas não foi possível. No entanto, fez-se uma análise qualitativa, e as comparações entre os resultados medidos e calculados mostraram que as principais características das tensões registradas podem ser bem reproduzidas por simulações considerando condições típicas. Demonstra-se claramente que as tensões induzidas por descargas atmosféricas podem apresentar oscilações mesmo no caso de uma linha casada, sem para-raios, cabo guarda ou condutor neutro, o que certamente não é um resultado óbvio. As tensões induzidas medidas, mesmo as unipolares, diferiram significativamente da tensão de impulso atmosférico normalizada (impulso 1,2/50 μs). O estudo permitiu uma melhor compreensão das características das tensões induzidas por descargas atmosféricas em uma linha simples e casada. A caracterização de tais surtos é um passo importante para uma estimativa mais precisa do desempenho de linhas de aéreas de distribuição, bem como para a seleção dos métodos de proteção mais eficientes frente a descargas atmosféricas.

Palavras-chave: Transitórios eletromagnéticos. Descargas atmosféricas. Tensões induzidas por descargas atmosféricas. Sobretensões.

FIGURE LIST

TABLE LIST

SUMMARY

1. INTRODUCTION

Lightning is one of the phenomena that most affect the performance of electric power systems. During storms, in regions of high and moderate keraunic levels, lightning overvoltages are often responsible for a significant amount of damages to equipment and unscheduled supply interruptions in overhead lines. Examples of damages include failures of sensitive electronic devices in consumer units and distribution transformers [1] – [9].

Disturbances in overhead distribution lines can be caused both in the case of direct and indirect strokes, that is, both when lightning strikes the line or the ground in its vicinity. Lightning-induced overvoltages occur much more frequently than those resulting from direct lightning strikes and represent one of the most important problems for overhead distribution lines, especially in regions with high ground flash densities and high resistivity soils [10] - [12].

In order to reduce the effects of lightning on power distribution lines and improve their reliability and power quality levels, it is necessary to adopt efficient solutions to improve their lightning performance.

A solution against direct lightning consists of the use of a shield wire together with surge arresters installed in all poles and in all phases. This protection method theoretically eliminates flashovers. However, the cost of this solution does not allow it to be generally applied. In practice, a cost-benefit analysis must be carried out to find the most effective protection measure for each specific case.

It is essential to understand the main characteristics of the lightning overvoltages, especially those induced by nearby strokes, to estimate the lightning performance of a distribution line and compare the effectivenesses of different protection alternatives more precisely [13].

The occurrence of a flashover depends not only on the overvoltage peak, but also on its polarity and waveshape. The amplitudes and waveforms of induced overvoltages vary widely and depend on various lightning parameters, the network configuration and soil characteristics [1], [2], [14] – [19].

The search for a better understanding of the behavior and the characteristics of lightning-

induced overvoltages has motivated the development of several studies on the subject.

By means of a Monte Carlo procedure applied to analytical formulations, Andreotti *et al*. [20] focused on the statistical characterization of lightning-induced voltage peak values. The cases of lines with and without shield wires, above a perfectly conducting ground, were considered.

Based on simulations using a multivariate Monte Carlo procedure and lightning current waveforms represented by Cigré functions, Napolitano *et al*. [21] provided a statistical characterization of the typical waveform parameters of lightning overvoltages induced on a single conductor medium voltage overhead line for soil conductivities of 1 and 10 mS/m.

Paulino *et al.* [22] analyzed the front times and times-to-half-value of lightning-induced voltages at the center of an overhead line above lossy ground, considering typical parameters for first negative strokes. The computer simulations showed that lightning-induced voltage waveforms are strongly dependent on the line length and soil resistivity.

Full-scale experiments involving measurements of voltages induced on overhead lines by natural lightning were carried out by Erikson and Meal [23], Yokoyama *et al*. [9], [24], [25], Master *et al.* [26], Cooray and De la Rosa [27], De la Rosa *et al.* [28], Rubinstein *et al.* [29], Michishita *et al*. [30], Piantini *et al.* [31], [32], and Santos and Piantini [33], [34]. The triggered-lightning technique was employed by Barker *et al.* [35], while the investigations by Yokoyama [36], Piantini and Janiszewski [37] - [40], and Ishii, Michishita, and Hongo [41] were performed using reduced-scale models.

Just to illustrate the difficulties in comparing these results, because of the different experimental conditions, let us consider two of the investigations cited above. More than 90% of the lightning-induced voltages recorded by Eriksson and Meal [23] on a three-phase line about 9.9 km long and 7.4 m high were unipolar and of positive polarity; only about 2-3% of the records displayed a bipolar shape. At one end of the line, the conductors were bonded and grounded directly to a double counterpoise buried electrode system. At the other end, they were terminated in individual spark gaps adjusted to have an impulse flashover voltage of about 200 kV. On the other hand, Rubinstein *et al.* [29] recorded two types of induced-voltage waveforms: oscillatory (six cases) and impulsive (five cases). The induced voltages were measured on the top wire of an un-energized, 448 m long three-conductor distribution line. The top wire was approximately 10 m above the ground and terminated by the total 10.8 kΩ impedance of the voltage divider plus the ground impedance, which was estimated to be tens of ohms. The characteristic impedance of the line was about 600 Ω, so that the end was

effectively an open circuit. The bottom wires were open.

Lightning-induced voltages were measured on low-voltage distribution lines by Hoidalen and Dahlslett [42], Cai *et al.* [43], and Nanayakkara *et al.* [44]. In [42], most of the measured transients were bipolar, and the front and half value times of the recorded transients were found to have a 50% value of 9 and 23 μs, respectively. On the other hand, all the recorded induced voltage waveforms were unipolar [43], either positive or negative; the majority of the induced voltages measured in [44] were unipolar, of negative polarity, and the front and half value times of the recorded transients were found to have a geometric mean value of 7.45 and 11.31 μs.

In [45], most of the 55 lightning-induced voltages measured on a rural branched network, with common components of a distribution system, showed oscillatory behavior. The 159 km long, 13.2 kV, three-phase distribution line had a horizontal configuration. The low-voltage (LV) side was typically single-phase, with three conductors arranged vertically. The measurements were made in four different points, three at the MV side and one at the LV side. Voltages with longer durations, with an average of approximately 940 μs, were observed at the MV side, but higher peak values were observed at the LV side, where the average value was 30.7 kV.

Wang et al. analyzed in [46] the front times and the times to half value of lightning-induced overvoltages on a 220 kV three-phase overhead line, 40 km long and 25 m high. The measurements were performed at the two substations connected by the line. About 54% (52 out of 97) of the front times of the induced voltages at the two substations were longer than 27.5 μs, and the highest value of the probability density was 19.5 μs. About 50% (50 out of 99) of the times to half value were shorter than 55 μs; the highest value of the probability density was 38.8 μs.

In order to establish a correlation between faults along the distribution system and lightning strokes, Lazarreti et al. presented in [47] a monitoring system that measures fast electromagnetic transients on energized distribution networks (both on high and low voltage circuits) and the local atmospheric electric field. The system has been installed in the city of Guaraniaçu-PR, Brazil, where the ground flash density is about 5 flashes/km^2/year. In a period of 15 months, a data series of 196 identified lightning occurrences was obtained, 84 of which were related to lightning strikes and short-circuits, i.e., lightning-related events that were followed by voltage variations possibly related to short-circuits. The remaining 112 events were

lightning strikes unrelated to short-circuits, i.e. they did not present subsequent voltage variations.

Based on an analysis of lightning-related faults in power distribution feeders using the monitoring system developed in [47] and integrating experimental data and digital simulations, Ravaglio et al. [48] presented an experimental case study to better understand the factors that influence when a lightning-related fault self-extinguishes or sustains itself causing the circuit protection to act, resulting in a feeder outage. The analysis was based on a single field case study, but the results of the digital simulation are relatively close to those of the actual case.

All of these studies indicate that lightning-induced voltages' amplitudes and waveshapes vary widely. This is expected, as they depend significantly on the characteristics of the soil and the stroke current, the relative position of the line and stroke location, the observation point, and the network configuration [1], [2], [14] – [19]. Due to the different line lengths, configurations, and termination conditions, in most of the cases the lightning-induced voltages obtained in different experimental studies cannot be compared directly.

However, as the behavior of equipment insulation under an impulse voltage depends on both the impulse amplitude and waveshape, it is essential to know the characteristics of the lightning overvoltages to which power equipment are subject to assess their lightning withstand capabilities [49] – [51]. As the line configuration has a significant effect on the lightning-induced voltages, the first step is to find out the main voltage characteristics for the case of a simple, basic line configuration.

This Dissertation involves the analysis of lightning-induced voltages recorded by two measurement systems implemented by the Institute of Energy and Environment of the University of São Paulo (IEE/USP) through the Lightning and High Voltage Research Center (CENDAT). The systems were developed for the study of overvoltages induced by natural lightning on experimental lines adopting the pioneering methodology of simultaneous measurements of lightning currents and induced voltages on lines with different configurations developed in [6], [37], [52]. These two systems will be better described in Chapter 2 of this Dissertation.

Despite the large number of researches on voltages induced by indirect lightning (for instance, [3], [5], [7], [25], [35], [53] – [57]), no work in the literature can be used to characterize

lightning-induced voltages based on measurements performed on a matched line with a simple configuration and without equipment such as transformers and surge arresters. This is mainly due to the difficulties in implementing a system for this purpose, the long observation time required to obtain a large volume of data, and the fact that lightning-induced voltages are affected by several lightning parameters, as well as by the soil and the network configuration [18], [31], [58], [59].

A better knowledge of the lightning-induced voltages and the statistical distributions of their main parameters is important for the design of power distribution lines with superior performance and power quality indexes. The characterization of these overvoltages will enable more precise analysis regarding the most effective measures for improving the lightning performance of distribution lines taking into account both the technical and economic points of view.

1.1. Objective

The main objective of this Dissertation is to evaluate the characteristics of the lightning-induced voltages measured on a matched line with a simple configuration, i.e., with no equipment such as transformers and surge arresters. It comprises the following specific objectives:

- to establish waveform parameters for classification of the induced voltages;
- to identify representative types of lightning-induced voltage waveforms;
- to compare the characteristics of typical measured lightning-induced voltage waveforms with simulation results using a validated model for calculating lightning transients;
- to present and discuss the statistical distributions of the induced voltage parameters.

1.2. Outline

This Dissertation is organized into six chapters. The first one presents the introduction, the objective, and the structure of the Dissertation.

The second chapter describes the experimental systems developed by the Lightning and High Voltage Research Center of the University of São Paulo (CENDAT / USP) and implemented in the campus of the University of São Paulo, in São Paulo, and in the campus of the Universidade Regional Integrada do Alto Uruguai e das Missões (URI) in Santo Ângelo–RS, for experimental studies of lightning-induced voltages on overhead lines. The first system operated from 2002 to 2009, while the other one was set up in 2017.

The third chapter presents a methodology for the classification of lightning-induced voltage waveforms, establishes the waveform parameters corresponding to each group, and discusses the obtained results.

In the fourth chapter it is shown that the basic characteristics of the induced voltage waveforms identified in Chapter 3 can be reproduced by means of calculations using a using a validated and consolidated model - the Extended Rusck Model (ERM) - considering realistic situations.

The fifth chapter presents and discusses the statistical distributions of the parameters of the induced voltage waveforms recorded on the experimental line.

Finally, in Chapter 6, the final conclusions and main contributions of the Dissertation are presented, as well as topics for future work.

2. EXPERIMENTAL SYSTEM

As mentioned in the previous chapter, the line configuration has a significant effect on the lightning-induced voltages, and therefore it is important to find out the main voltage characteristics for the case of a simple, basic line configuration. Therefore, this chapter presents the two systems developed by the Lightning and High Voltage Research Center of the University of São Paulo (CENDAT / USP) to study lightning transients on overhead lines. Both systems were designed to record, simultaneously, lightning currents and the corresponding voltages induced on an experimental line. The first system was implemented in the campus of the University of São Paulo, in São Paulo [31], [32], [60], while the other one was installed in the campus of the Universidade Regional Integrada do Alto Uruguai e das Missões (URI) in Santo Ângelo – RS. The analysis carried out in this work considers only the voltages recorded in the first system as, up to now, just a few voltages have been obtained in System 2. However, one of the voltages measured in System 2 is shown in section 2.2, for illustration.

2.1. System 1 - Campus of the University of São Paulo in São Paulo (USP/SP)

The first system was implemented in the campus of the University of São Paulo in São Paulo, Brazil, and operated in the period 2002 – 2009. It consisted of a 62.5 m high instrumented tower isolated from the ground and located at a distance of 67 m from a two-conductor, 2.7 km long, 10 m high un-energized overhead line. The experimental line was above a soil with resistivity of about 170 Ω.m. The conductors, with a diameter of 17.48 mm, one with and the other without surge arresters, were installed on 6 m wooden crossarms; the reason for this separation between the two conductors was to decrease their mutual coupling [31], [32].

The conductor without arresters was matched at both ends in order to avoid reflections. A matching resistor was placed at one of the terminations of the other conductor (the farther from the measuring points), while a surge arrester was installed at the other end, as illustrated in Fig. 2.1. A section of the experimental line is shown in Fig. 2.2. Although lightning-induced voltages were measured at two points in each conductor, the results presented in this Dissertation refer only to the voltages induced on the conductor matched at both ends. This

conductor had not any equipment connected, except for the two 15 kΩ resistive voltage dividers (whose ratios were 588:1 and 590:1).

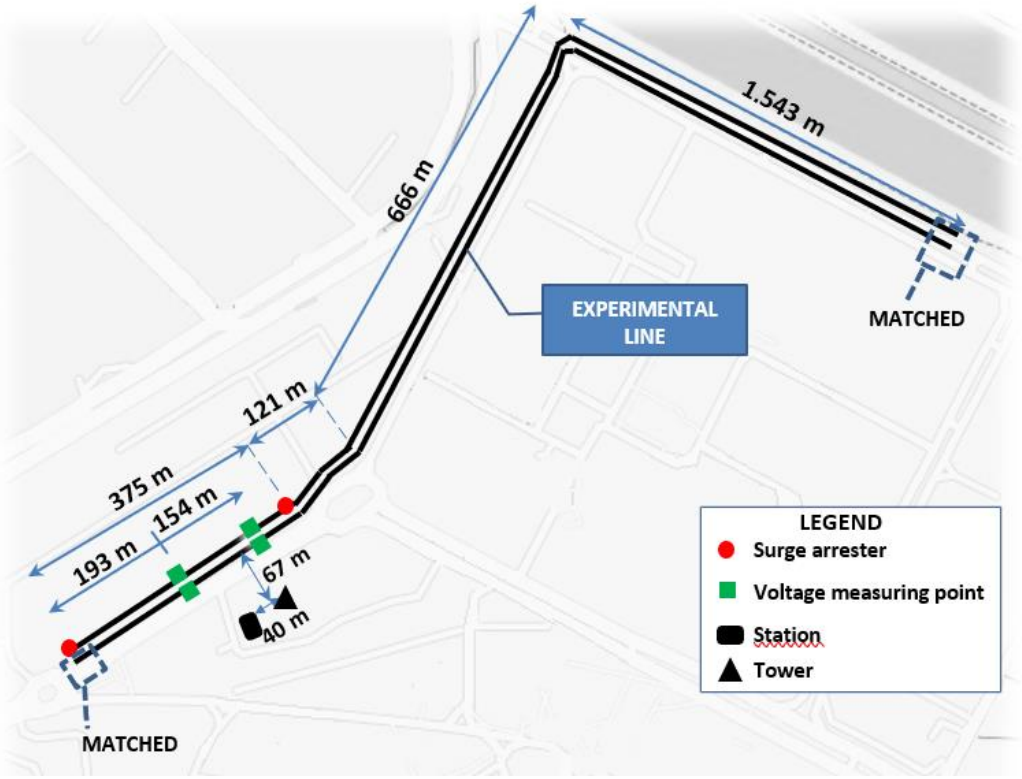

Figure 2.1. Sketch of the experimental system in the campus of the University of São Paulo [34].

Figure 2.2. Section of the experimental line in the campus of the University of São Paulo [33].

The voltages across the low-voltage arms of the voltage dividers located in the four measuring points were recorded in the respective oscilloscopes and transmitted through optical fiber cables to a computer located in a measuring station. The 2-channel oscilloscopes, Tektronix® TDS3012B, had a bandwidth of 100 MHz, sampling rate of 1.25 GSa/s, vertical resolution of 9 bits, and 10,000 points record length per channel. Mini modems were responsible for the electrical/optical and optical/electrical signals conversion. Further details of the system can be found in [31], [32], [60].

The system had to be dismounted and a new system [53] was implemented in the campus of the Universidade Regional Integrada do Alto Uruguai e das Missões (URI), as described in subsection 2.2.

2.2. System 2 - Campus of the URI in Santo Ângelo/RS

System 2 was implemented in the campus of the Universidade Regional Integrada do Alto Uruguai e das Missões (URI) in Santo Ângelo – RS in 2017. Santo Ângelo is located in the state of Rio Grande do Sul, in the south of Brazil, and is characterized by one of the highest ground flash densities in the country, of around 12 flashes/km²/year, as indicated in Fig. 2.3 (the ground flash density in the city of São Paulo is approximately 9 flashes/km²/year).

The system consists of a 70 m high instrumented tower, an experimental line for induced voltage measurements, a measuring station with the automated equipment control and the data acquisition system, an electric field mill, and a GPS time receiver, as shown in Fig. 2.4. The line has two conductors, one with and the other without surge arresters. The distance between the conductors is 6 m. The vertical electric field is used to turn the system on when a thunderstorm is imminent; the GPS clock is used to obtain the timestamp of the current and voltage measurements.

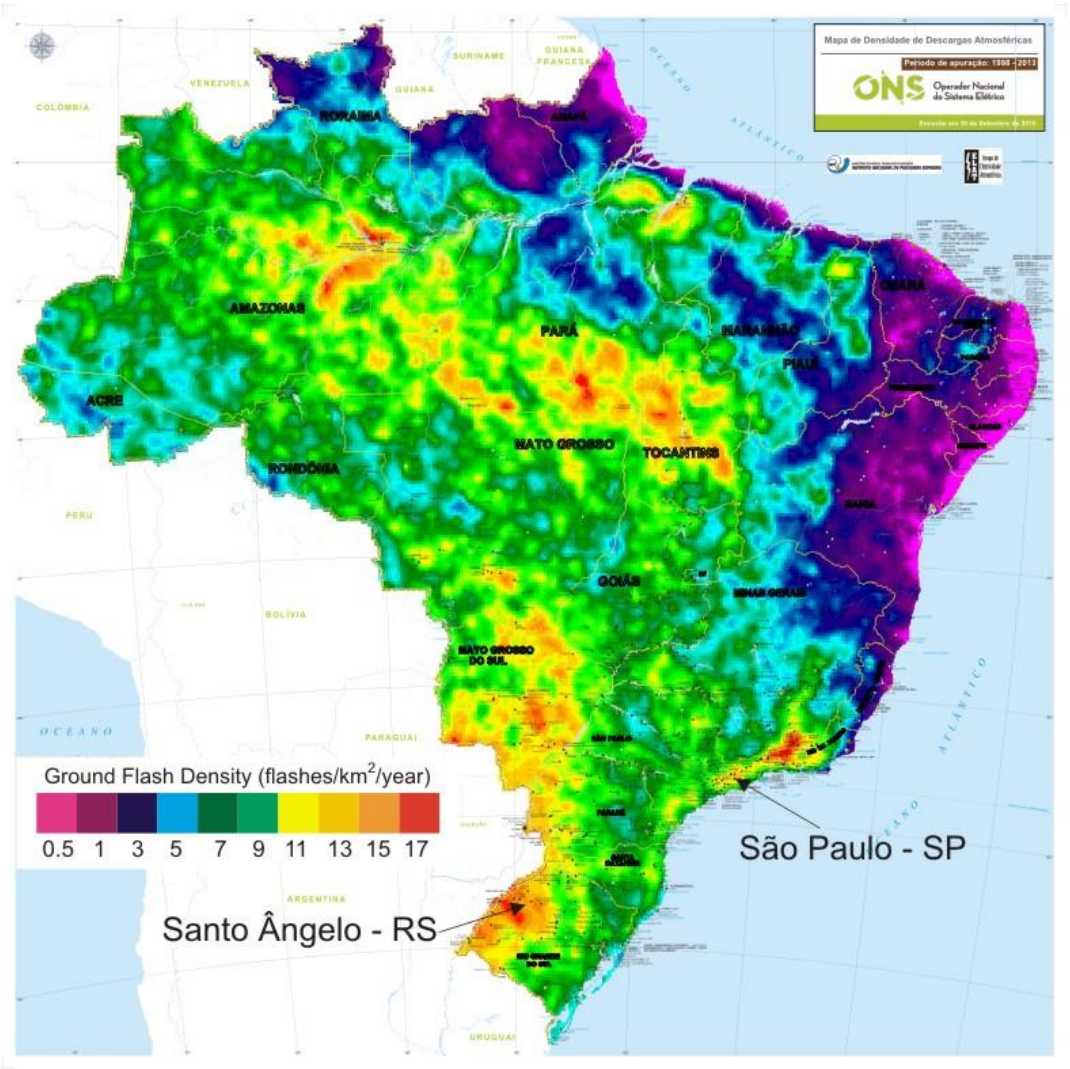

Figure 2.3. Map of the ground flash density in Brazil. Adapted from [66].

At approximately 50 m from the line, a room used as measuring station houses the computer that executes the main control and acquisition software, the electrical-optical and optical/electrical converters, and the backup and no-break systems. The computer is connected to the internet and the measured waveforms can be sent to a remote file server.

A microcontroller system is used to turn on and off the oscilloscopes via DC/AC power inverter. It also controls the battery charge and the temperature and humidity inside the equipment box.

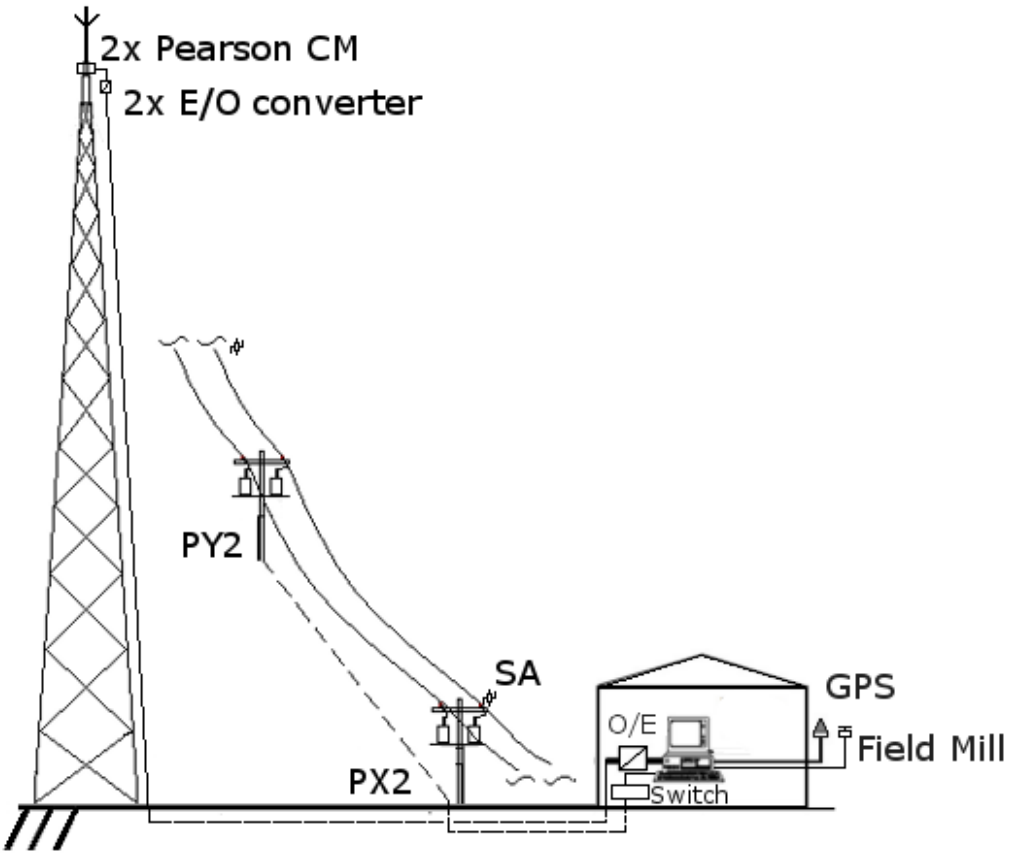

Figure 2.4. Sketch of the system overview. CM: Current monitor; E/O: electrical - optical converter; O/E: optical - electrical converter; PX2 and PY2 - poles where the induced voltages are measured; SA: surge arrester [52].

2.2.1. Tower and Experimental Line

The 70 m high tower, shown in Fig. 2.5, is located at a distance of 50 m from the line. The current measuring system, installed at its top, is described in detail in subsection 2.2.2. As shown in Fig. 2.6, the top of the tower is insulated from the rest of the structure so that the entire lightning current passes through the measuring system.

Figure 2.5. Instrumented tower [52].

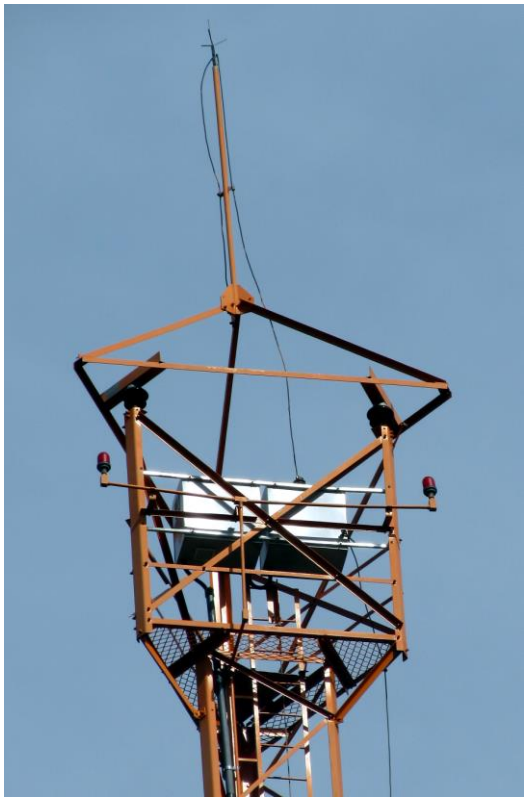

Figure 2.6. Current measuring system installed at the tower top [52].

The non-energised, non-conventional experimental line where the lightning-induced voltages are measured has two conductors supported by concrete poles. Surge arresters are installed in one of the conductors, while the other has no protection. The height and diameter of the conductors are 9 m and 5.2 mm, respectively. A metallic crossarm is used; the distance between the conductors is about 6 m to reduce the mutual coupling. The conductors are matched at both ends in order to avoid reflections. The line length is approximately 819 m and, as illustrated in Fig. 2.7, it has a "L" shape. A picture of the line is presented in Fig. 2.8.

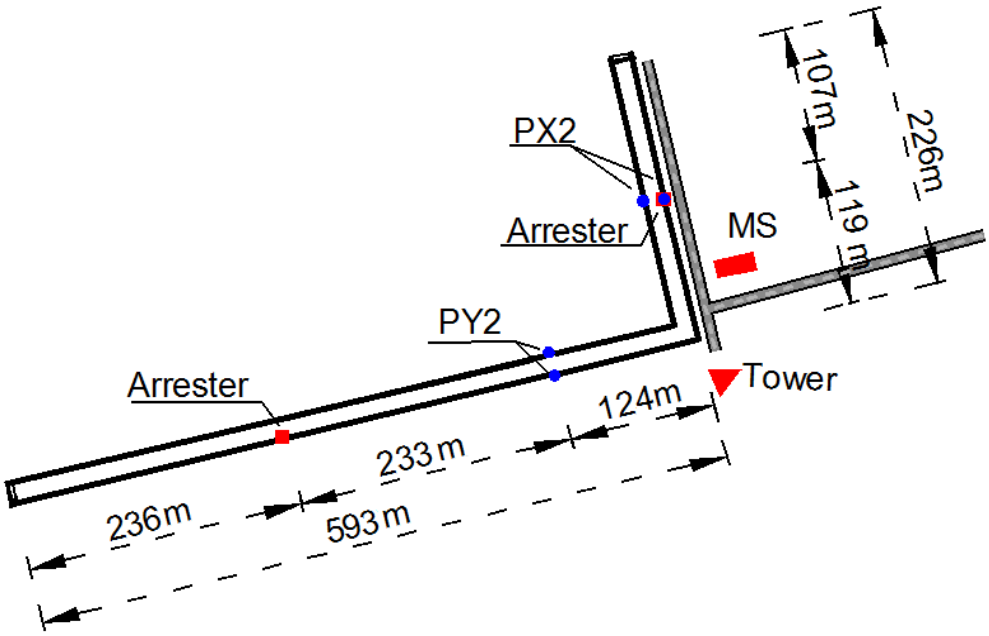

Figure 2.7. Sketch of the experimental line and location of measuring points (PX2 and PY2), arresters, tower and measuring station in Santo Ângelo – RS.(MS: measuring station) [52].

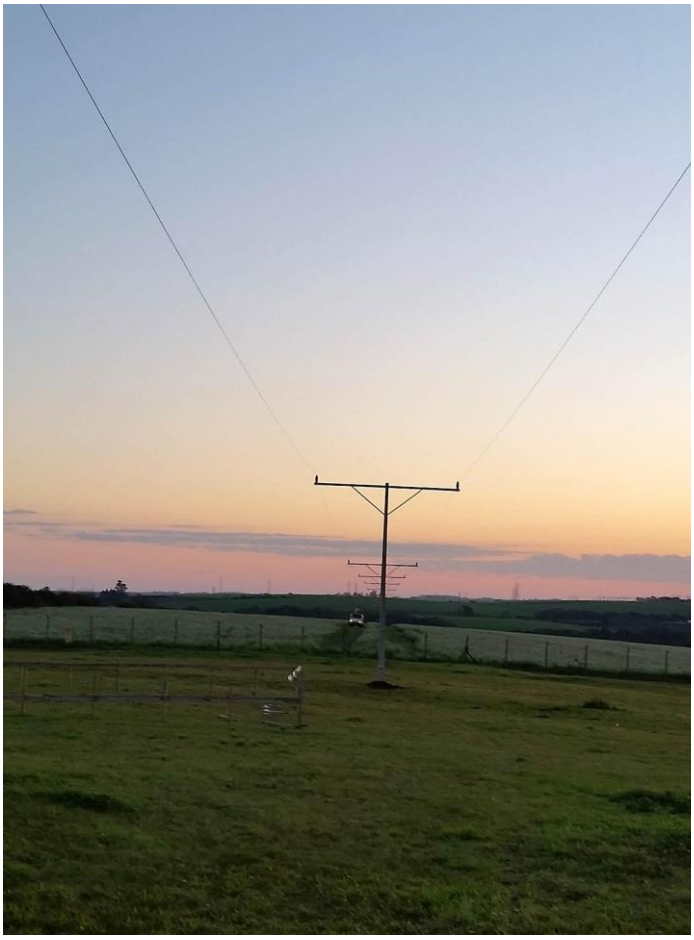

Figure 2.8. Experimental distribution line [52].

2.2.2. Control and Measuring Systems

This section presents the main features of the current and voltage measuring systems and describes the operation of the data acquisition and control systems.

2.2.2.1. Current Measuring System

The lightning current is measured at the top of the tower using two Pearson Current Monitors, one with sensitivity of 0.025 V/A (maximum peak current of 20 kA) and the other with sensitivity of 0.005 V/A (maximum peak current of 100 kA). The current is recorded by a high-speed data acquisition board (Gage CompuScope 4327) installed on a personal computer (PC) at the measurement station. This data acquisition board has two channels, one for each current monitor, with 65 MHz bandwidth, sampling rate of 100 MS/s, 14-bit vertical resolution, and

total memory of 1 GSamples. This memory allows the recording of 5.12 s of the current waveform (in both channels), so that first and also subsequent stroke currents can be measured.

The electrical signals of the current monitors are coupled to the acquisition board installed in the measuring station through analog-to-digital/digital-to-analog fiber links. The links have a DC-40 MHz bandwidth and a 14-bit vertical resolution. The input voltage is $\pm$ 100 V, and the links use single mode fiber. Two links are used, one for each current monitor.

The current timestamp is performed by a GPS clock installed in the computer used for data acquisition. The GPS clock has two capture inputs, which are used for current and induced voltage timestamps. The GPS board has an overall time uncertainty of 100 ns. The acquisition board has a trigger-out connector which is connected to one capture input of the GPS clock.

2.2.2.2. Voltage Measuring System

The induced voltages are measured at two different points of each conductor, i.e., at four points of the line: two points at pole PX2 and two at pole PY2. At each of these poles, there is a metallic box used as the base for two high voltage resistive dividers, enclosure of the oscilloscope, microcontroller, communication system, battery and battery charger, circuit-breakers and surge protective devices (SPDs), inverter, and temperature and humidity control systems. Fig. 2.9 shows the measuring system installed at pole PX2. An example of a lightning-induced voltage measured by oscilloscope 1, channel 1, at the measuring point PX2, on the conductor without surge arrester, is shown in Fig. 2.10.

Figure 2.9. Voltage measuring system (pole PX2) [52].

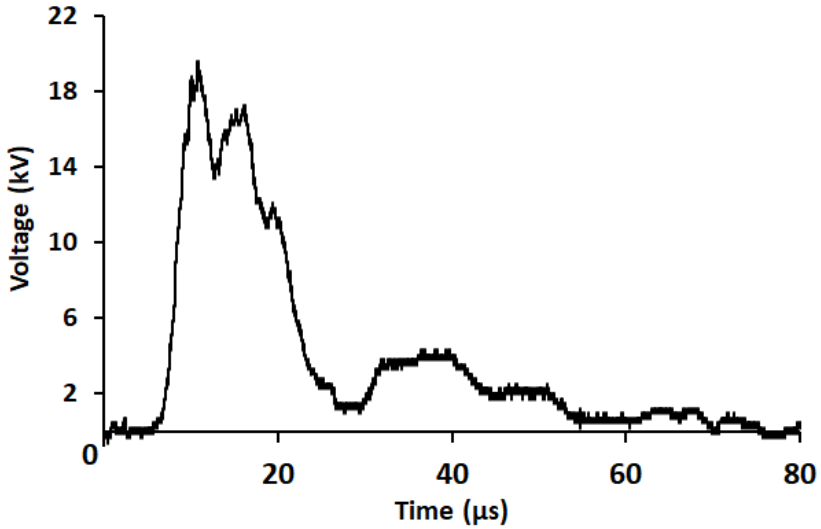

Figure 2.10. Example of a lightning-induced voltage measured in the campus of the Universidade Regional Integrada do Alto Uruguai e das Missões (URI) in Santo Ângelo - RS.

The maximum impulse voltage (standard lightning impulse) that the resistive voltage dividers can withstand is 250 kV. The low voltage resistors are installed inside the metallic box. The oscilloscopes are four-channel, two channels being used for each measuring point. Channel attenuations at each measuring point are adjusted to allow a wide measuring range. While one channel, for example, is set to measure from -6 kV to 42 kV, the other channel has a range of -30 kV to 210 kV, for the same measuring point. The oscilloscopes have 8-bit vertical resolution, trigger input and output BNC connectors, and maximum memory of 2 MS/channel. The Ethernet port via optical fiber converter is used for communicating with the computer.

The triggering system of the oscilloscopes installed at poles PX2 and PY2 are physically interleaved via TTL to optical fiber transmitter/receiver. This configuration ensures that the measurements made on the two poles refer to the same lightning event. Two additional TTL to Optical Fiber Transmitter/Receiver are installed at pole PY2 and at the measuring station to obtain the timestamp of the induced voltage measurements. The oscilloscopes have segmented memory. This feature allows the acquisition memory to be divided into a set of equal-length sub-records. The oscilloscope memory has been divided into 5 segments, resulting in 5 blocks with about 333.3 kS/channel. The oscilloscope sweep speed was set equal to 50 μs/div, which results in 5 blocks with 500 μs of measurement. The resulting sampling rate is 667 MS/s. The oscilloscope is able to re-arm the trigger system for new segments in about 1 μs, a feature that allows to record voltages induced by subsequent strokes or by different flashes which occur at short intervals.

2.2.2.3. Control System

The data acquisition and control system is performed by two programs. The main program is implemented into the personal computer located at the measuring station, and the secondary program is implemented into the microcontrollers (Arduino UNO) installed at the instrumented boxes (poles PX2, PY2, and top of tower). The main program, developed in LabVIEW, is responsible for most of the tasks, including the setup of the oscilloscopes and acquisition board, sending the command to turn the equipment on and off, acquiring measured waveforms and so on. The program that is executed at the microcontrollers is responsible, together with the main

program, for relay actuation and monitoring of the environmental conditions inside the instrumented boxes.

The main program allows configuring the setup of the oscilloscopes and data acquisition board. The oscilloscopes can be turned on manually, prescheduled, or when the vertical electric field exceeds a certain value. The electric field is always monitored and its value is recorded on the computer hard disk. During the measurements, the main program sends commands to the Arduino to disconnect the battery chargers from the low voltage circuit (220 V AC underground) and to turn on the DC-AC power inverter. The oscilloscopes are powered from a stationary lead-acid battery through the inverters. The previously saved setup of the oscilloscopes and acquisition board is restored and can be changed at any time in the main program. In case of a lightning strike to the tower or nearby, the induced voltages will be recorded in the oscilloscope memory and the waveforms will be acquired and saved in a specific folder in the computer hard disk. The timestamps of the voltage measurements are obtained from a GPS card installed on the computer. After acquiring the waveforms, the oscilloscopes are put in single acquisition mode again. At the end of the measurement cycle, the oscilloscopes are switched off and the battery charger is switched on. The main program creates Log files that record all the events measured by the system.

The oscilloscopes can be turned on independently of the prescheduled time if the vertical electric field exceeds a certain value. In this case, the oscilloscopes are kept on for a given time.

The control of the current measuring system is independent of the oscilloscopes. It can be switched on/off manually or prescheduled. In case of a lightning stroke to the tower, the signals of the current monitors will be sent to the acquisition card installed in the PC and the main program will write the data in a specific folder. The timestamp of the current measurements are also obtained from the GPS card.

The microcontrollers installed in the instrumented boxes are also responsible for monitoring the battery voltage and the temperature and humidity inside the boxes. If the system indicates that the battery voltage is low, it automatically switches off the oscilloscopes. The temperature control is done by exhausters installed in the boxes. Humidity can be controlled through the exhausters and also through a heater. This system is also adjusted and monitored by the main program.

3. ANALYSIS OF THE LIGHTNING-INDUCED VOLTAGE WAVEFORMS

This chapter aims to analyze the 64 lightning-induced voltages with magnitudes above 2 kV recorded by the system that operated at the campus of the University of São Paulo (System 1), described in section 2.1. The analysis is focused on the time parameters, which, unlike the voltage amplitude, do not depend on the current peak value. About one-third of the recorded voltages (21 out of 64) were classified as bipolar. This high percentage of bipolar voltages was somewhat unexpected – or at least it was not obvious -, as the line was matched at both ends and had no equipment other than distribution insulators and the two resistive dividers.

3.1. General

As mentioned in Chapter 2, the voltages were measured on an un-energized conductor matched at both ends, so that reflections are not present. This conductor did not have any equipment connected except for the distribution insulators and the two voltage dividers. The analysis refers to the voltages induced by 64 lightning strokes that reached magnitudes higher than 2 kV. As the voltages were measured simultaneously at two points of the conductor, in principle the 64 lightning events should result in 128 induced voltage waveforms. However, the differences between the voltages induced on the two points were always negligible and, in addition, in some cases the voltages were recorded only at one point. Therefore, only one voltage waveform was considered for each lightning event, so the data considered in the analysis consisted of 64 induced voltage waveforms.

Although the locations of the lightning strokes that induced the recorded voltages were not available, none of the voltages were induced by flashes that hit the tower described in Chapter 2.

Fig. 3.1 shows the monthly occurrence statistics of the measured induced voltages. It can be seen that 72% of the measurements were obtained in the period January - March, which corresponds to summer in the Southern Hemisphere.

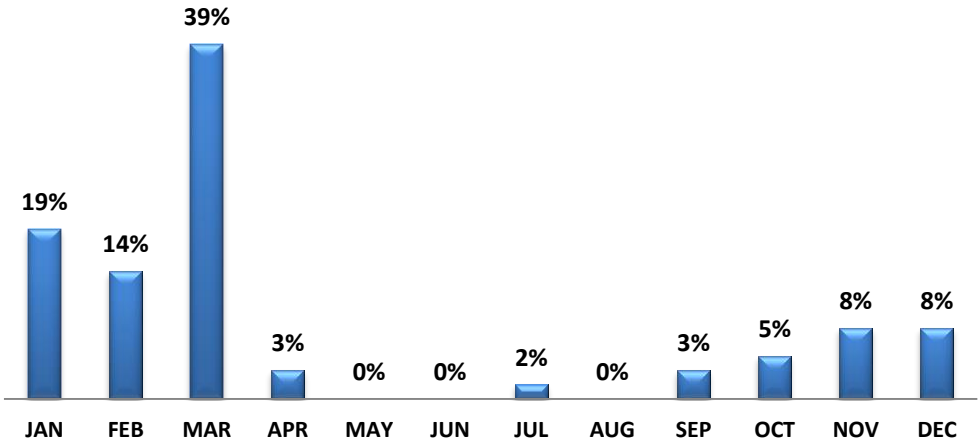

Figure 3.1. Monthly occurrence statistics of the lightning-induced voltages measured at the experimental line [33].

The Savitzky-Golay digital filter [61] was applied to the raw data to smooth the noise slightly. This filter smooths the noisy signal by fitting a polynomial function piecewise to the signal. Some examples of lightning-induced voltages waveforms before and after being filtered are shown in Fig. 3.2 to Fig. 3.5.

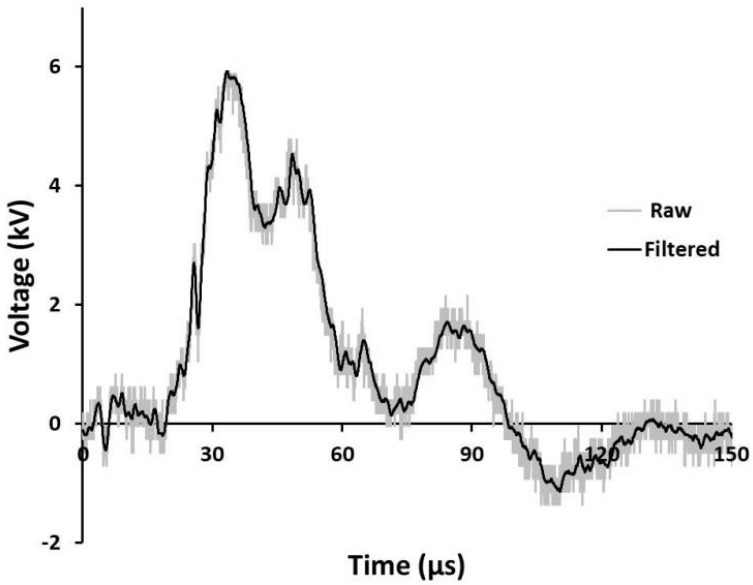

Figure 3.2. Lightning-induced voltage waveshape (#5) with and without filtering [33].

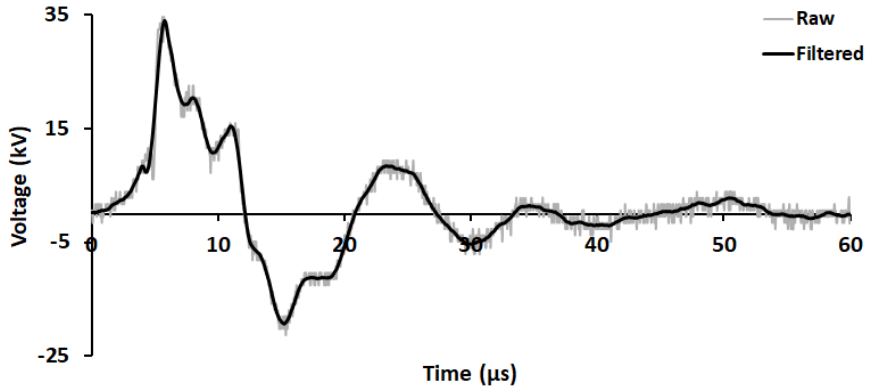

Figure 3.3. Lightning-induced voltage waveshape (#17) with and without filtering.

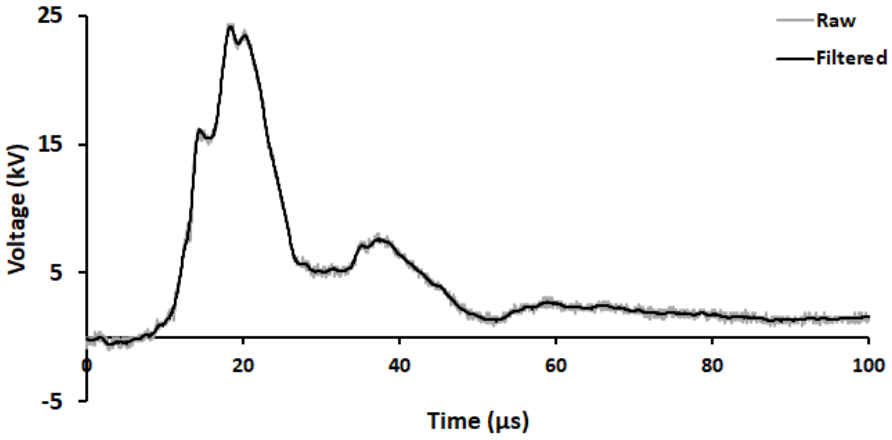

Figure 3.4. Lightning-induced voltage waveshape (#23) with and without filtering.

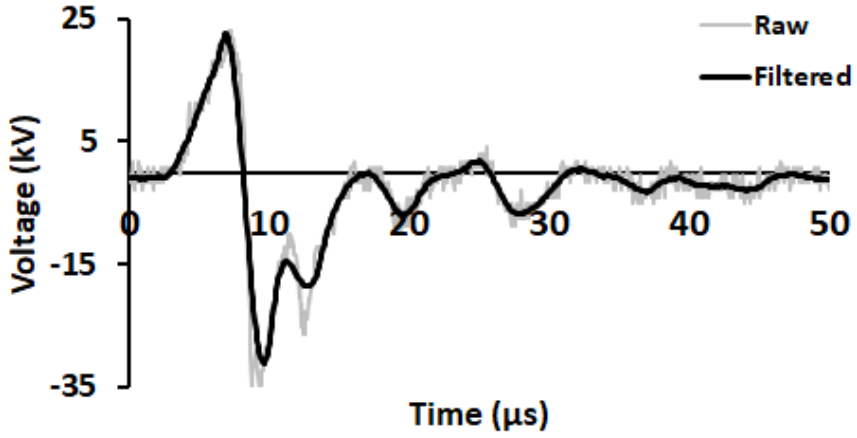

Figure 3.5. Lightning-induced voltage waveshape (#57) with and without filtering.

The wavetails of the recorded induced voltages are shorter in comparison with the standard lightning impulse voltage (1.2 / 50 μs), a result which is coherent with calculations [10] – [12], [20], [24], [14] – [17] and measurements performed in other studies [9], [18], [19], [24], [25], [42] – [44], [51], [62]. A typical voltage induced by a nearby downward negative lightning flash usually has positive polarity, at least at the points of the line close to the stroke location. However, lightning-induced voltages are significantly affected by the stroke current waveshape and many other parameters and conditions. As shown in [1], [16], [17], depending on the observation point and the relative position of the stroke location with respect to the line, the induced voltage may be positive, negative, or bipolar. The occurrence of an upward leader may also lead to a bipolar voltage with a short negative peak in the initial part (in the case of downward negative lightning flashes) [1], [63]. The channel tortuosity influences the induced voltages remarkably [64]; channel branches may also affect the voltage characteristics.

Strictly speaking, all the recorded lightning-induced voltages were bipolar. However, in many cases the initial part of the voltage and the semi-cycles that occur after the maximum absolute value (*Vmax*) have no significant effects on the behavior of power equipment insulation subjected to these voltages.

The analysis revealed that the measured voltage waveshapes could be classified into four categories. These four voltage types are derived from a “basic” waveshape with three semi-cycles (A, B, and C), as shown in Fig. 3.6. Type I corresponds to the unipolar waveshape, for which the semi-cycles A and C can be neglected. The bipolar voltages are subdivided into Types II, III, and IV. If the semi-cycles A or C can be disregarded, the voltage is classified as Type II or Type III, respectively. If the three semi-cycles are important, it is considered as Type IV.

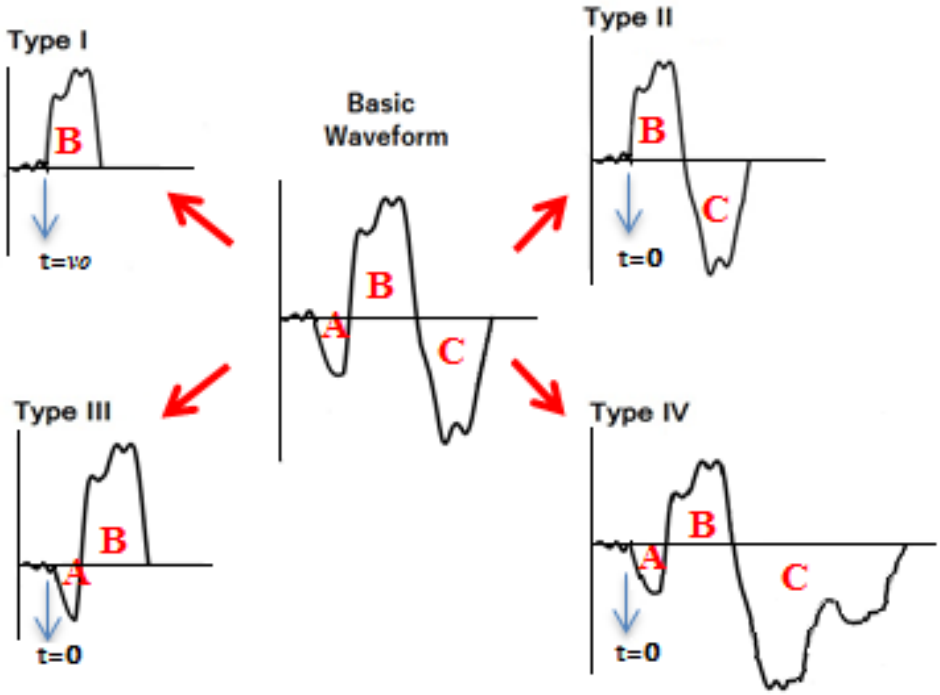

Figure 3.6. Schematic lightning-induced voltage types derived from the 'basic' waveform [34].

The criterion adopted to neglect semi-cycles of the 'basic' waveshape and classify the voltage into one of the four types is: semi-cycle A is disregarded if its peak value is less than 20% of the maximum absolute voltage values (*Vmax*); semi-cycle C is neglected if its voltage peak is less than 40% of *Vmax*. The criterion for neglecting semi-cycle C may be controversial. However, considering the recorded waveforms, if the magnitude of the voltage peak corresponding to semi-cycle C is lower than 40% of the maximum absolute voltage value, this semi-cycle will not have an important effect on the insulation behavior in the great majority of the cases.

For the induced voltage shown in Fig. 3.2, *Vmax* = 5.9 kV. As the absolute values of the peaks of the semi-cycles that precede the one at which *Vmax* is reached are lower than 20% (1.18 kV) and 40% (2.36 kV) of *Vmax*, respectively, both semi-cycles are disregarded. Therefore, according to the adopted criteria, the voltage has been classified as unipolar, that is, as Type I.

For the unipolar waveshapes (Type I), the instant t = 0 corresponds to the virtual origin (*vo*) defined in section 3.2. For the bipolar waveshapes, the instant t = 0 is the instant at which the voltage crosses the horizontal axis just before semi-cycle B (Type II) or semi-cycle A (Types III and IV), as indicated in Fig. 3.6.

The parameters that characterize the four voltage types are discussed in the next sections.

3.2. Type I

About 67% of the recorded lightning-induced voltages, that is, 43 out of 64, were classified as Type I. Except for one case, all the voltages have positive polarity. Five examples of this voltage type are shown in Figs. 3.7 to 3.11. The only recorded induced voltage of negative polarity is depicted in Fig. 3.11.

As described in [65], the first stroke current waveshape starts with a concave front followed by an abrupt rise around the half-peak that leads to the first peak. This initial peak is usually followed by a second peak which is normally higher than the first one; the medium of the ratio of the first and second peaks is 0.9 [65]. The virtual origin, from which the wavefront parameters of lightning currents are calculated, is obtained taking the first peak as reference.

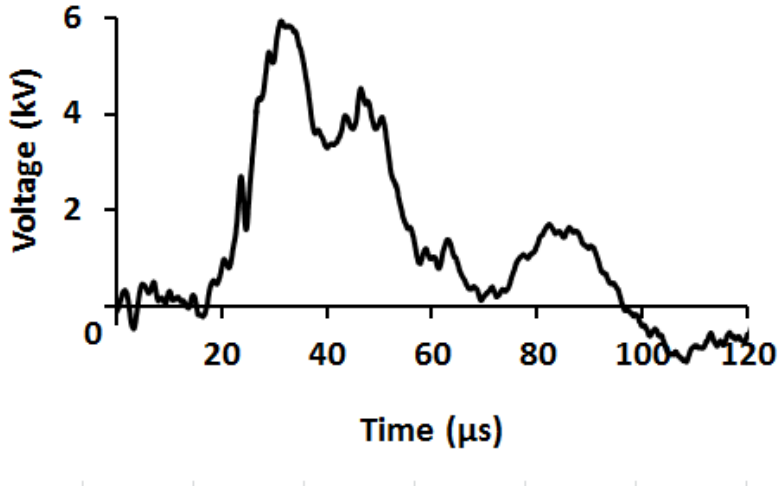

Figure 3.7. Example of a Type I lightning-induced voltage with positive polarity (Waveshape #5) [34].

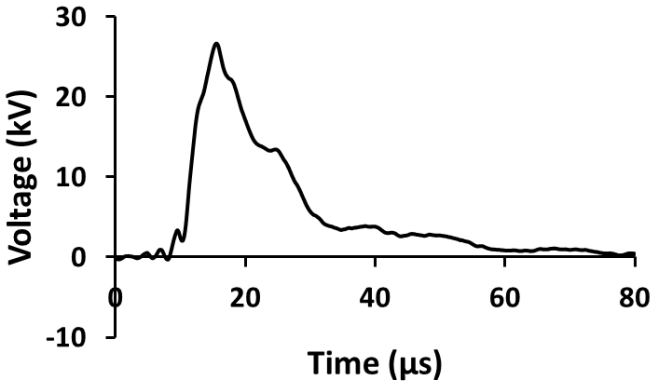

Figure 3.8. Example of a Type I lightning-induced voltage with positive polarity (Waveshape #22) [34].

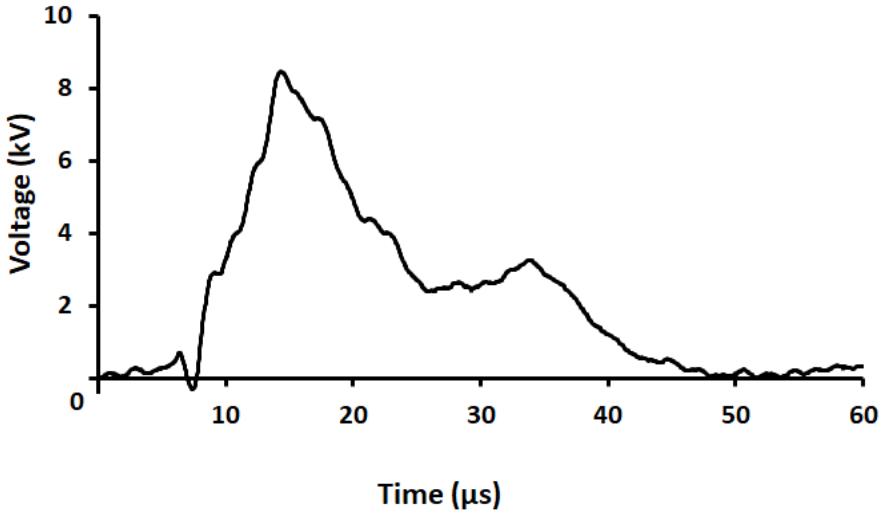

Figure 3.9. Example of a Type I lightning-induced voltage with positive polarity (Waveshape #7).

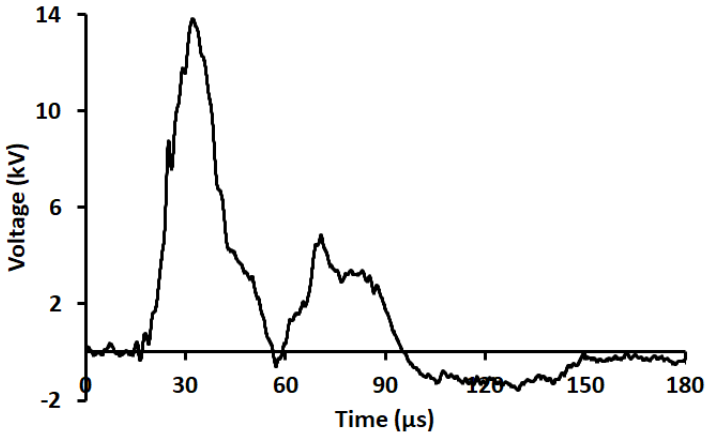

Figure 3.10. Example of a Type I lightning-induced voltage with positive polarity (Waveshape #9).

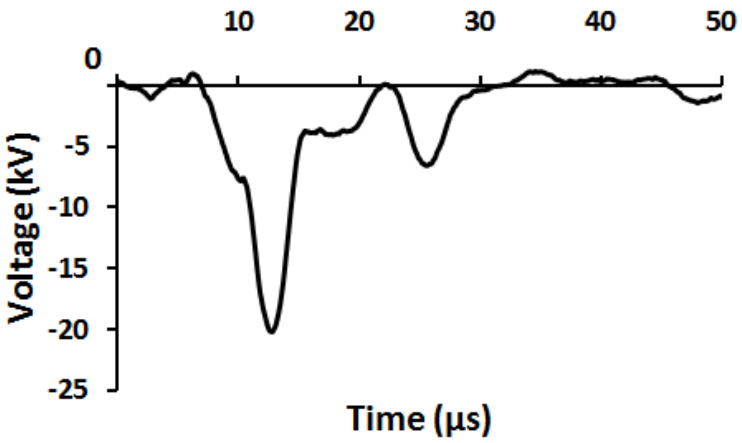

Figure 3.11. Example of a Type I lightning-induced voltage with negative polarity (Waveshape #59) [34].

Regarding the measured lightning-induced voltages, more than 40% (20 out of 43) of those classified as Type I have more than one peak preceding the maximum value, as illustrated in Fig. 3.7. The amplitudes of these peaks vary over a wide range, from 5% to 90% of *Vmax*, and a criterion should be defined for choosing which of these peaks should be used as reference for the calculation of the wavefront parameters.

Three situations were considered regarding the reference V_1 for calculating T_{10}, T_{30}, T_{90}, and vo:

- *Vmax*: the reference is the maximum voltage value (*Vmax*);
- 0.75 *Vmax*: the reference V_1 is the highest peak among the peaks in the range 75% *Vmax* to *Vmax*, that is, the maximum voltage peak V_1 such that $0.75\ Vmax \leq V_1 < Vmax$;
- 0.65 *Vmax*: the reference V_1 is the highest peak among the peaks in the range 65% *Vmax* to *Vmax*, that is, the maximum voltage peak V_1 such that $0.65\ Vmax \leq V_1 < Vmax$.

The parameters which characterize Type I voltages are the equivalent front times $tf_{(10/90)}$ and $tf_{(30/90)}$ and the time to half-value (th), which are calculated according to (3.1) – (3.3).

Equivalent front time $tf_{(10/90)}$:

$$tf_{(10/90)} = \frac{(T_{90}-T_{10})}{0.8}\ \frac{Vmax}{V1} \qquad (3.1).$$

Equivalent front time $tf_{(30/90)}$:

$$tf_{(30/90)} = \frac{(T_{90}-T_{30})}{0.6}\ \frac{Vmax}{V1} \quad (3.2).$$

Time to half-value, th:

$$th = T_{l50} - vo \quad (3.3).$$

The virtual origin, vo, is calculated as:

$$vo = T_{30} - 0.3\ tf_{(30/90)} \quad (3.4).$$

In (3.1) – (3.3), T_{10}, T_{30} and T_{90} are, respectively, the 10%, 30%, and 90% intercepts along the induced voltage waveshape. V_1 is the reference for calculating T_{10}, T_{30}, and T_{90}. T_{l50} is the instant corresponding to the value of 50% of the maximum voltage on the wavetail; in the case of oscillating voltages for which more than one point on the wavetail crosses the line corresponding to 50% of *Vmax*, T_{l50} is the longest time. The time to half-value *th* is the difference between T_{l50} and the virtual origin *vo*.

Fig. 3.12 shows an example of an induced voltage waveform whose front time $tf_{(30/90)}$ was calculated according to the three criteria presented. If the "0.65 *Vmax*" criterion is adopted, $tf_{(30/90)}$ = 2.7 μs, whereas a front time about seven times longer (namely, 18.2 μs) is obtained if either the "*Vmax*" or the "0.75 *Vmax*" criteria are used. If, for example, an insulator is to be tested in a laboratory with an impulse voltage with the same amplitude and front time of the voltage depicted in Fig. 3.12, it is recommended to be on the safe side, i.e., to apply an impulse voltage with front time of 2.7 μs, for which the insulation presents a lower insulation strength.

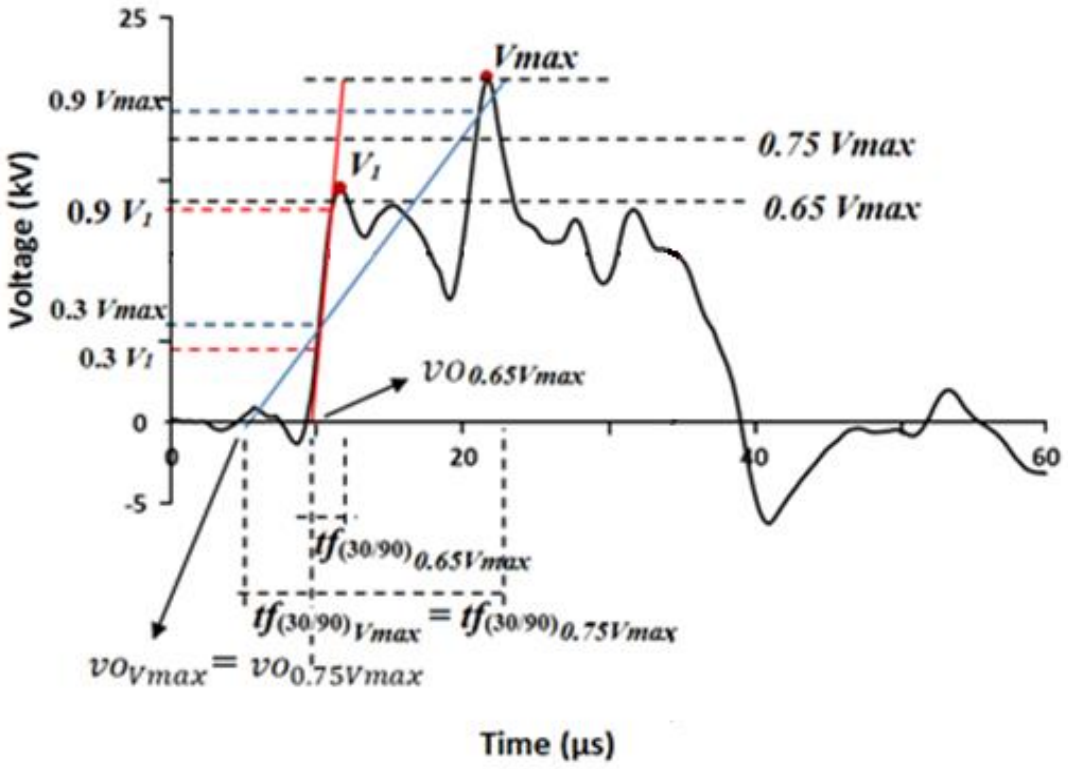

Figure 3.12. Criteria for determining the virtual origin and waveshape parameters (Waveshape #46), adapted from [33].

Table 3.1 presents the average ($\bar{x}$), median (μ), and standard deviation (σ) of the waveshape parameters $tf_{(10/90)}$, $tf_{(30/90)}$, and *th* calculated according to these three criteria. Concerning the time to half-value, the differences obtained using the three criteria are insignificant. Larger variations are observed on the front time $tf_{(30/90)}$ (maximum differences of about 25% and 15% for the average and median, respectively).

Table 3.1. Waveshape parameters $tf_{(10/90)}$, $tf_{(30/90)}$, and *th* calculated according to three different criteria.

Criterion	$tf_{(10/90)}$ (µs)			$tf_{(30/90)}$ (µs)			*th* (µs)		
	$\bar{x}$	μ	σ	$\bar{x}$	μ	σ	$\bar{x}$	μ	σ
Vmax	6.4	4.4	4.7	8.5	5.5	6.3	19.6	17.1	11.8
0.75 *Vmax*	7.0	5.7	3.9	7.6	5.3	5.6	19.2	16.8	12.1
0.65 *Vmax*	7.3	5.9	4.2	6.8	4.8	5.2	19.0	16.8	11.9

An individual analysis of the induced voltage waveshapes indicated that the best results are obtained when the reference for calculating T_{10}, T_{30}, T_{90}, and *vo* is the highest peak among the

peaks in the range 65% *Vmax* to *Vmax*. That is, the reference is the peak voltage V_1 such that 0.65 *Vmax* ≤ V_1 <*Vmax*. By "best results" we mean that this criterion leads to voltages with shorter front times, and when an insulation is subjected to two impulses with the same amplitude and wavetail but different front times, more severe stress is caused by the impulse with shorter front time. From the defined criterion, the parameters which characterize Type I voltages are the equivalent front times $tf_{(10/90)}$ and $tf_{(30/90),}$ and the time to half-value (*th*), indicated in Fig. 3.13.

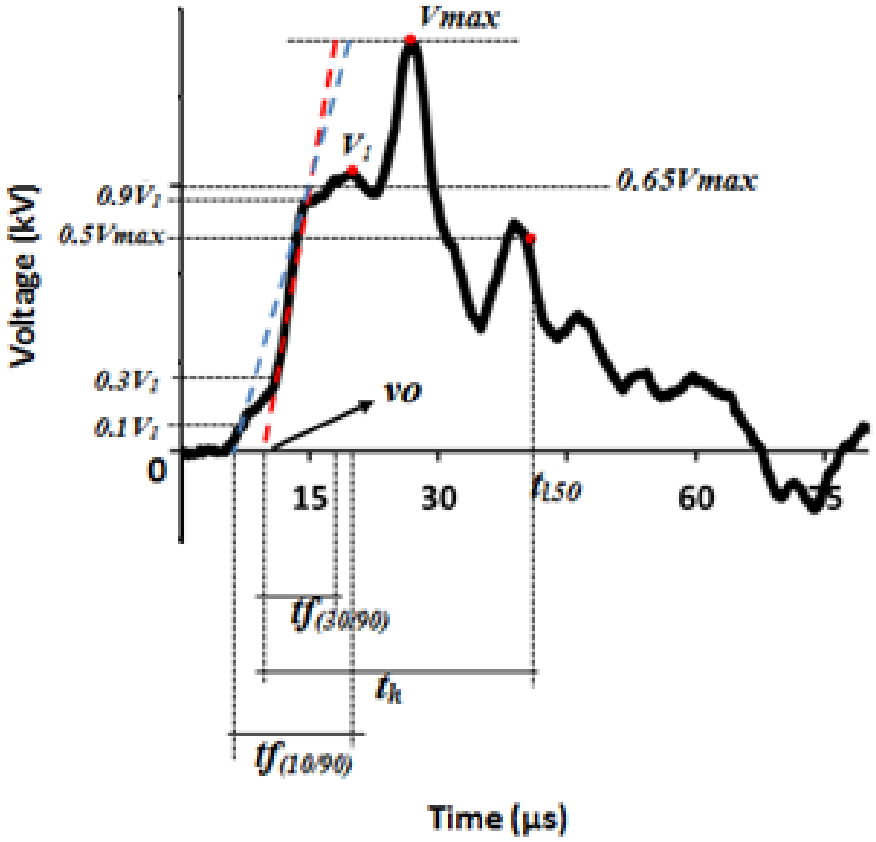

Figure 3.13. Wavefront parameters of a Type I voltage (Waveshape #51). Blue and red lines pass through the points corresponding to 10% and 90% of V_1 and 30% and 90% of V_1, respectively [34].

For about 65% of Type I voltages, including those shown in Figs. 3.7 to 3.11, the equivalent front time $tf_{(10/90)}$ is longer than $tf_{(30/90)}$. The medians (μ_{ln}) and standard deviations (σ_{ln}) of the Type I voltage waveshape parameters, assuming the log-normal distribution, are presented in Table 3.2 along with the arithmetic mean ($\bar{x}$). The medians of $tf_{(10/90)}$, $tf_{(30/90)}$, and *th* are, respectively, 6.1 µs, 5.2 µs, and 15.8 µs. The front times are longer and the times to half-value

are shorter in comparison with the standard lightning impulse voltage.

Table 3.2. Type I Voltage waveshape parameters $tf_{(10/90)}$, $tf_{(30/90)}$, and *th*.

Parameter	$\bar{x}$	μ_{ln}	σ_{ln}
$tf_{(10/90)}$ **(μs)**	7.3	6.1	5.0
$tf_{(30/90)}$ **(μs)**	6.8	5.2	5.9
***th* (μs)**	19.0	15.8	13.5

3.3. Type II

The induced voltages classified as Type II correspond to about 20% (13 out of 64) of the recorded voltages. They are composed of two semi-cycles, the first one of positive polarity, as indicated in Fig. 3.6. The maximum absolute voltage value can occur either in the first or the second semi-cycle. Examples of Type II induced voltages are shown in Figs. 3.14 to 3.17.

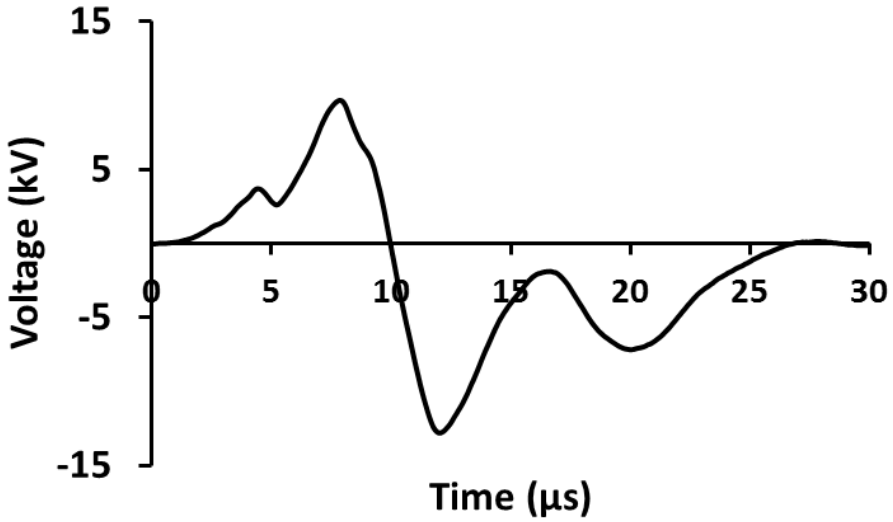

Figure 3.14. Type II induced voltage waveshape with maximum absolute voltage value in the second semi-cycle (Waveshape #48).

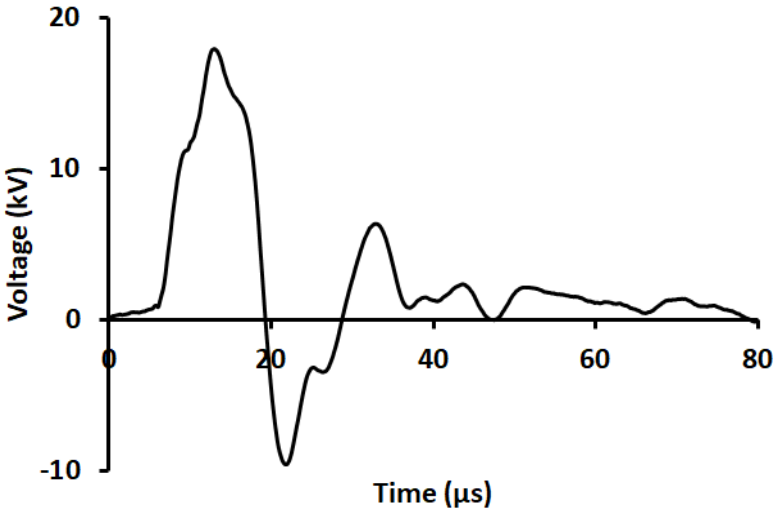

Figure 3.15. Type II induced voltage waveshape with maximum absolute voltage value in the first semi-cycle (Waveshape #43).

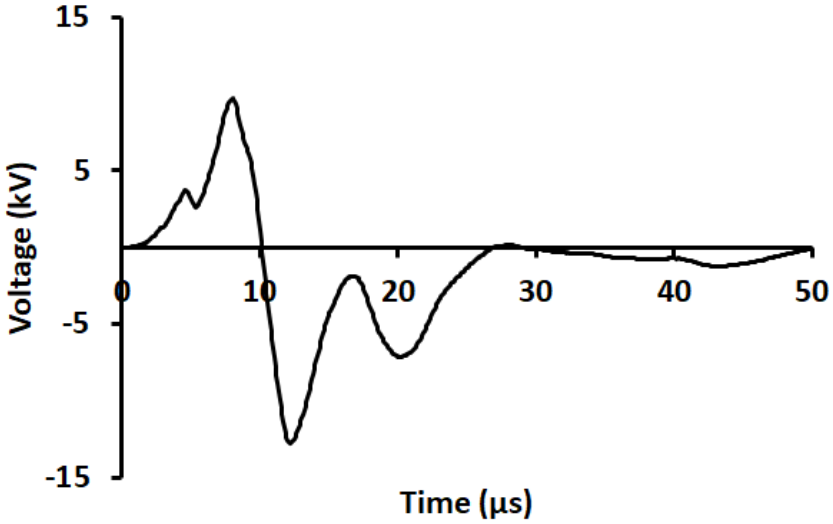

Figure 3.16. Type II induced voltage waveshape with maximum absolute voltage value in the second semi-cycle (Waveshape #49).

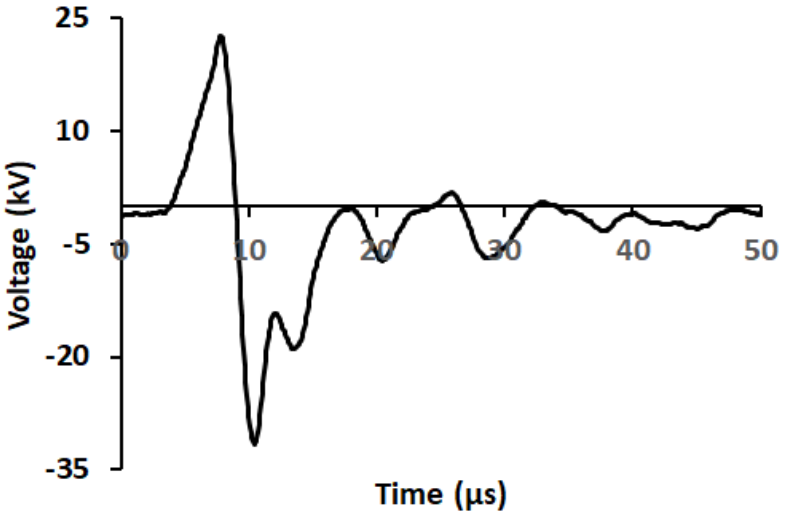

Figure 3.17. Type II induced voltage waveshape with maximum absolute voltage value in the second semi-cycle (Waveshape #57).

The duration of the first semi-cycle of the voltage shown in Fig. 3.14 is 9.4 μs. The voltage reaches its maximum (absolute value of 12.8 kV) in the second semi-cycle, whose duration is 16.8 μs.

In 69% of the cases, the maximum absolute value of the voltage occurs in the first semi-cycle. The ratio of the absolute values of the peak voltages of the second and first semi-cycles ranges from 0.46 to 1.38, as shown in Fig. 3.18 The average times at which the voltage reaches its peaks in the first and second semi-cycles are 5.3 μs and 13.3 μs, respectively.

For most Type II induced voltages, the second semi-cycle is longer than the first one. The first and second semi-cycles have average durations of 9.4 μs and 14.3 μs, respectively.

The medians (μ_{ln}) and the standard deviations (σ_{ln}) of the durations are 8.2 μs and 11.2 μs for the first semi-cycle and 5.5 μs and 15.5 μs for the second one, respectively. The ratio of the durations of the second and first semi-cycles varies in the range of 0.16 to 6.57. As shown in Fig. 3.19, in 10 out of the 13 cases (about 77%) the duration of the second semi-cycle is longer than that of the first one.

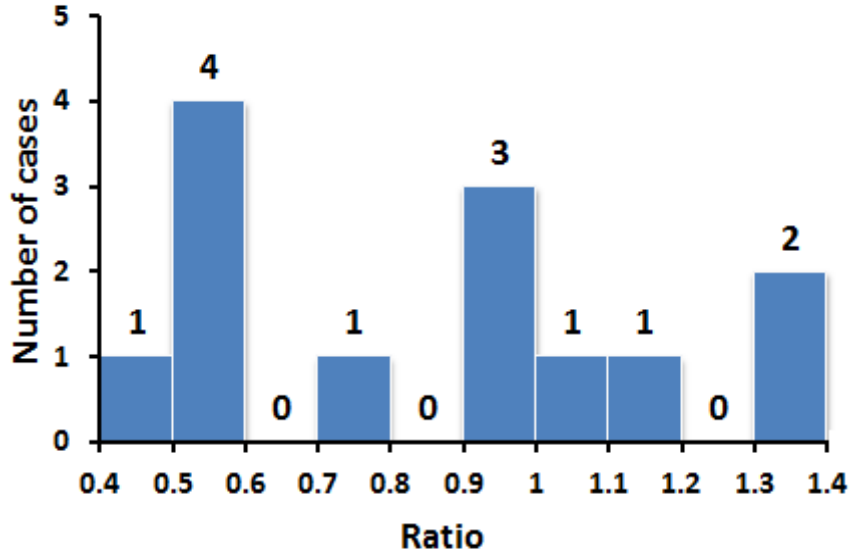

Figure 3.18. Histogram of the ratios of the absolute values of the maximum voltages of the second and first semi-cycles [34].

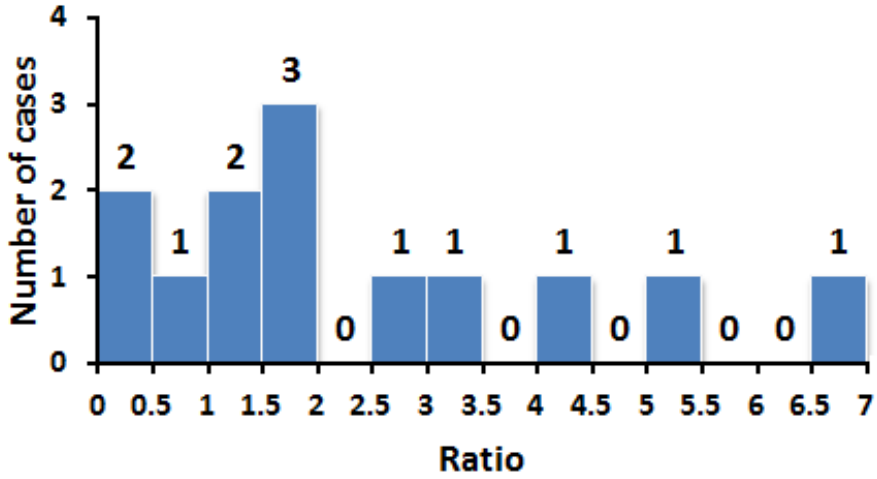

Figure 3.19. Histogram of the ratios of the durations of the second and first semi-cycles [34].

3.4. Type III

The induced voltages classified as Type III correspond to 9.4% (6 out of 64) of the recorded voltages. They are composed of two semi-cycles and, except for one case, the first one has negative polarity, shorter duration, and lower magnitude, as indicated in Fig. 3.6. Typical examples of Type III voltage waveshapes are given in Figs. 3.20 to 3.23. Fig. 3.23 shows the only recorded induced voltage with polarities of the first and second peaks (positive and

negative, respectively) inverted compared with the other voltages.

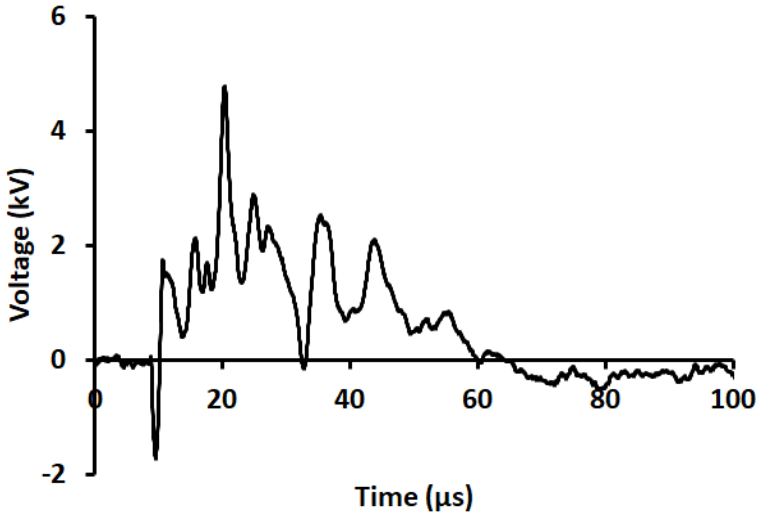

Figure 3.20. Type III induced voltage waveshape with first semi-cycle of positive polarity and maximum absolute voltage value in the second semi-cycle (Waveshape #11).

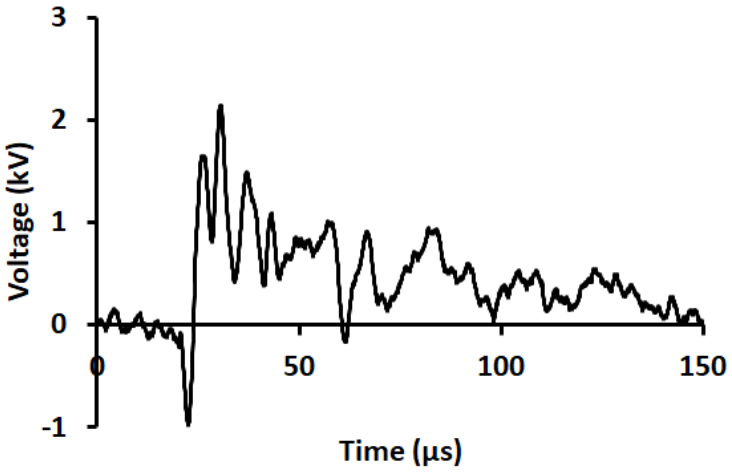

Figure 3.21. Type III induced voltage waveshape with first semi-cycle of positive polarity and maximum absolute voltage value in the second semi-cycle (Waveshape #34).

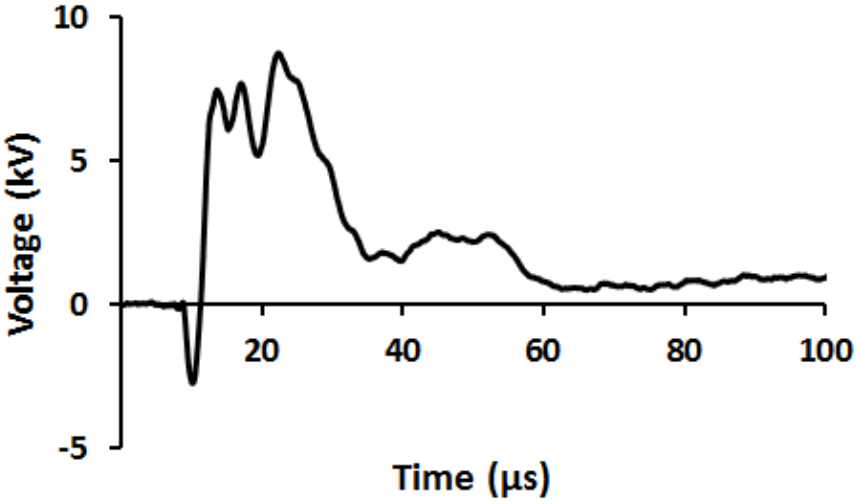

Figure 3.22. Type III induced voltage waveshape with first semi-cycle of negative polarity and maximum absolute voltage value in the second semi-cycle (Waveshape #36) [34].

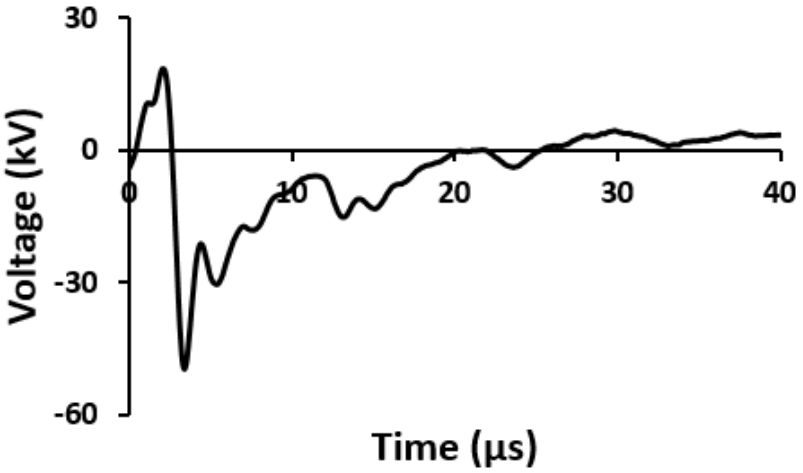

Figure 3.23. Type III induced voltage waveshape with first semi-cycle of positive polarity and maximum absolute voltage value in the second semi-cycle (Waveshape #18) [34].

Although the polarities of the semi-cycles of the induced voltage shown in Fig. 3.23 are inverted in relation to the other voltages classified as Type III, the durations of the first and second semi-cycles are coherent with those of the other voltages. This indicates that it is likely to have been induced by a positive downward lightning flash. The average durations of the first and second semi-cycles of Type III induced voltages are 3.3 µs and 47.4 µs, respectively. The medians (μ_{ln}) and standard deviations (σ_{ln}) are, respectively, 2.7 µs and 2.5 µs for the first semi-cycle and 30.1 µs and 63.5 µs for the second one. The average ratio of the absolute values of the peak voltages of the first and second semi-cycles is 0.4.

The average times at which the peak values occur are 2.5 μs for the first and 10.2 μs for the second semi-cycle.

The ratios of the maximum absolute voltage value of the first and second semi-cycles varied in the range of 0.26 to 0.45, the average being 0.4. The histogram of the ratios is shown in Fig. 3.24. The ratios of the durations of the second and first semi-cycles varied in the range of 4 to 67, as shown in Fig. 3.25.

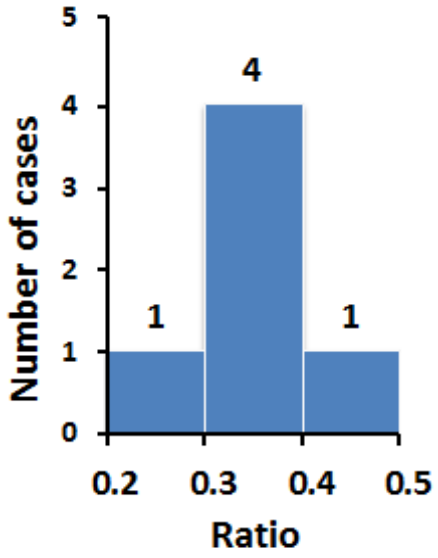

Figure 3.24. Histogram of the ratios of the absolute values of the lowest and highest induced voltage.

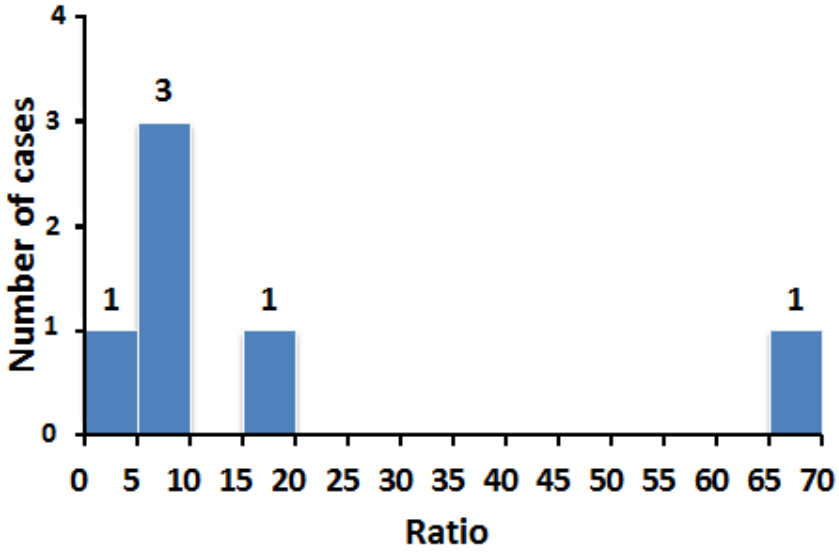

Figure 3.25. Histogram of the ratios of the durations of the second and first semi-cycles.

3.5. Type IV

The induced voltages classified as Type IV correspond to 3.1% (2 out of 64) of the recorded voltages. They are composed of three semi-cycles, as indicated in Fig. 3.6. Type IV has a particularity in that the occurrence of the maximum absolute voltage value is in the third semi-cycle, which has negative polarity and the longest duration. The two induced voltage waveshapes classified as Type IV are presented in Fig. 3.23 and Fig. 3.24.

The durations are 4.2 μs and 4 μs for the first semi-cycle, 2.7 μs and 4.9 μs for the second semi-cycle, and 35.5 μs and 23.9 μs for the third semi-cycle of the voltages shown in Fig. 3.26 and Fig. 3.27 respectively. The ratios of the absolute values of the maximum voltages of the first and third semi-cycles are 0.62 and 0.46; the ratio of the absolute values of the maximum voltages of the second and third semi-cycles are 0.54 and 0.86.

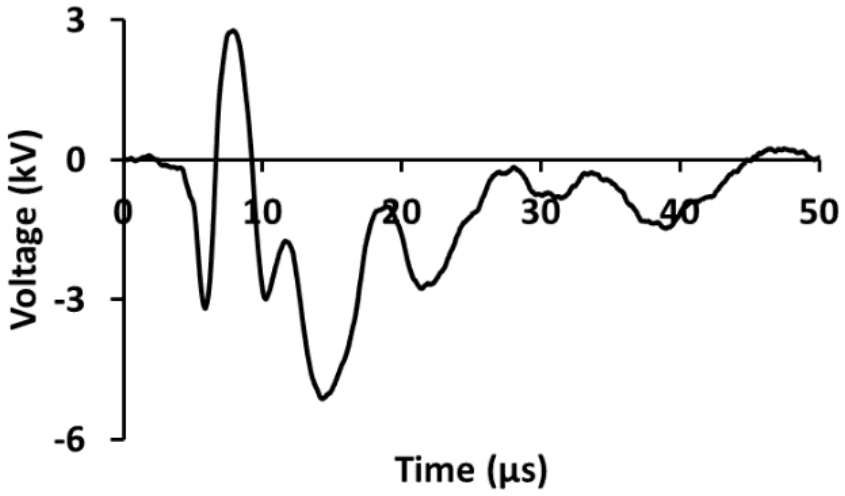

Figure 3.26. Type IV induced voltage waveshape (Waveshape #2) [34].

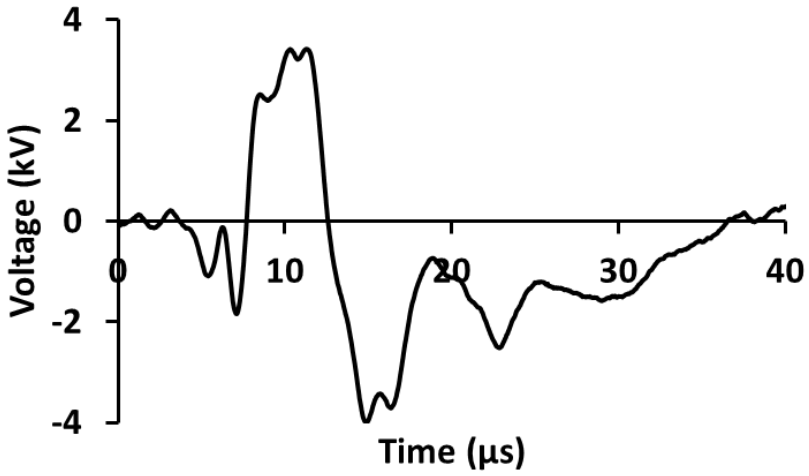

Figure 3.27. Type IV induced voltage waveshape (Waveshape #13) [34].

4. GENERAL ASSESSMENT OF THE MEASURED LIGHTNING-INDUCED VOLTAGES - COMPARISONS WITH CALCULATION RESULTS

The analysis presented in Chapter 3 indicated that about 67% of the recorded lightning-induced voltages, that is, 43 out of 64, were unipolar (Type I). In other words, about one-third of the recorded voltages were classified as bipolar. As the line was matched at both ends and had no equipment other than distribution insulators and the two resistive dividers, this result was far from obvious. Bipolar lightning surges appeared to be more common than expected.
In this chapter, an investigation is performed aiming at finding at which conditions voltages with characteristics similar to those observed on the measured ones, considering a similar line, could be obtained. The calculations are performed using the Extended Rusck Model (ERM) [56].

4.1. The Extended Rusck Model (ERM)

The ERM is a model for calculating lightning-induced surges that enables to take into account realistic situations such as, e.g., a multi-conductor line with a multi-grounded neutral or shield wire over a finitely conducting ground [67]. The incidence of lightning flashes to nearby elevated objects and the occurrence of upward leaders can also be considered [67], as well as the presence of equipment such as transformers and surge arresters [18]. The effect of a multi-grounded conductor is evaluated by calculating the currents that flow to ground at the various grounding points taking into account the multiple reflections and, then, the voltages associated with these currents that, due to the coupling between the wires, are induced on the phase conductors [14]. The ERM has been validated with experimental data obtained using different techniques: rocket-triggered lightning, lightning flashes to instrumented towers, and reduced scale modeling [10], [18], [56], [67].

It represents an extension of the Rusck model [53] in the sense that, unlike the original model, which was developed under the assumption of a perfectly conducting ground, it enables the analysis of situations of practical interest. The good agreement observed between measured and calculated induced voltages in hundreds of situations, including the case of finite soil

conductivity, confirms the suitability of the ERM for the analysis of lightning-induced transients. Details of the model can be found in [56].

4.2. Comparisons

The purpose of the comparisons presented in this section is to investigate under which conditions voltages with characteristics similar to the recorded ones, especially those classified as belonging to Types I, II, and III, could be induced on a matched line without surge arresters, shield wire, and a neutral conductor. The voltages classified as these three types correspond to approximately 97% of the measurements. Negative downward flashes are assumed in all the calculations, though in the figures the currents are represented as if they had positive polarity.

The number of simulations required to obtain the conditions under which the calculated voltages were similar to the measured ones varied from case to case. The first case, corresponding to a Type I voltage, was the simplest one, and it was relatively easy to find the combination of the parameters. The second case, corresponding to a Type II voltage, required more time, but it was also not so difficult. On the other hand, it took much more time to identify the combination of the parameters relevant to the third case, corresponding to a Type III voltage.

The first case considered refers to the induced voltage #22 (Type I). In Fig. 4.1 the measured voltage is compared with the one calculated with the ERM assuming a typical stroke current with amplitude (*Ip)* of 25 kA, front time $tf_{(30/90)}$ of about 4.5 μs, and propagation velocity of 40% that of light in free space. The line is 2 km long, 9 m high, and the distance *(d)* between the stroke location and the line center, where the voltage is calculated, is 500 m, as indicated in Fig. 4.2. The soil resistivity (ρ) is 100 Ω.m, and the relative permittivity is equal to 10. The current waveshape is represented by the Heidler Function [68], with I_0 = 23.7 kA, τ_1 = 1.5 μs, τ_2= 160 μs and n = 2.

$$i(t) = \frac{I_0}{\eta}\frac{(t/\tau_1)^n}{[(t/\tau_1)^n + 1]} e^{-(t/\tau_2)}; \qquad \eta = e^{-\left(\frac{\tau_1}{\tau_2}\right)\cdot\left(n.\frac{\tau_2}{\tau_1}\right)^{1/n}} \qquad (4.1).$$

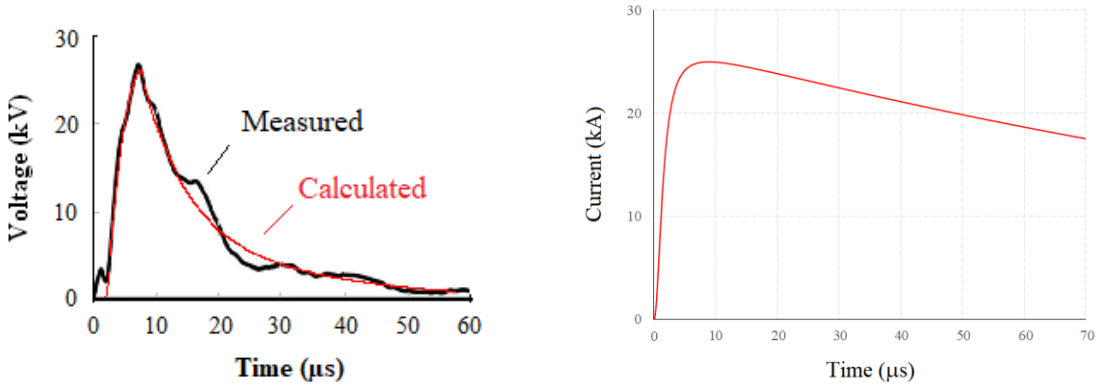

(a) (b)

(a) Measured and calculated induced voltages. (b) Stroke current

Figure 4.1. Comparison between measured and calculated induced voltages (Type I – Waveshape #22).

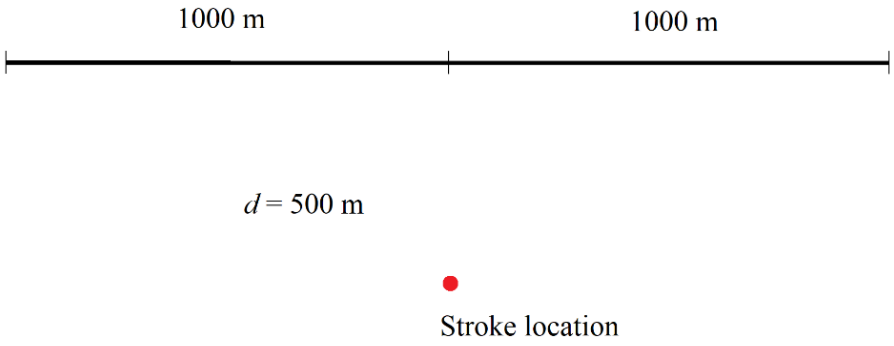

Figure 4.2. Simulation conditions for the calculated voltages depicted in Fig. 4.1 and in Fig. 4.3 (both voltages were calculated at the line center).

The second case refers to the induced voltage #17 (Type II), which in Fig. 4.3 is compared with the one calculated with the ERM assuming a stroke current with an amplitude of 37 kA and front time of 3 μs. The current has a short wavetail, with time to half-value of 9 μs. All the other conditions are the same as in the previous case. Although, in general, the times to half-value of lightning currents are typically of the order of tens of microseconds [65], much shorter values may occur. In [25], for instance, cases are shown of stroke currents with times to half-value of about 3 μs (Case 83-03), 5 μs (Case 82-10), 10 μs (Case 82-09), and 20 μs (Case 83-09).

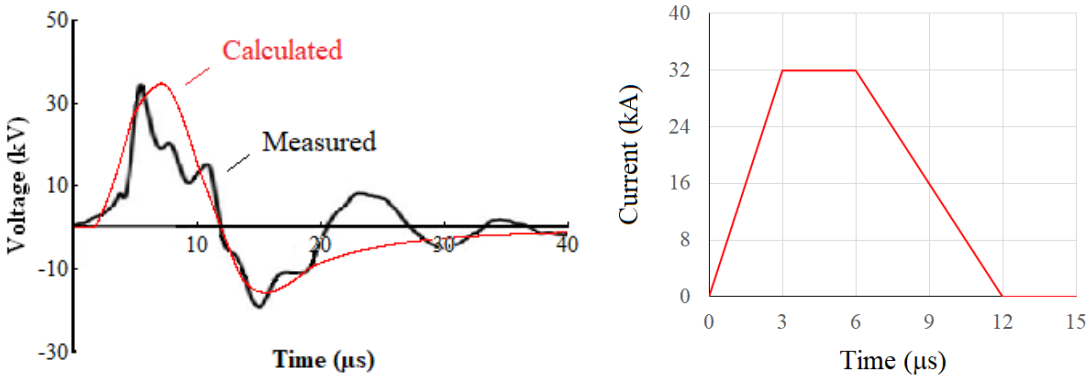

(a) (b)

(a) Measured and calculated induced voltages. (b) Stroke current

Figure 4.3. Comparison between measured and calculated induced voltages (Type II – Waveshape #17).

The third case refers to an induced voltage classified as Type III (#36), which is depicted in Fig. 4.4 together with the voltage calculated with the ERM, assuming a stroke current with an amplitude of 35 kA and front time $tf_{(30/90)}$ of about 4.5 μs. The current waveshape is the same as the one corresponding to the first case, shown in Fig. 4.1b; only the amplitude is different. The line is the same, but its relative position in relation to the stroke location is different, and the voltage is calculated at the point located at a distance of 550 m from the line termination closest to the lightning strike point, as shown in Fig. 4.5. The soil resistivity is equal to 400 Ω.m. The other conditions are the same as in the previous cases.

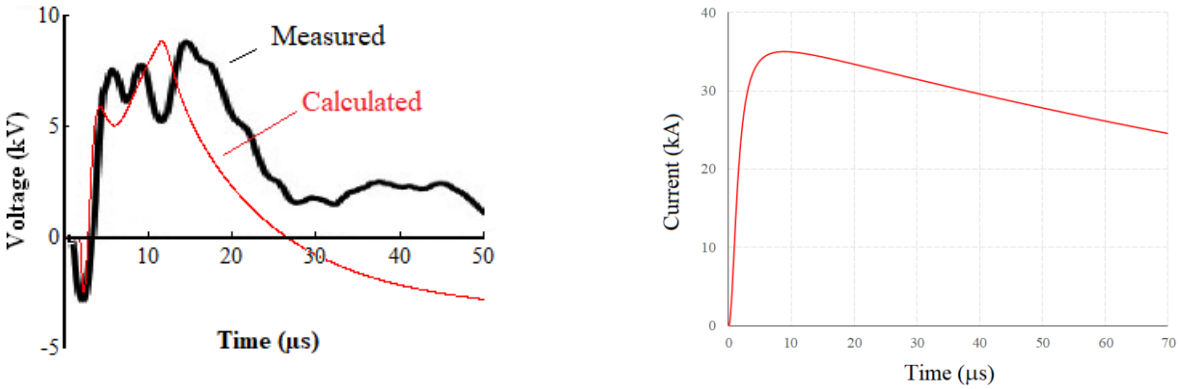

(a) (b)

(a) Measured and calculated induced voltages. (b) Stroke current

Figure 4.4. Comparison between measured and calculated induced voltages (Type III – Waveshape #36).

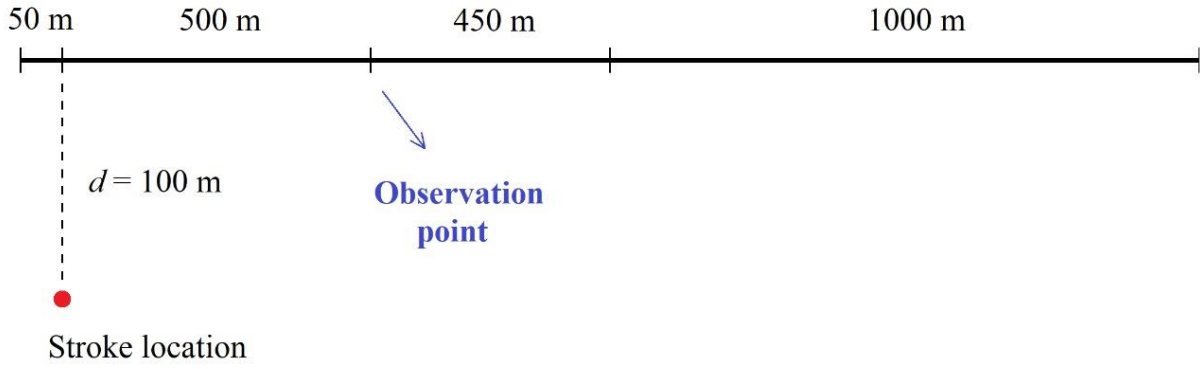

Figure 4.5. Simulation conditions for the calculated voltage depicted in Fig. 4.4.

Although just a qualitative analysis is possible since the strike point location and the characteristics of the lightning currents were not known, the comparisons presented in this chapter clearly showed that the main features of the recorded voltages can be well reproduced by the simulation results considering typical conditions. In particular, the occurrence of bipolar induced voltages can be explained based on different combinations between the values of parameters such as the relative position between the line and the stroke location, the current waveform, the ground resistivity, and the observation point.

5. STATISTICAL ANALYSIS OF THE WAVEFORM PARAMETERS OF THE RECORDED LIGHTNING-INDUCED VOLTAGES

This chapter presents and discusses the statistical distributions of the waveform parameters of the four voltage types presented in Chapter 3. The voltage amplitudes are not important in the analysis since the line has neither arresters nor transformers and, therefore, the system is linear and the voltage waveforms do not depend on the current peak values. In other words, if a certain stroke current I_1 induces on the line the voltage V_1, the current I_2, with the same waveform and under the same conditions (except for the peak value), will induce on the line the voltage V_2, with amplitude equal to V_1 x (I_2 / I_1) but with the same waveform as V_1. Hence, information is given on the recorded voltage peak values, but the chapter aims at discussing the statistical distributions of the waveform parameters.

The analysis is divided into four parts: initially, all the 64 recorded voltage waveforms are considered and information is presented on the distribution of their peak values. Then, the discussion involves only the 43 unipolar waveforms (Type I). After that, the bipolar voltages (Types II, III, and IV) are considered. Initially, the analysis refers to the parameters that these three voltage types have in common; then, the voltage types are discussed separately. Finally, some remarks are presented highlighting the main findings of the chapter.

5.1. Distribution of the recorded voltage peak values

The histogram of the maximum absolute voltage values, considering all the recorded induced voltages, is shown in Fig. 5.1. Actually, although the total number of recorded voltages is 64, the histogram shows data corresponding to 63 induced voltages only, as one of them (Waveshape # 15) has been excluded. The reason is that, although the voltage waveform is coherent and similar to other waveforms, its maximum value (about 7315 kV) is too high and indicates a measurement error. This voltage, which is presented in Fig. 5.2, was considered in the analysis of the waveshape parameters (section 5.2), but its maximum value was disregarded.

The maximum absolute voltage values (*Vmax*) varied in a wide range, from about 2 to 69 kV. In 47 out of the 63 voltages (i.e., in approximately 75% of the cases), *Vmax* was lower than 20 kV.

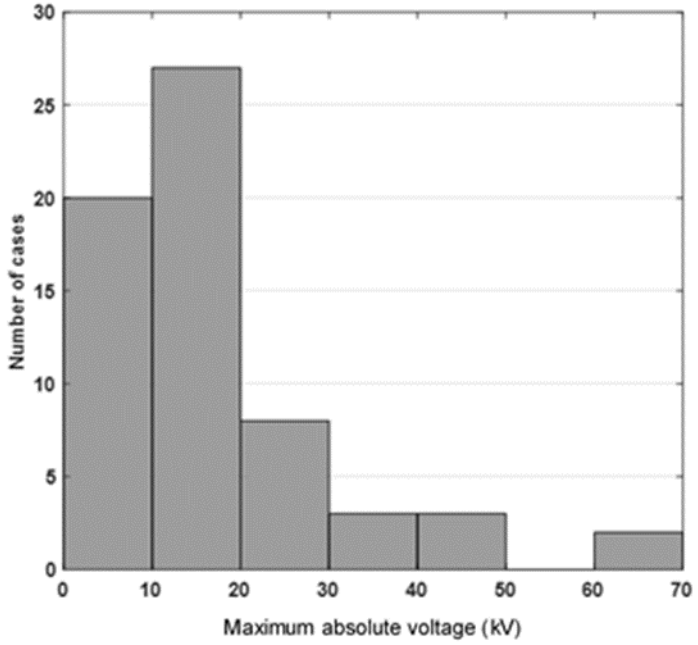

Figure 5.1. Histogram of the maximum absolute voltage values (63 voltages).

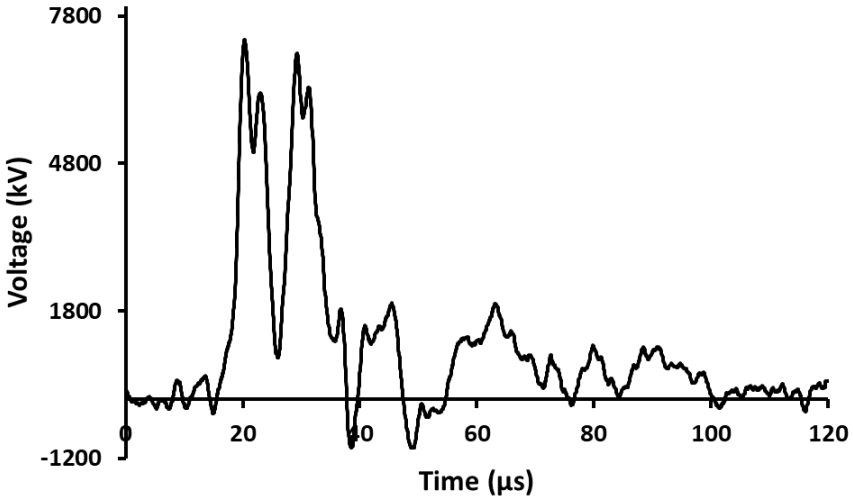

Figure 5.2. Induced voltage excluded from the histogram shown in Fig. 5.1 due to measurement error in the voltage values (Waveshape #15).

The cumulative frequency distribution curve of the maximum absolute voltage values is presented in Fig. 5.3, along with its log-normal approximation (the slanted straight line). Based

on the log-normal approximation, the median value of the voltage maximums is 12.6 kV, and 95% of the voltage amplitudes are lower than 44.5 kV. The average ($\bar{x}$), median (μ_{ln}), standard deviation (σ_{ln}), and the 5% and 95% values of the maximum absolute voltage values calculated based on the log-normal approximation are presented in Table 5.1.

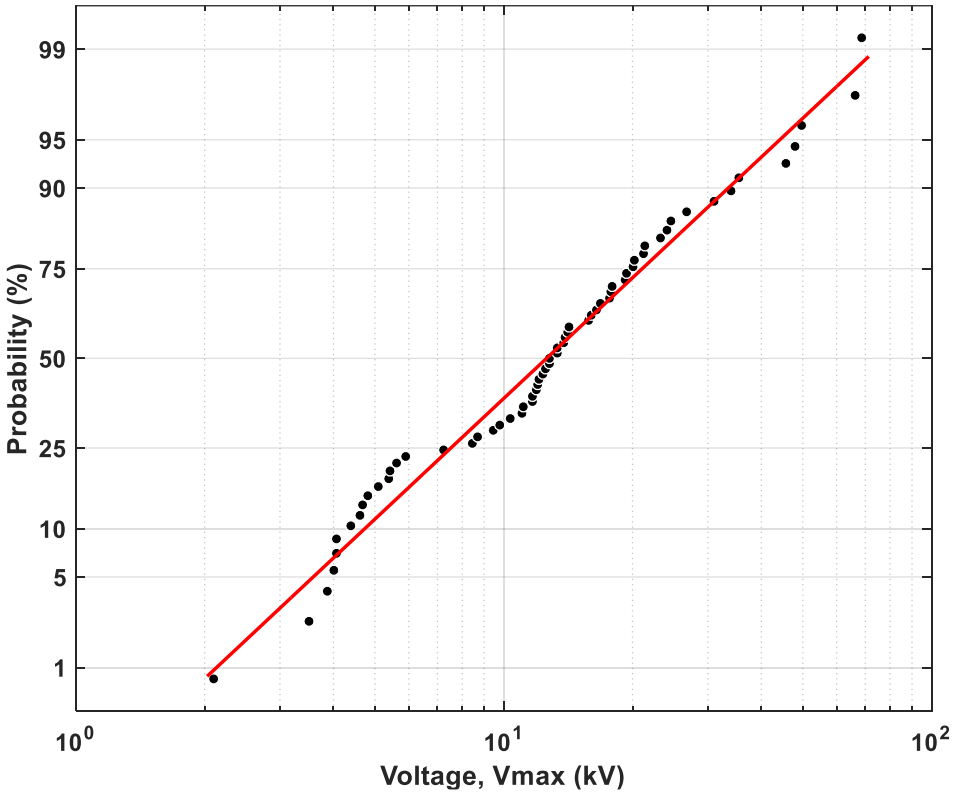

Figure 5.3. Cumulative statistical distribution of the maximum absolute voltage values and its log-normal approximation. It gives the percent of cases less than the value specified in the abscissa (63 waveforms).

Table 5.1. Statistic results of the maximum absolute voltage values (63 lightning-induced voltages).

Parameter	V_{max} **(kV)**
Minimum	2.1
Maximum	68.9
Average ($\bar{x}$)	16.7
Median (μ_{ln})	12.6
Std. deviation (σ_{ln})	14.9
5% value	3.6
95% value	44.5

5.2. Distributions of the parameters of the unipolar (Type I) waveforms

The histogram of the maximum absolute voltage values of the unipolar induced voltages is shown in Fig. 5.4. The maximum values varied widely, from about 3 to 69 kV. In 32 out of the 42 voltage waveforms (i.e., in approximately 76% of the cases), *Vmax* was lower than 20 kV. As explained in section 5.1, one of the recorded induced voltages (Waveform #15, Fig. 5.1) had to be disregarded in the analysis of the distribution of the maximum values due to a measurement error. The voltage was classified as Type I, and despite the error in its maximum value, the waveform was coherent and the time parameters were considered in the analysis. Therefore, the number of maximum values of the Type I voltages is 42, but the number of time parameters is 43.

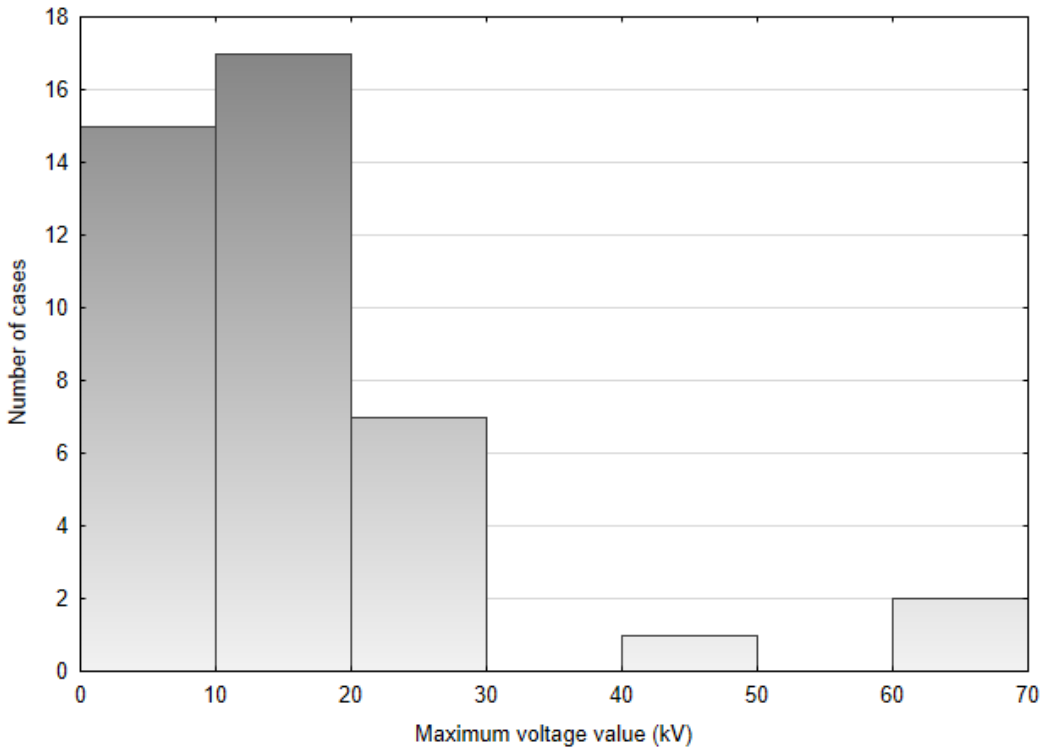

Figure 5.4. Histogram of the maximum absolute voltage values (42 voltages).

The cumulative frequency distributions of the maximum absolute voltage values and the time parameters $tf_{(10/90)}$, $tf_{(30/90)}$, and *th* are shown in Figs. 5.5 to 5.8, respectively, together with the corresponding log-normal approximations (slanted straight lines).

Unless otherwise indicated, all the values of the statistical parameters presented hereafter refer to the log-normal approximation.

Fig. 5.5 indicates that the median value of the V_{max} is 12.1 kV and that 95% of the measured voltages are lower than 40 kV.

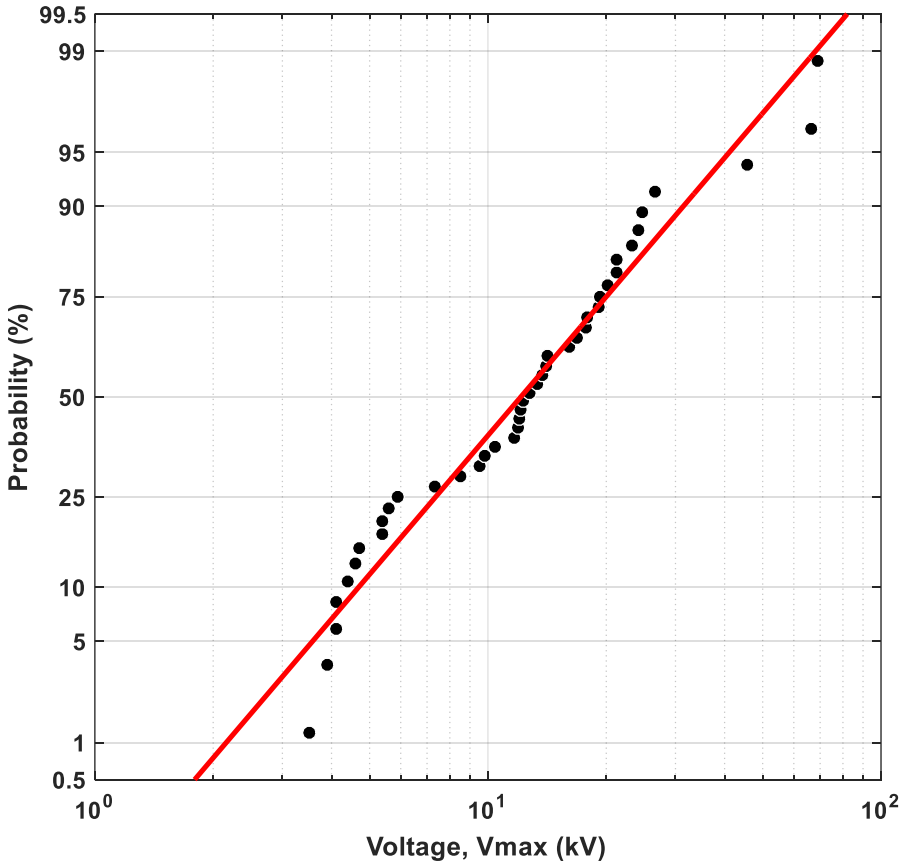

Figure 5.5. Cumulative statistical distribution of the maximum absolute voltage values and its log-normal approximation. It gives the percent of cases less than the value specified in the abscissa (42 voltages).

The median values of the time parameters $tf_{(10/90)}$ and $tf_{(30/90)}$, whose curves are shown in Fig. 5.6 and Fig. 5.7, are 6.1 μs and 5.2 μs, respectively. In about 95% of the cases, $tf_{(10/90)}$ is

shorter than 16 μs, and in 5% of the cases it is shorter than 2.3 μs. The corresponding values for $tf_{(30/90)}$ are, respectively, 17.6 μs (95% of the cases) and 1.5 μs (5% of the cases).

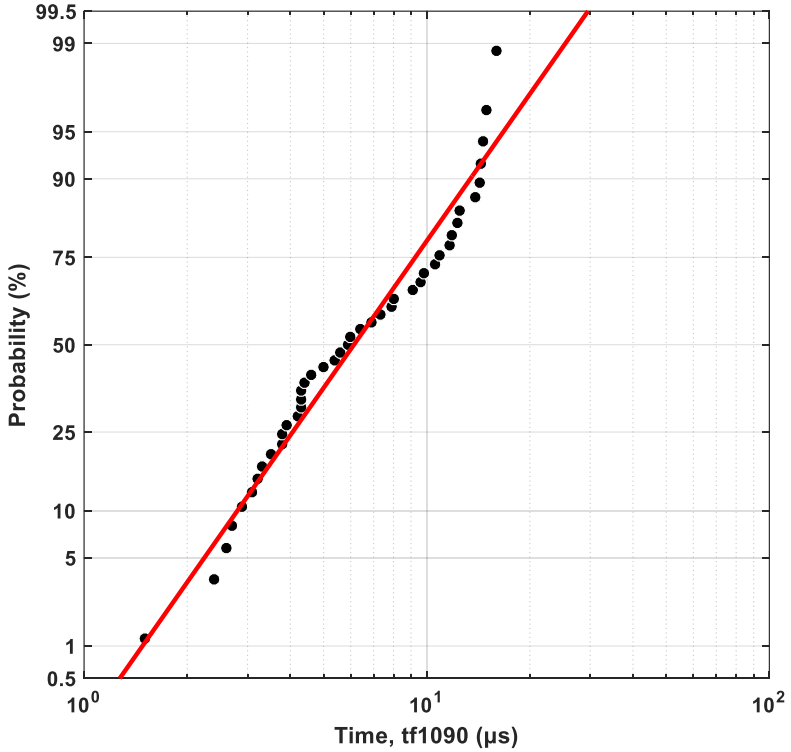

Figure 5.6. Cumulative statistical distribution of the $tf_{(10/90)}$ and its log-normal approximation. It gives the percent of cases less than the value specified in the abscissa (43 waveforms).

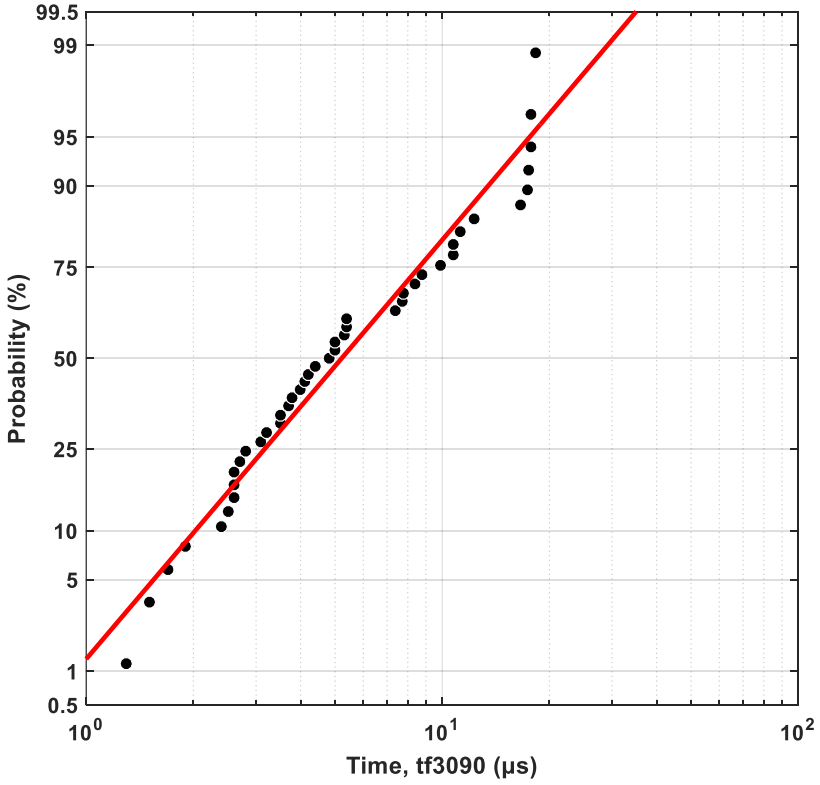

Figure 5.7. Cumulative statistical distribution of the $tf_{(30/90)}$ and its log-normal approximation. It gives the percent of cases less than the value specified in the abscissa (43 waveforms).

The cumulative frequency distribution curve of the time to half-value (*th)* is presented in Fig. 5.8. The median is equal to 15.8 μs. In 95% of the cases, *th* is shorter than 45.4 μs, and in 5% of the cases it is shorter than 5.5 μs.

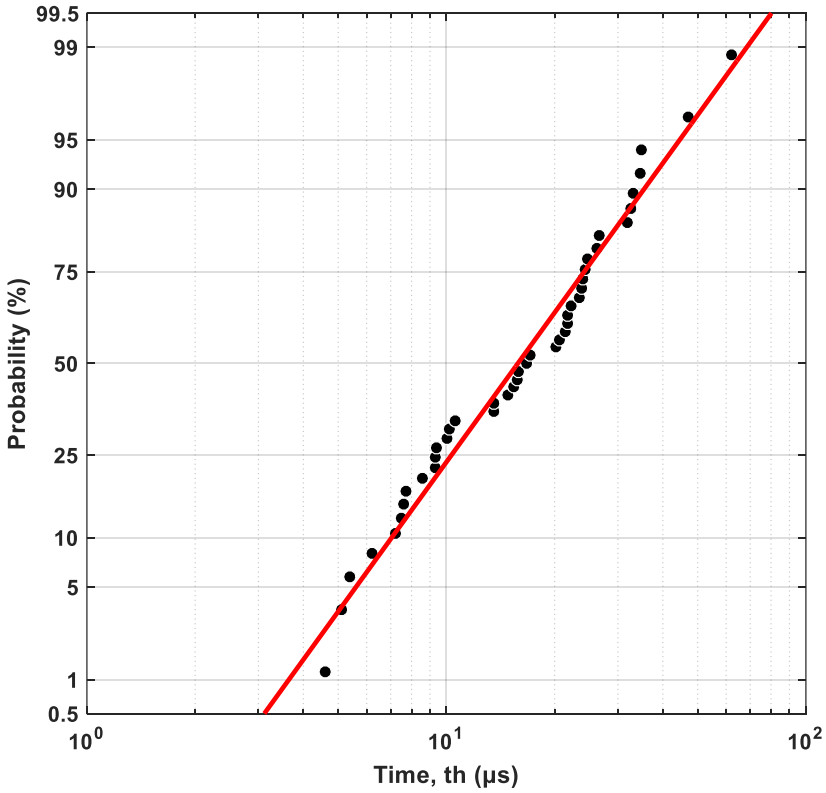

Figure 5.8. Cumulative statistical distribution of the time to half-value *th* and its log-normal approximation. It gives the percent of cases less than the value specified in the abscissa (43 waveforms).

In Fig. 5.9 the cumulative frequency distributions of the $tf_{(10/90)}$, $tf_{(30/90)}$, and *th* are presented in the same graph to facilitate the comparison.

The average ($\bar{x}$), median (μ_{ln}), standard deviation (σ_{ln}), and the 5% and 95% values of the maximum absolute voltage and the time parameters $tf_{(10/90)}$, $tf_{(30/90)}$, and *th*, values calculated from the log-normal approximation curve are presented in Table 5.2.

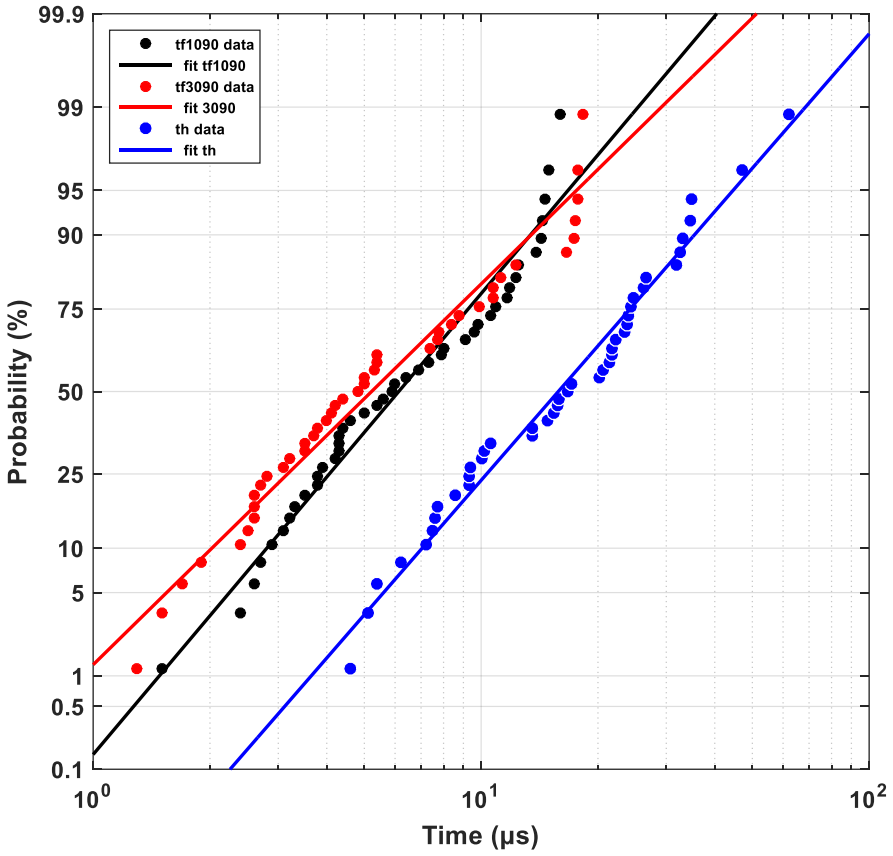

Figure 5.9. Comparison of the cumulative statistical distributions of the $tf_{(10/90)}$, $tf_{(30/90)}$, and *th*, and their log-normal approximations. It gives the percent of cases less than the value specified in the abscissa (43 waveforms).

Table 5.2. Statistic results for the maximum absolute voltage values (42 voltages) and time parameters $tf_{(10/90)}$, $tf_{(30/90)}$, and *th* (43 voltages).

Parameter/Variable	V_{max} **(kV)**	$tf_{(10/90)}$ **(µs)**	$tf_{(30/90)}$ **(µs)**	***th*** **(µs)**
Minimum	3.5	1.5	1.3	4.6
Maximum	68.9	16	18.3	62.2
Average ($\bar{x}$)	16.1	7.3	6.8	19.0
Median (μ_{ln})	12.1	6.1	5.2	15.8
Std. deviation (σ_{ln})	13.7	5.0	5.9	13.5
5% value	3.6	2.3	1.5	5.5
95% value	41.4	16	17.6	45.4

5.3. Distributions of the parameters of the bipolar waveforms (Types II, III, and IV)

This section presents the statistical distributions of the waveforms parameters of the bipolar induced voltages (Types II, III, and IV). Initially, the results are given for the three voltage types together, that is, for the 21 bipolar voltages. Then, the results are presented for each of the voltage types. The parameters of the bipolar voltages are the maximum absolute voltage values, the durations of the first and second semi-cycles, the time interval between the peaks of the first and second semi-cycles ($t_{vp2\text{-}vp1}$), and the ratio of the maximum absolute voltage values of the second and first semi-cycles.

Although the analysis presented in this section comprehends the 21 voltages classified as bipolar, 20 were considered for the analysis of the duration of the second semi-cycle, as one of them (Waveshape #36), shown in Fig. 5.10, did not cross the zero axis within the time window and therefore the duration of the second semi-cycle could not be determined. The curves corresponding to all the other parameters were obtained considering the 21 recorded voltages.

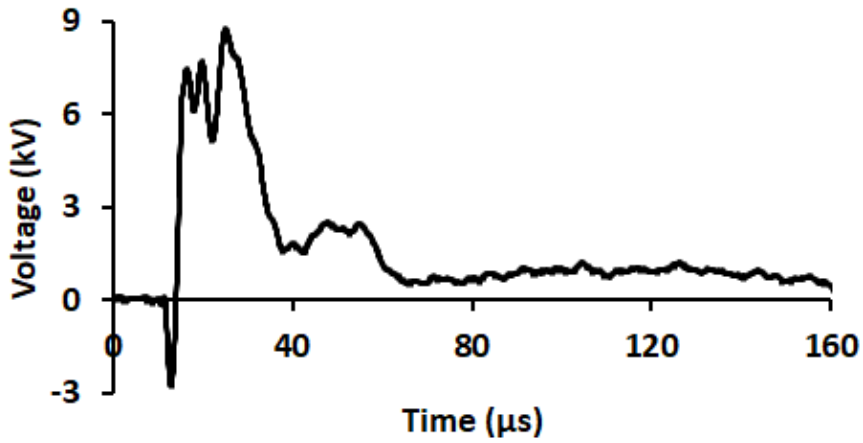

Figure. 5.10. Induced voltage that was not considered in the analysis of the duration of the second semi-cycle because it does not cross the zero axis within the time window, and the duration of the second semi-cycle could not be determined (Waveshape #36).

5.3.1. Types II, III, and IV

The histograms of the maximum absolute voltage values of the first and second semi-cycles are shown in Fig. 5.11 and Fig. 5.12, respectively. The maximum values varied in the ranges of 0.97 to 41.3 kV and 2.14 to 49.6 kV for the first and second semi-cycles, respectively. In the first semi-cycle, the voltage *Vmax* was lower than 20 kV in 16 out of the 21 induced voltages

(i.e., in approximately 76% of the cases), while in the second semi-cycle it was lower than 20 kV in 18 out of the 21 voltages (about 86% of the total).

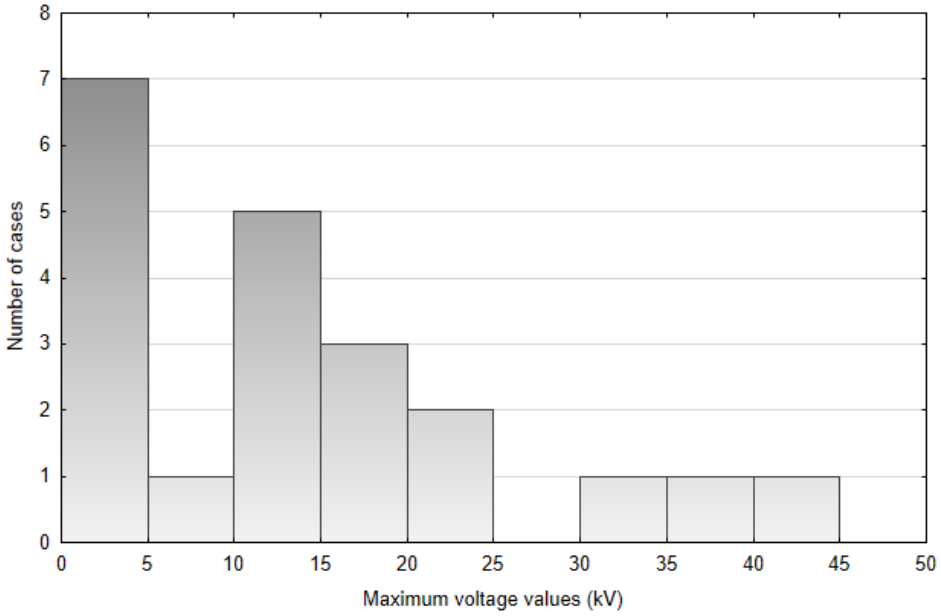

Figure 5.11. Histogram of the maximum absolute voltage values of the first semi-cycle (21 voltages).

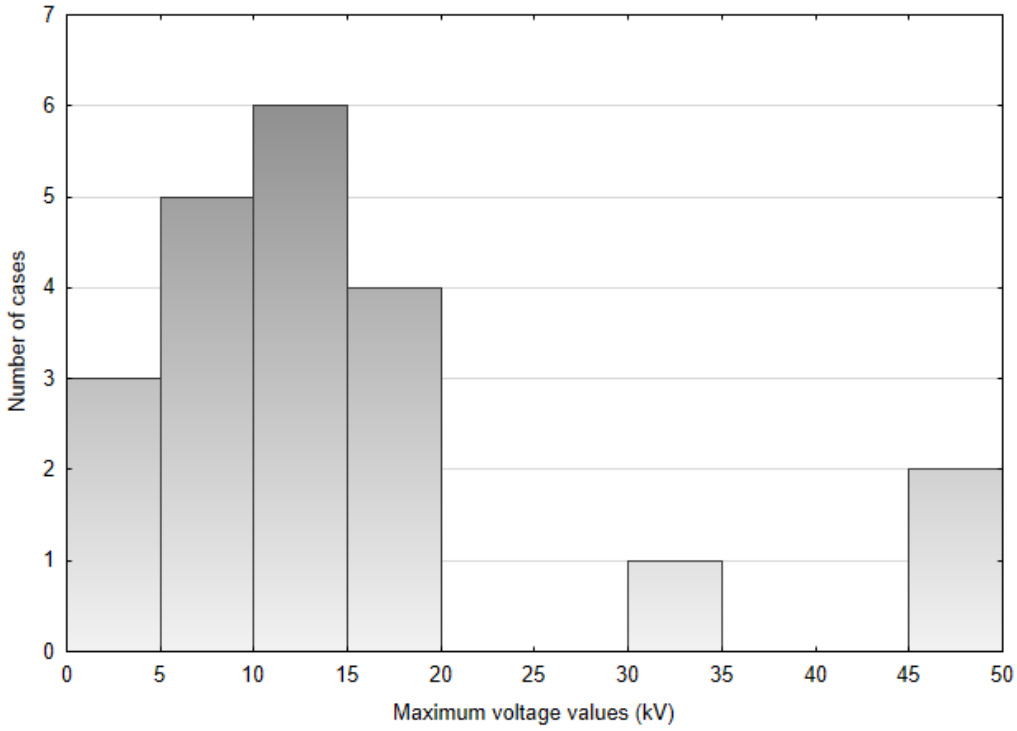

Figure 5.12. Histogram of the maximum absolute voltage values of the second semi-cycle (21 voltages).

The cumulative frequency distributions of the maximum absolute voltage values, durations of the first and second semi-cycles, and time intervals between the peaks of the first and second semi-cycles are presented in Figs. 5.13 to 5.18, respectively, together with the corresponding log-normal approximations (slanted straight lines), giving the percent of cases less than the values indicated in the abscissa.

Unless otherwise indicated, all the values of the statistical parameters presented hereafter refer to the log-normal approximation.

Figs. 5.13 and 5.14 indicate that the median values of the maximum absolute voltage values of the first and second semi-cycles are, respectively, 9.1 kV and 11.2 kV. Regarding the first semi-cycle, in 5% of the cases the maximum voltage is lower than 1.5 kV, and in 95% of the cases it is lower than 55 kV (this is the value obtained from the log-normal approximation; the maximum measured value was about 41 kV). The values relative to the second semi-cycle are 3.1 kV (5% of the cases) and 41.5 kV (95% of the cases).

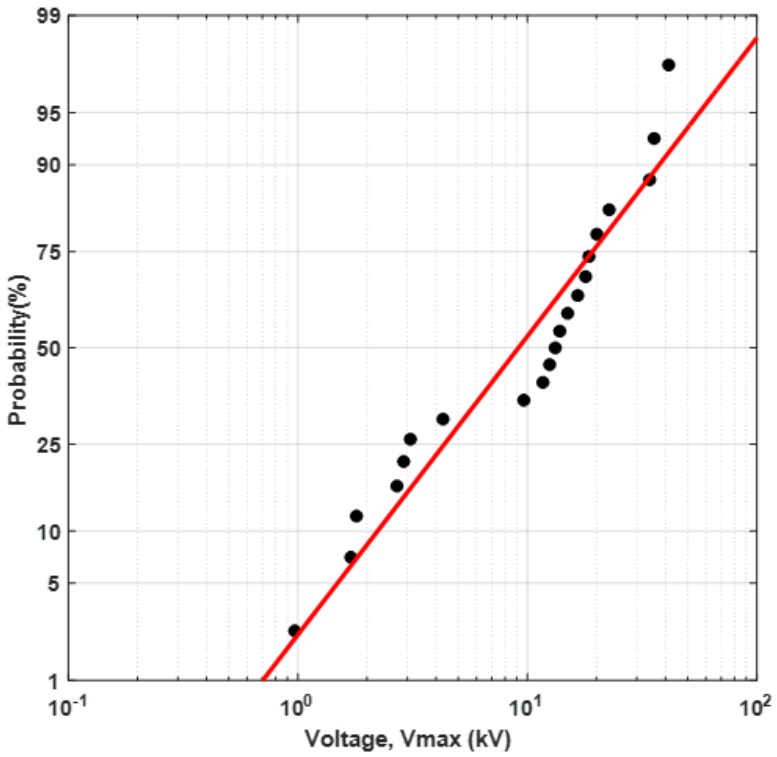

Figure 5.13. Cumulative statistical distribution of the maximum absolute voltage values of the first semi-cycle and its log-normal approximation. It gives the percent of cases less than the value specified in the abscissa (21 induced voltages).

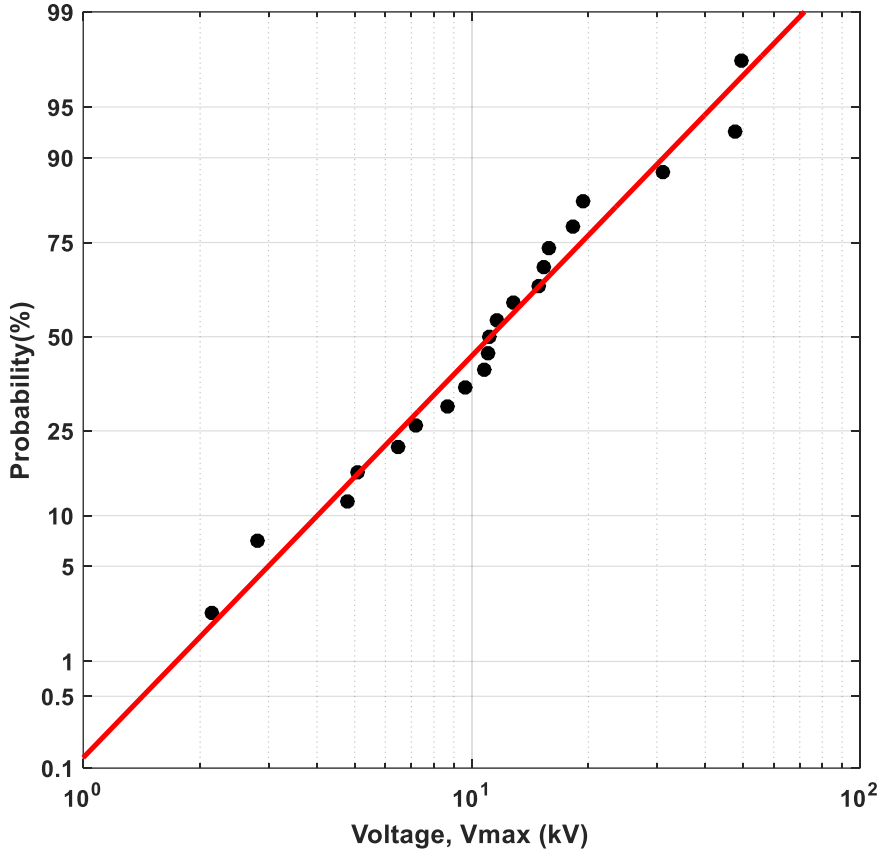

Figure 5.14. Cumulative statistical distribution of the maximum absolute voltage values of the second semi-cycle and its log-normal approximation. It gives the percent of cases less than the value specified in the abscissa (21 induced voltages).

In Fig. 5.15 the cumulative frequency distributions of the maximum absolute voltage values of the first and second semi-cycles are presented in the same graph to facilitate the comparison.

Fig. 5.16 and Fig. 5.17 indicate that the median values of the durations of the first and second semi-cycles are, respectively, 5.5 μs and 13.4 μs. In 5% of the cases, the duration of the first semi-cycle is shorter than 1.6 μs and in 95% of the cases it is lower than 18.9 μs. The values corresponding to the second semi-cycle are 2.5 μs (5% of the cases) and 71 μs (95% of the cases).

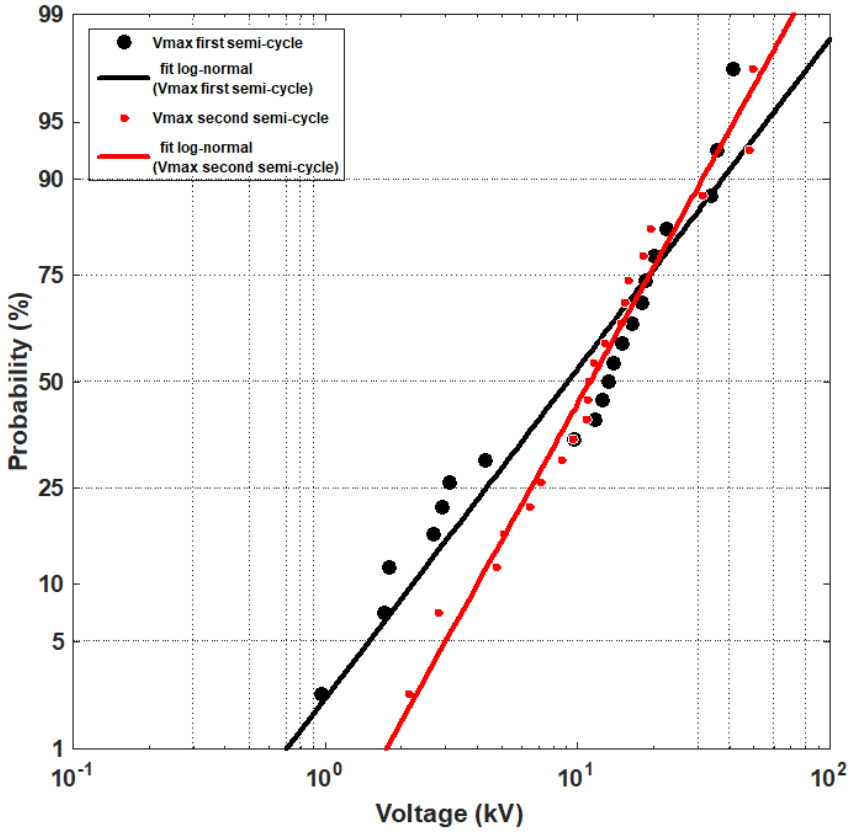

Figure 5.15. Comparison of the cumulative statistical distributions of maximum absolute voltage values of the first and second semi-cycles and their log-normal approximations. It gives the percent of cases less than the value specified in the abscissa (21 induced voltages).

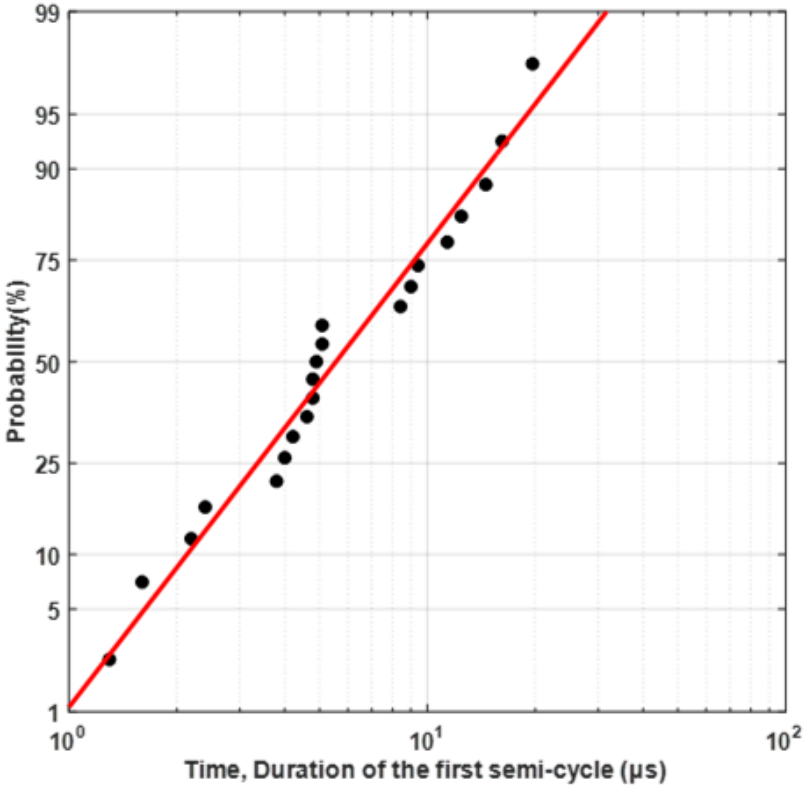

Figure 5.16. Cumulative statistical distribution of the duration of the first semi-cycle and its log-normal approximation. It gives the percent of cases less than the value specified in the abscissa (21 waveforms).

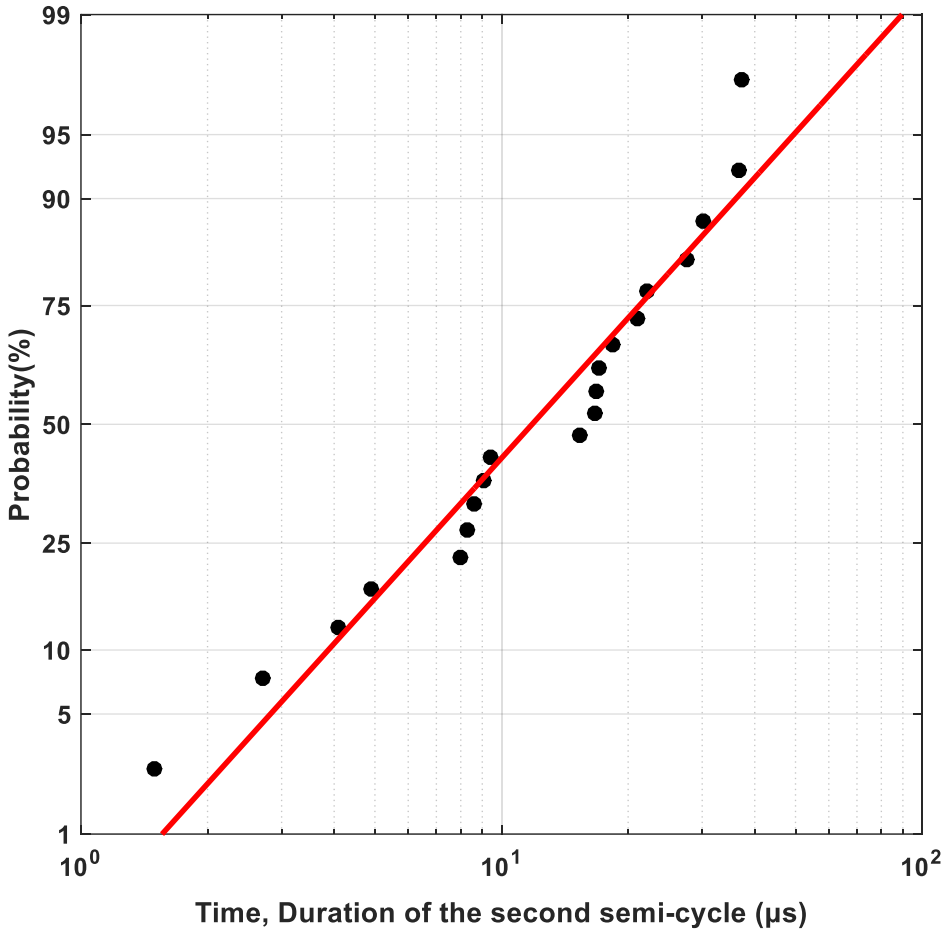

Figure 5.17. Cumulative statistical distribution of the duration of the second semi-cycle and its log-normal approximation. It gives the percent of cases less than the value specified in the abscissa (20 waveforms).

The cumulative frequency distribution of the time intervals between the peaks of the first and second semi-cycles ($t_{vp2\text{-}vp1}$) is given in Fig. 5.18, which indicates that the median is 6 µs and that in 5% and 95% of the cases the values are shorter than 2 µs and 19 µs, respectively.

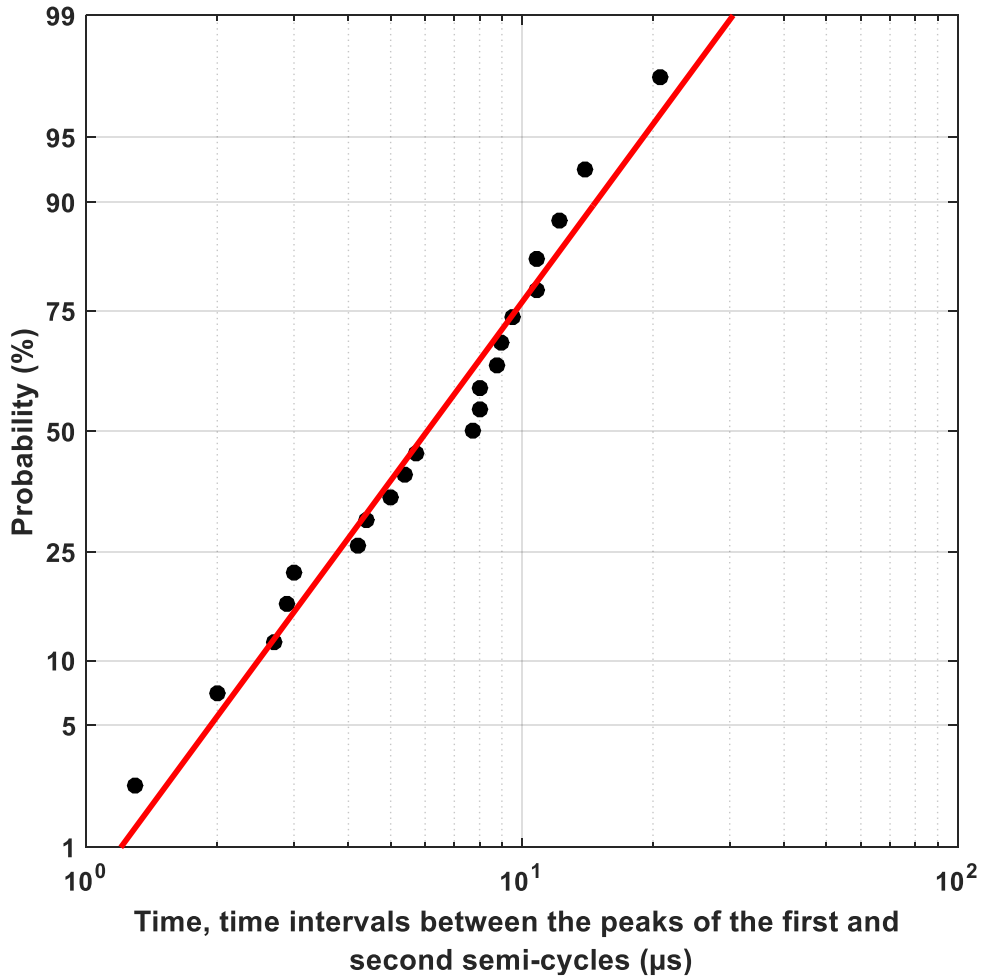

Figure 5.18. Cumulative statistical distribution of the time intervals between the peaks of the first and second semi-cycles $(t_{vp2\text{-}vp1})$, and its log-normal approximation. It gives the percent of cases less than the value specified in the abscissa (21 waveforms).

The minimum, maximum, average ($\bar{x}$), median (μ_{ln}), standard deviation (σ_{ln}), and the 5% and 95% values of the parameters that are common to the three bipolar voltage types are presented in Table 5.3. The medians and the standard deviations were calculated from the log-normal approximations.

Table 5.3. Statistic results of the maximum absolute voltage, durations of the first and second semi-cycles, and time intervals between the voltage peaks in the first and second semi-cycles (21 induced voltages).

Parameter/Variable	**First semi-cycle**		**Second semi-cycle**		
	Vmax (kV)	Duration (μs)	*Vmax* (kV)	Duration* (μs)	$t_{vp2\text{-}vp1}$ (μs)
Minimum	0.97	1.3	2.14	1.5	1.3
Maximum	41.3	19.6	49.6	37.3	20.8
Average ($\bar{x}$)	14.3	7.3	15.0	15.8	7.4
Median (μ_{ln})	9.1	5.5	11.2	13.4	6.0
Std. deviation (σ_{ln})	25.9	6.3	14.6	30.7	6.1
5% value	1.5	1.6	3.1	2.5	2.0
95% value	55	18.9	41.5	71.0	19.0

* Total of 20 induced voltages because the recorded voltage shown in Fig.5.10 did not cross the zero axis and the duration of the second semi-cycle could not be determined.

5.3.2. Type II

The histograms of the maximum absolute voltage values of the first and second semi-cycles are shown in Fig. 5.19 and Fig. 5.20, respectively. Regarding the first semi-cycle, *Vmax* was lower than 20 kV in 8 out of the 13 cases (61.5%); in the second semi-cycle, it was lower than 20 kV in 11 out of the 13 cases (84.6%). The maximum values varied in the ranges of 9.7 kV to 41.3 kV and 6.4 kV to 47.8 kV for the first and second semi-cycles, respectively.

The cumulative frequency distributions of the maximum absolute voltage values, durations of the first and second semi-cycles, of the ratios of the maximum absolute voltage values of the second and first semi-cycles, and time intervals between the peaks of the first and second semi-cycles are presented in Figs. 5.21 to 5.28, together with the corresponding log-normal approximations (slanted straight lines). The figures give the percent of cases less than the values indicated in the abscissa.

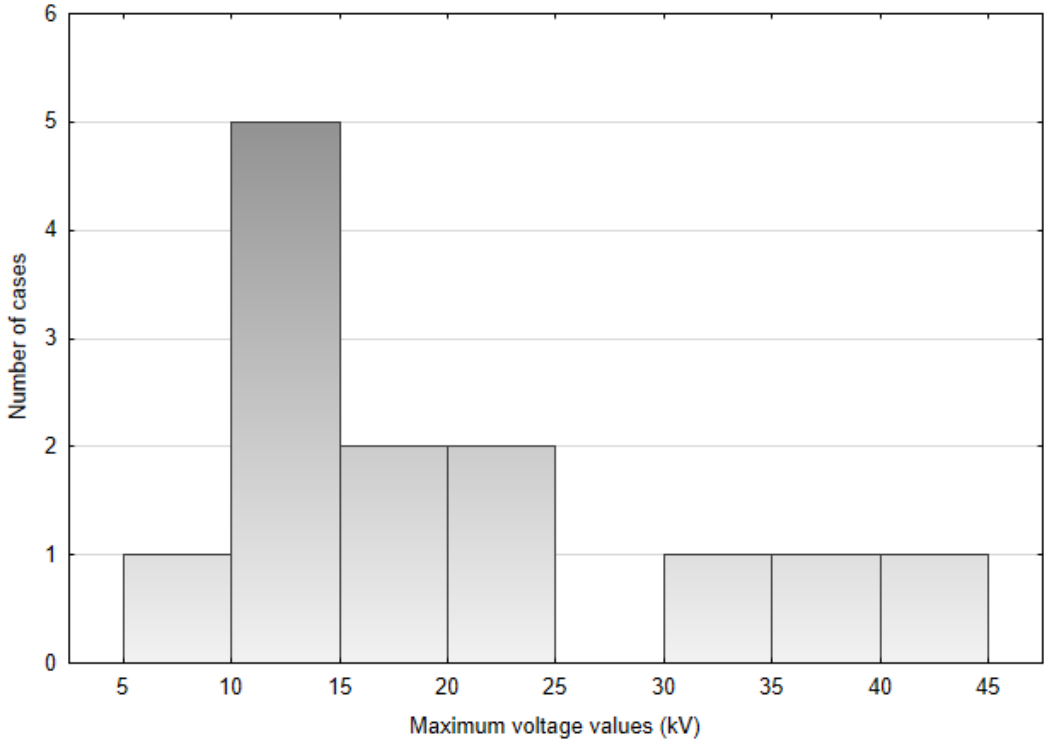

Figure 5.19. Histogram of the maximum absolute voltage values of the first semi-cycle (13 voltages).

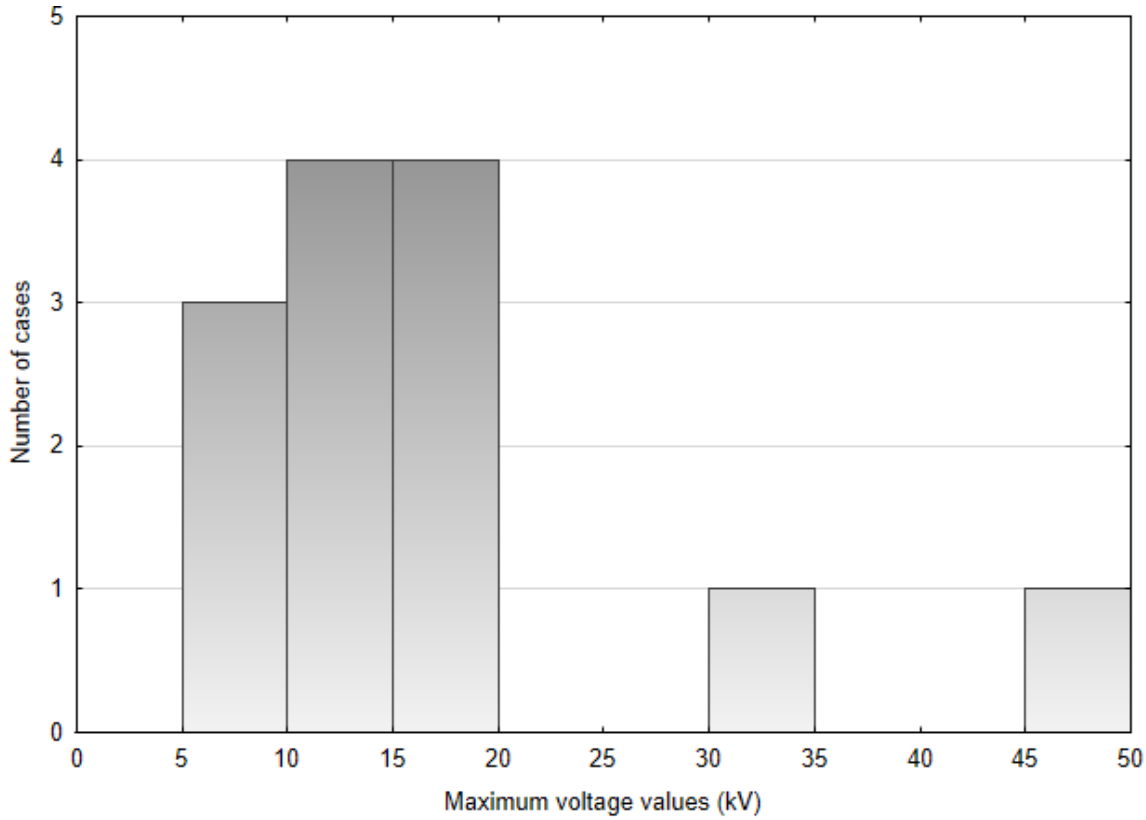

Figure 5.20. Histogram of the maximum absolute voltage values of the second semi-cycle (13 voltages).

Unless otherwise indicated, all the values of the statistical parameters presented hereafter refer to the log-normal approximation.

Figs. 5.21 and 5.22 indicate that the median values of the maximum absolute voltage values of the first and second semi-cycles are, respectively, 18.3 kV and 14.6 kV. Regarding the first semi-cycle, in 5% of the cases the maximum voltage is lower than 8.6 kV, and in 95% of the cases it is lower than 39 kV. The values relative to the second semi-cycle are 6 kV (5% of the cases) and 36 kV (95% of the cases).

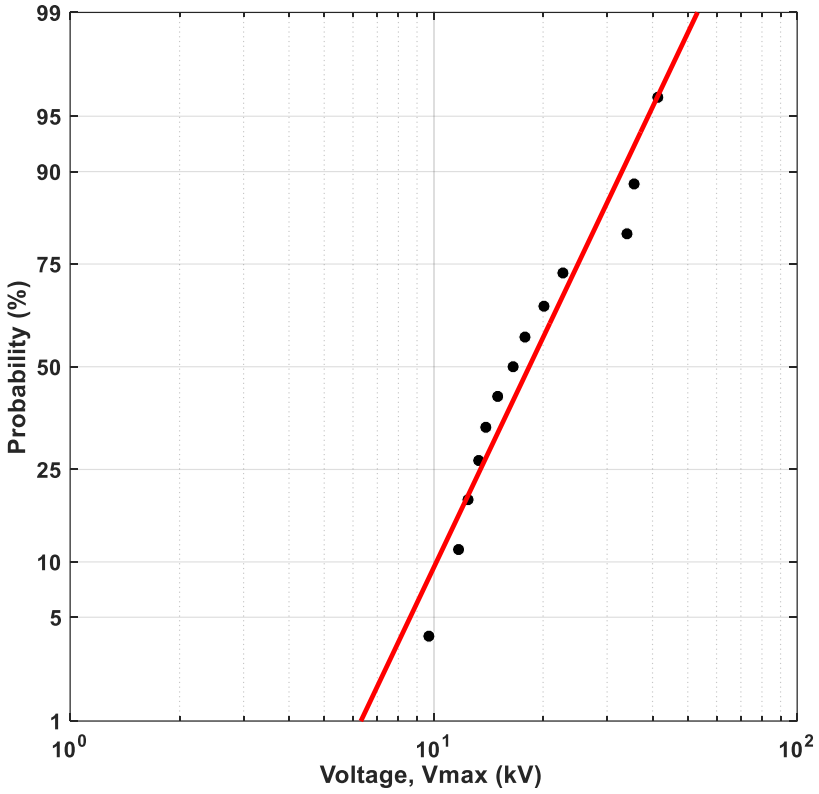

Figure 5.21. Cumulative statistical distribution of the maximum absolute voltage values of the first semi-cycle and its log-normal approximation. It gives the percent of cases less than the value specified in the abscissa (13 waveforms).

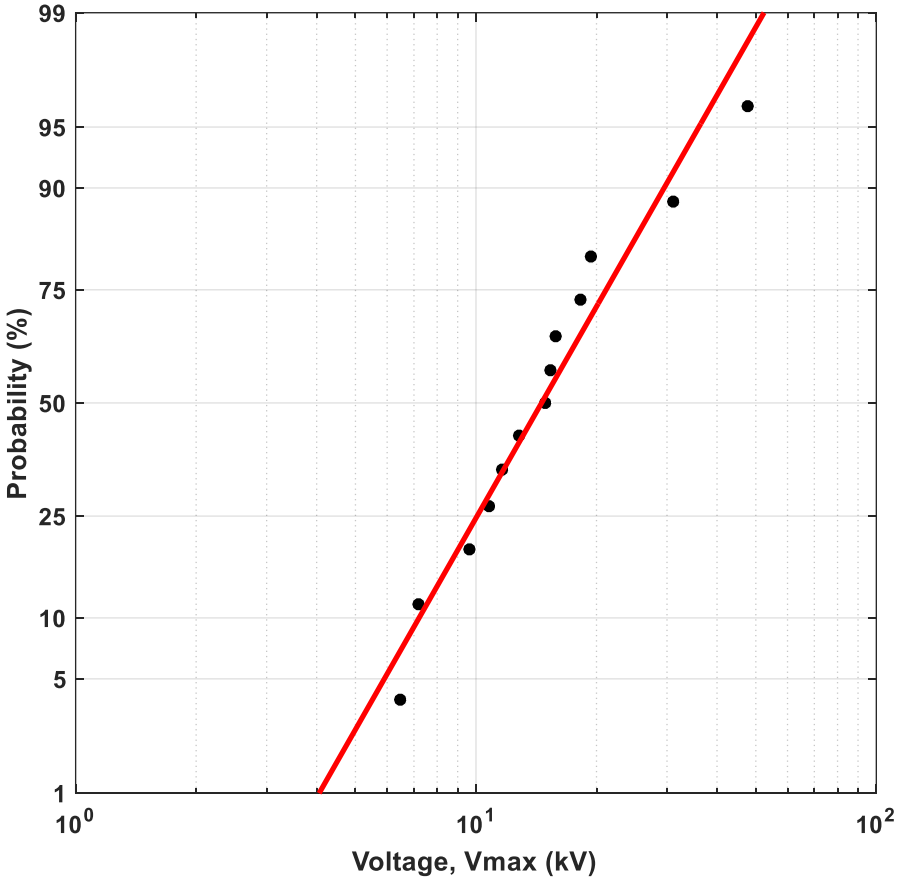

Figure 5.22. Cumulative statistical distribution of the maximum absolute voltage values of the second semi-cycle and its log-normal approximation. It gives the percent of cases less than the value specified in the abscissa (13 waveforms).

In Fig. 5.23 the cumulative frequency distributions of the maximum absolute voltage values of the first and second semi-cycles are presented in the same graph to facilitate the comparison.

Fig. 5.24 gives the cumulative frequency distribution of the ratios of the maximum absolute voltage values of the second and first semi-cycles (V_2p/V_1p). The median value is 0.8; in 5% of the cases the ratio is lower than 0.4, and in 95% of the cases it is lower than 1.5.

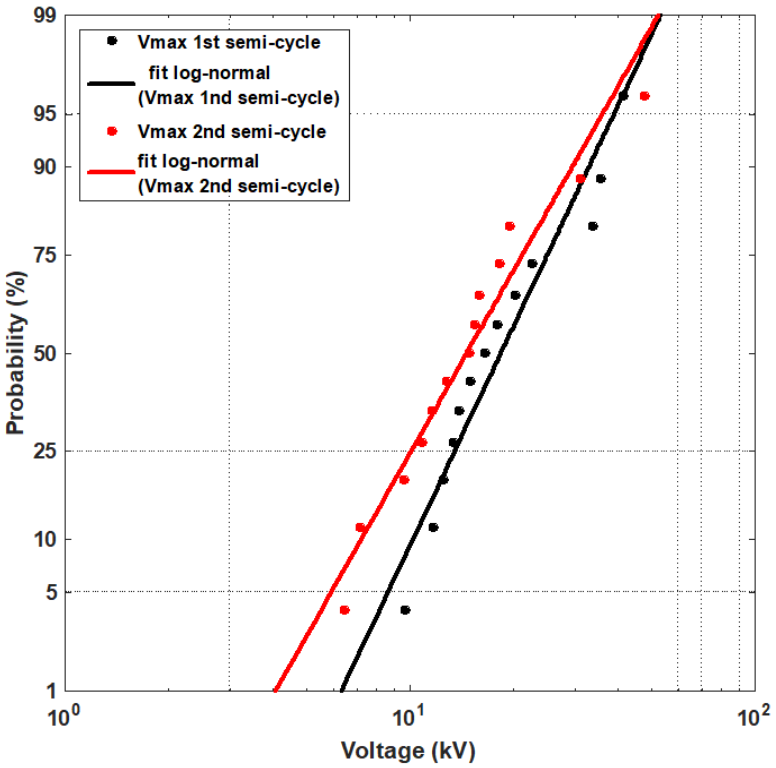

Figure 5.23. Comparison of the cumulative statistical distributions of the maximum absolute voltage values of the first and second semi-cycles and their log-normal approximations. It gives the percent of cases less than the value specified in the abscissa (13 waveforms).

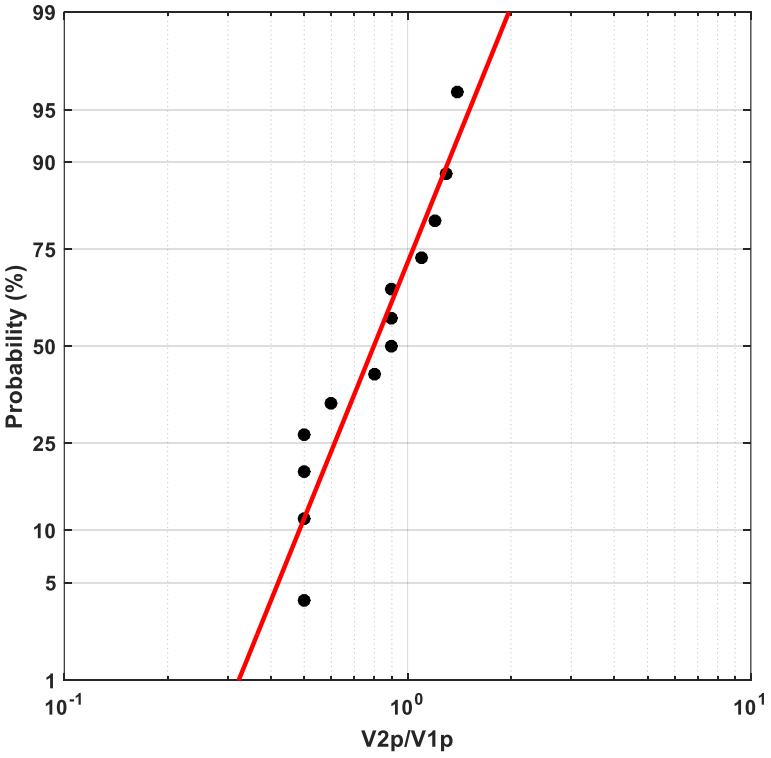

Figure 5.24. Cumulative statistical distribution of the ratios of the maximum absolute voltage values of the second and first semi-cycles (V_2p / V_1p) and its log-normal approximation. It gives the percent of cases less than the value specified in the abscissa (13 waveforms).

Fig. 5.25 and Fig. 5.26 indicate that the median values of the durations of the first and second semi-cycles are, respectively, 8.2 μs and 11.2 μs. In 5% of the cases the duration of the first semi-cycle is shorter than 3.4 μs, and in 95% of the cases it is shorter than 19.9 μs. The values corresponding to the second semi-cycle are 2.9 μs (5% of the cases) and 43.7 μs (95% of the cases).

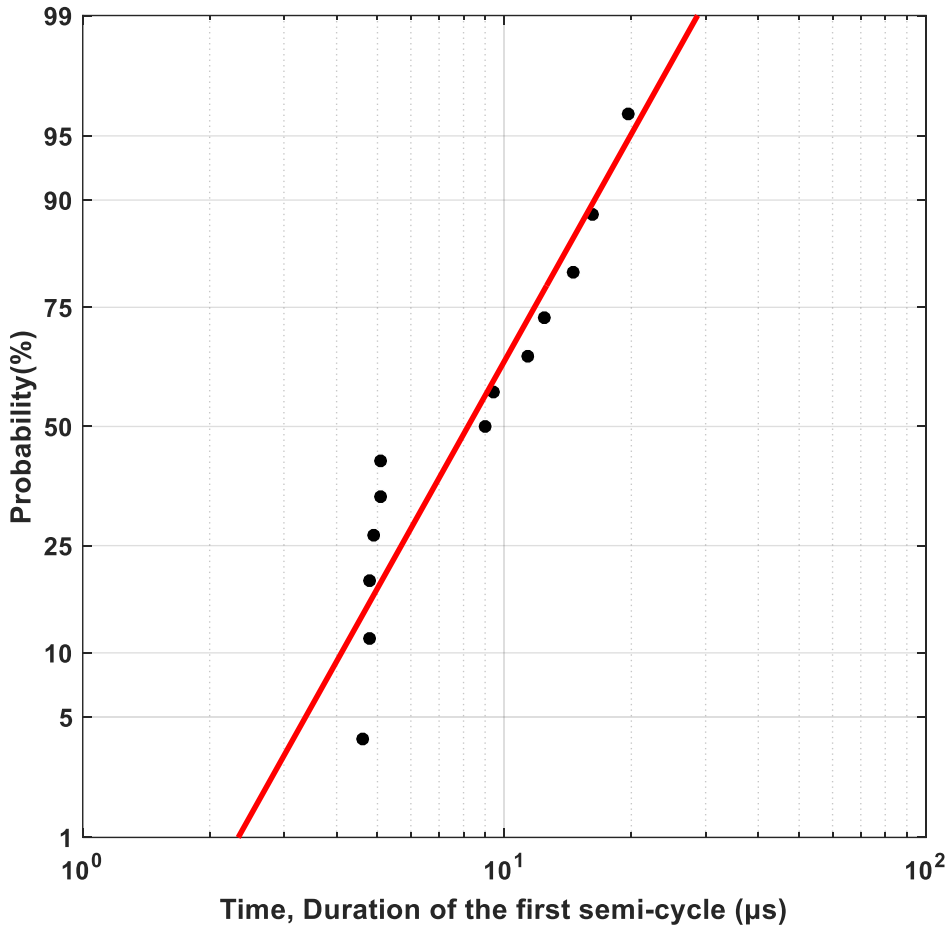

Figure 5.25. Cumulative statistical distribution of the durations of the first semi-cycle and its log-normal approximation. It gives the percent of cases less than the value specified in the abscissa (13 waveforms).

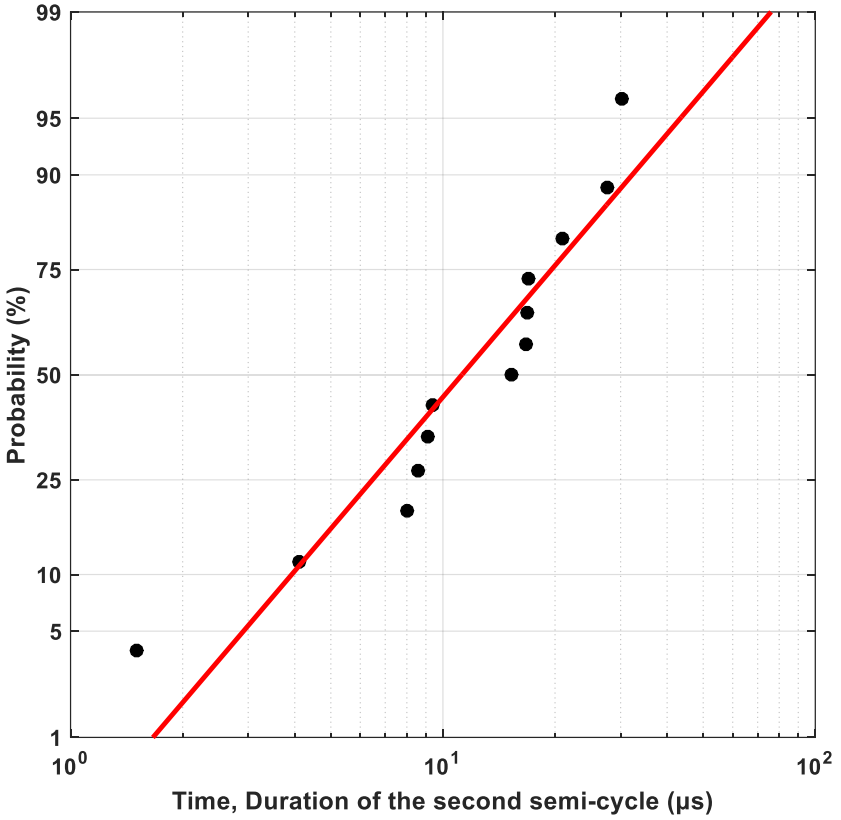

Figure 5.26. Cumulative statistical distribution of the durations of the second semi-cycle and its log-normal approximation. It gives the percent of cases less than the value specified in the abscissa (13 waveforms).

In Fig. 5.27 the cumulative frequency distributions of the durations of the first and second semi-cycles are presented in the same graph, together with their log-normal approximations, to facilitate the comparison.

The cumulative frequency distribution of the time intervals between the peaks of the first and second semi-cycles ($t_{vp2\text{-}vp1}$) is given in Fig. 5.28, which indicates that the median is 6.8 μs and that in 5% and 95% of the cases, the values are shorter than 2.6 μs and 17.5 μs, respectively.

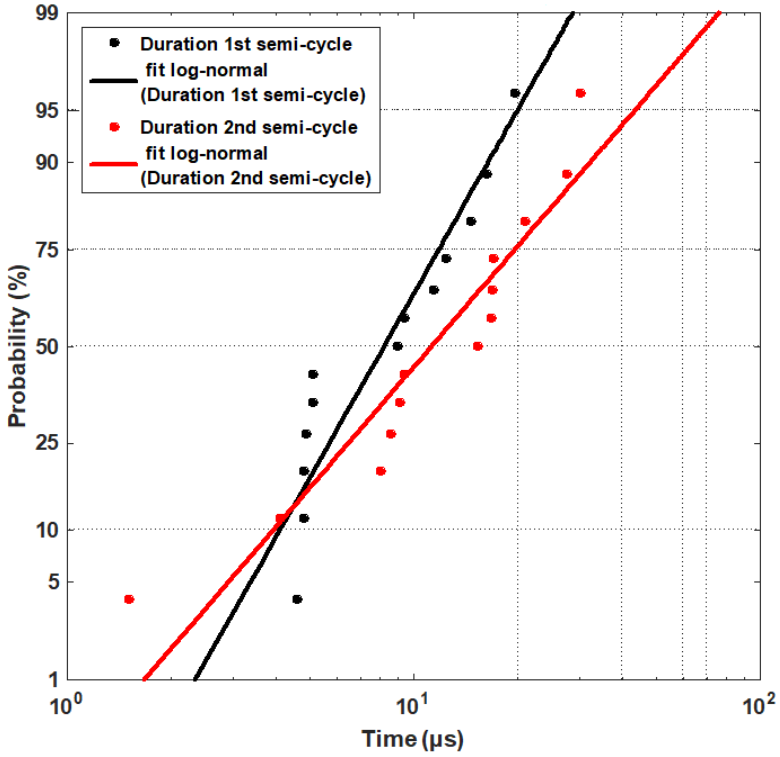

Figure 5.27. Comparison of the cumulative statistical distributions of the durations of the first and second semi-cycles and their log-normal approximations. It gives the percent of cases less than the value specified in the abscissa (13 waveforms).

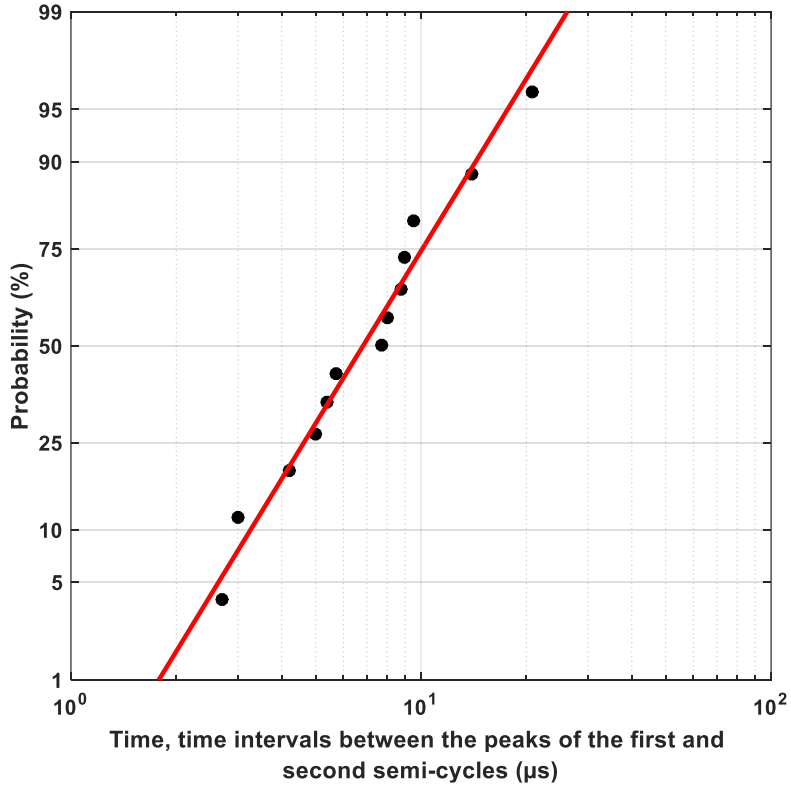

Figure 5.28. Cumulative statistical distribution of the time intervals between the peaks of the first and second semi-cycles ($t_{vp2\text{-}vp1}$) and its log-normal approximation. It gives the percent of cases less than the value specified in the abscissa (13 waveforms).

The minimum, maximum, average ($\bar{x}$), median (μ_{ln}), standard deviation (σ_{ln}), and the 5% and 95% values of the parameters of the measured induced voltages classified as Type II are presented in Table 5.4. The medians and the standard deviations were calculated from the log-normal approximations.

Table 5.4. Statistic results of the maximum absolute voltage values, durations of the first and second semi-cycles, time intervals between the peaks of the first and second semi-cycles, and ratio of the maximum absolute voltage values of the second and first semi-cycles (13 lightning-induced voltages).

Parameter/Variable	**First semi-cycle**		**Second semi-cycle**			
	Vmax (kV)	Duration (μs)	Vmax (kV)	Duration (μs)	$t_{vp2\text{-}vp1}$ (μs)	V_2p/V_{1p}
Minimum	9.7	4.6	6.4	1.5	2.7	0.5
Maximum	41.3	19.6	47.8	30.2	20.8	1.4
Average ($\bar{x}$)	20.3	9.4	17.0	14.2	7.9	0.8
Median (μ_{ln})	18.3	8.2	14.6	11.2	6.8	0.8
Std. deviation (σ_{ln})	9.8	5.5	10.1	15.5	5.1	0.3
5% value	8.6	3.4	6.0	2.9	2.6	0.4
95% value	39.0	19.9	36.0	43.7	17.5	1.5

5.3.3. Type III

The histograms of the maximum absolute voltage values of the first and second semi-cycles are shown in Fig. 5.29 and Fig. 5.30, respectively. Regarding the first semi-cycle, in 5 out of the 6 cases (83%) *Vmax* was lower than 6 kV; in the second semi-cycle, in the same percentage of the cases (83%) it was lower than 15 kV. The maximum values varied in the ranges of about 1 kV to 19 kV and 2 kV to 50 kV for the first and second semi-cycles, respectively.

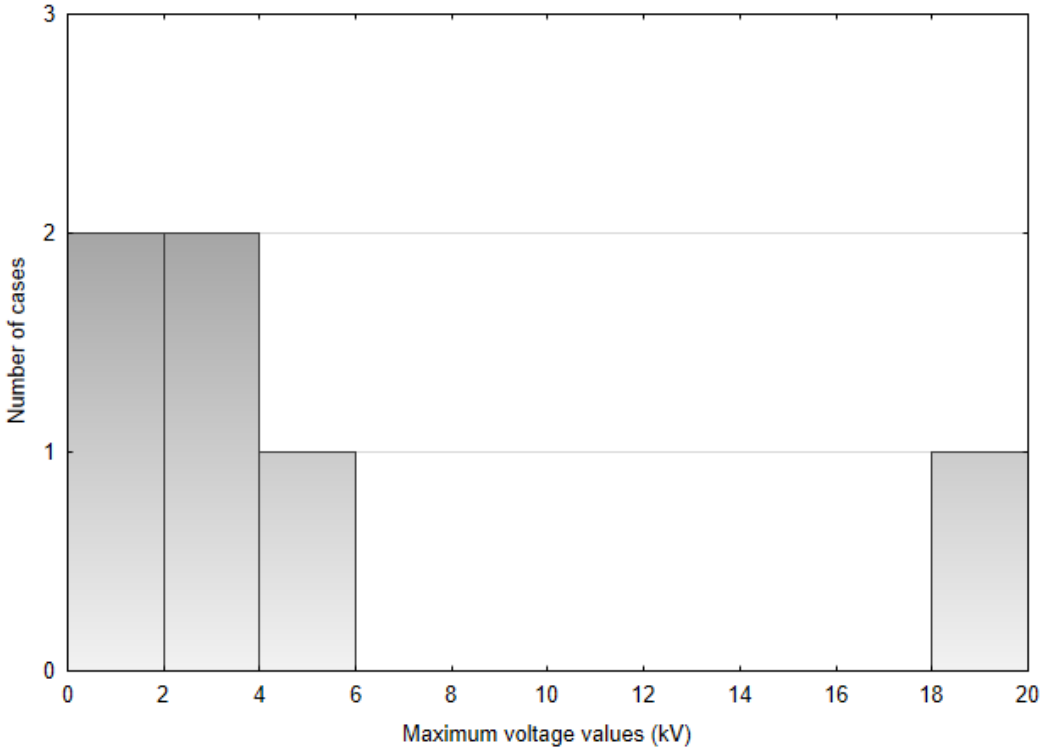

Figure 5.29. Histogram of the maximum absolute voltage values of the first semi-cycle (6 voltages).

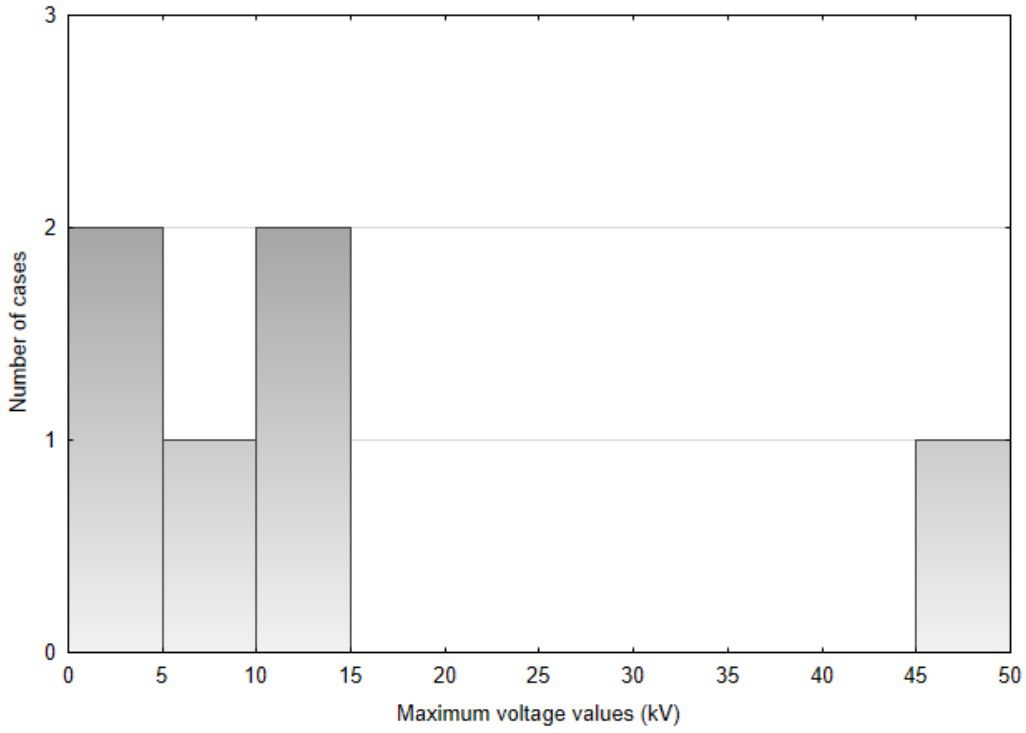

Figure 5.30 Histogram of the maximum absolute voltage value of the second semi-cycle (6 voltages).

The cumulative frequency distributions of the maximum absolute voltage values, durations of the first and second semi-cycles, ratios of the maximum absolute voltage values of the second and first semi-cycles, and time intervals between the peaks of the first and second semi-cycles are presented in Figs. 5.31 to 5.37, together with the corresponding log-normal approximations (slanted straight lines). The figures give the percent of cases less than the values indicated in the abscissa.

Unless otherwise indicated, all the values of the statistical parameters presented hereafter refer to the log-normal approximation.

Figs. 5.31 and 5.32 indicate that the median values of the maximum absolute voltage values of the first and second semi-cycles are, respectively, 2.8 kV and 9.8 kV. Regarding the first semi-cycle, in 5% of the cases the maximum voltage is lower than 0.6 kV, and in 95% of the cases it is lower than 16.5 kV. The values relative to the second semi-cycle are 1.6 kV (5% of the cases) and 50 kV (95% of the cases).

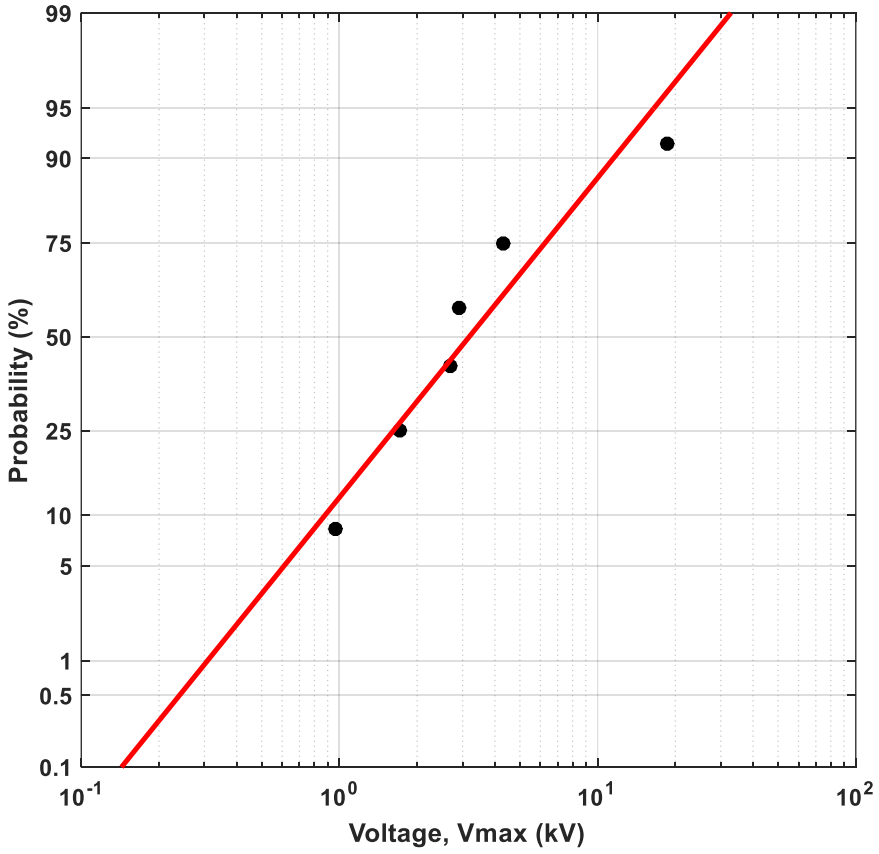

Figure 5.31. Cumulative statistical distribution of the maximum absolute voltage value of the first semi-cycle and its log-normal approximation. It gives the percent of cases less than the value specified in the abscissa (6 waveforms).

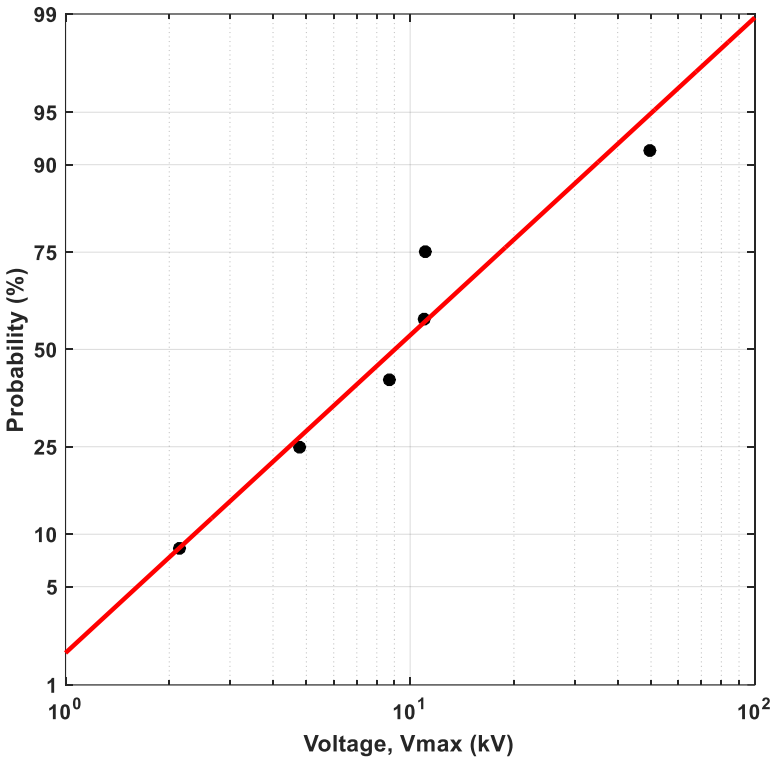

Figure 5.32. Cumulative statistical distribution of the maximum absolute voltage value of the second semi-cycle and its log-normal approximation. It gives the percent of cases less than the value specified in the abscissa (6 waveforms).

In Fig. 5.33 the cumulative frequency distributions of the maximum absolute voltage values of the first and second semi-cycles are presented in the same graph to facilitate the comparison.

Fig. 5.34 gives the cumulative frequency distribution of the ratios of the maximum absolute voltage values of the second and first semi-cycles (V_1p/V_2p). The median value is 0.3; in 5% of the cases the ratio is lower than 0.26, and in 95% of the cases it is lower than 0.48.

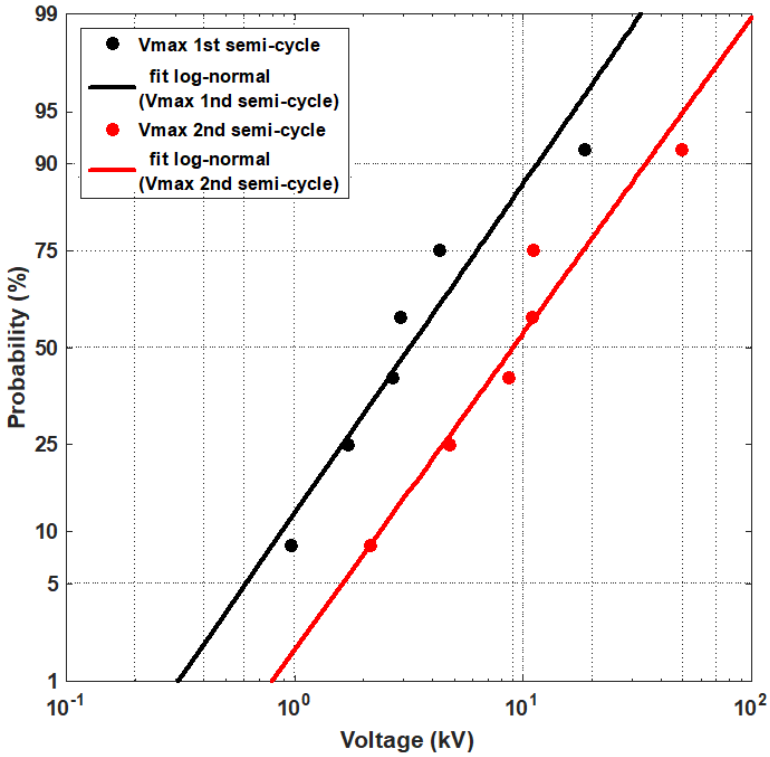

Figure 5.33. Comparison of the cumulative statistical distribution of the maximum absolute voltage value of the first and second semi-cycle and its log-normal approximation. It gives the percent of cases less than the value specified in the abscissa (6 waveforms).

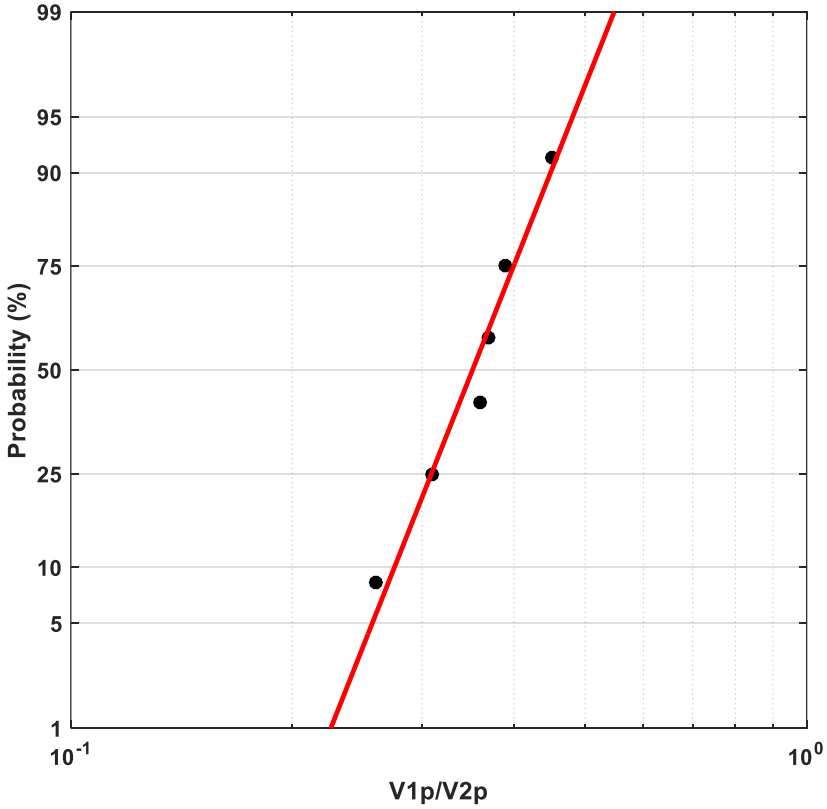

Figure 5.34. Cumulative statistical distribution of the ratios of the maximum absolute voltage value of the first and second semi-cycles (V_1p/V_2p) and its log-normal approximation. It gives the percent of cases less than the value specified in the abscissa (6 waveforms).

Fig. 5.35 and Fig. 5.36 indicate that the median values of the durations of the first and second semi-cycles are, respectively, 2.3 μs and 22 μs. In 5% of the cases, the duration of the first semi-cycle is shorter than 0.9 μs and in 95% of the cases it is lower than 8.1 μs. The values corresponding to the second semi-cycle are 7.9 μs (5% of the cases) and 59 μs (95% of the cases).

In Fig. 5.37 the cumulative frequency distributions of the durations of the first and second semi-cycles are presented in the same graph, together with their log-normal approximations, to facilitate the comparison.

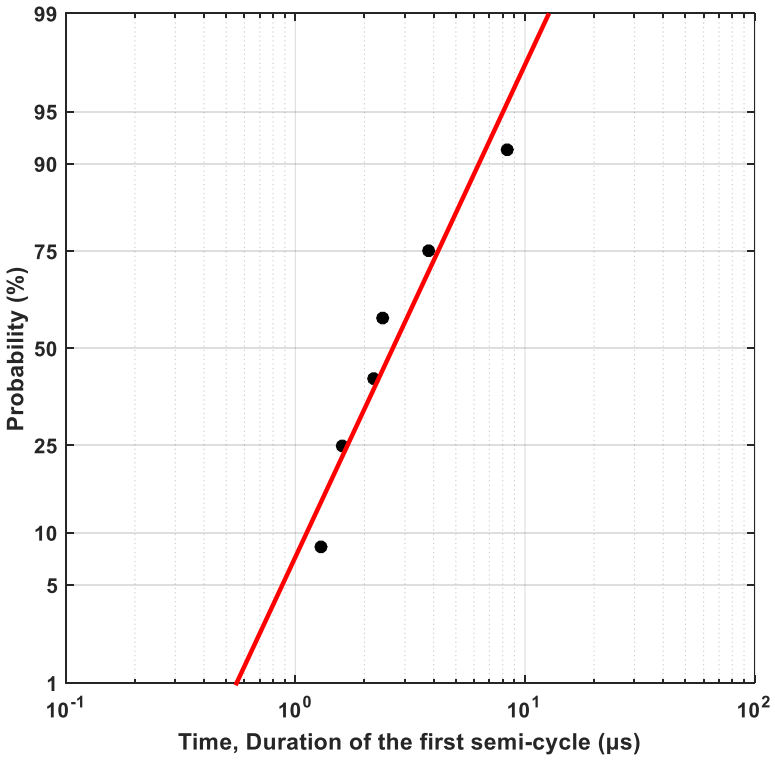

Figure 5.35. Cumulative statistical distribution of the duration of the first semi-cycle and its log-normal approximation. It gives the percent of cases less than the value specified in the abscissa (6 waveforms).

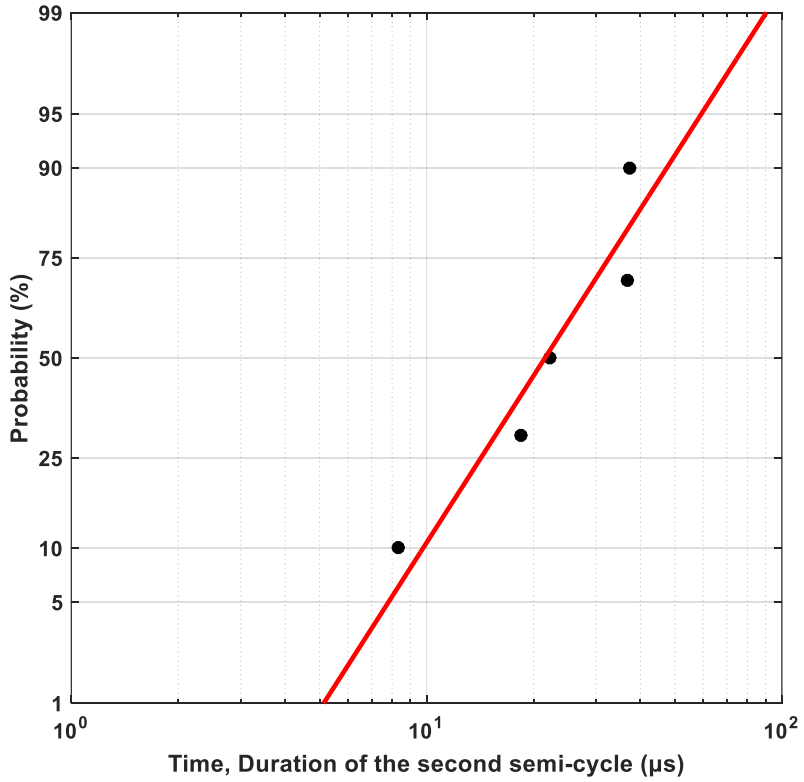

Figure 5.36. Cumulative statistical distribution of the duration of the second semi-cycle and its log-normal approximation. It gives the percent of cases less than the value specified in the abscissa (5 waveforms).

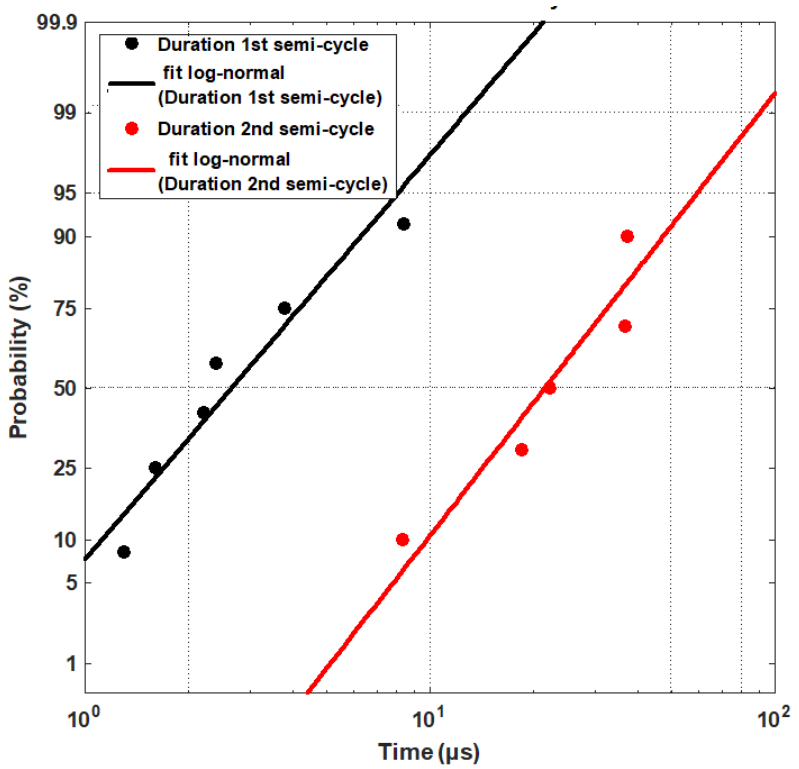

Figure 5.37. Comparison of the cumulative statistical distribution of the duration of the first (6 waveforms) and second semi-cycle (5 waveforms) and its log-normal approximation. It gives the percent of cases less than the value specified in the abscissa.

The cumulative frequency distribution of the time intervals between the peaks of the first and second semi-cycles ($t_{vp2\text{-}vp1}$) is given in Fig. 5.38, which indicates that the median is 9.4 μs and that in 5% and 95% of the cases, respectively, the values are shorter than 1.3 μs and 26.5 μs.

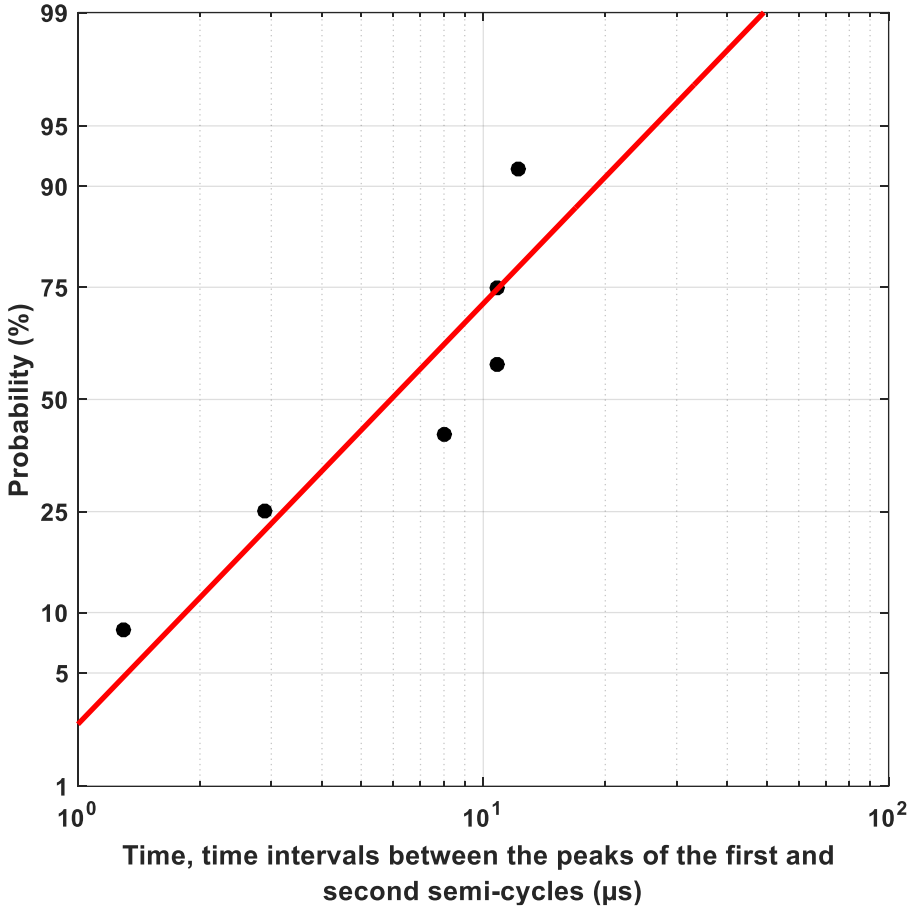

Figure 5.38. Cumulative statistical distribution of the time intervals between the peaks of the first and second semi-cycles and its log-normal approximation. It gives the percent of cases less than the value specified in the abscissa (6 waveforms).

The minimum, maximum, average ($\bar{x}$), median (μ_{ln}), standard deviation (σ_{ln}), and the 5% and 95% values of the parameters of the measured lightning-induced voltages classified as Type III are presented in Table 5.5. The medians and the standard deviations were calculated from the log-normal approximations.

Table 5.5. Statistic results of the maximum absolute voltage value, durations of the first and second semi-cycles, time intervals between the peaks of the first and second semi-cycles, and ratio of the maximum absolute voltage value of the second and first semi-cycles (6 lightning-induced voltages).

Parameter/Variable	**First semi-cycle**		**Second semi-cycle**			
	Vmax (kV)	Duration (μs)	*Vmax* (kV)	Duration* (μs)	$t_{vp2\text{-}vp1}$ (μs)	V_{1p}/V_{2p}
Minimum	0.97	1.3	2.1	8.3	1.3	0.26
Maximum	18.6	8.4	49.6	37.3	10.8	0.45
Average ($\bar{x}$)	5.2	3.3	15.5	24.6	7.7	0.4
Median (μ_{ln})	2.8	2.3	9.8	22.0	9.4	0.3
Std. deviation (σ_{ln})	6.6	2.6	17.5	12.4	10.2	0.1
5% value	0.6	0.9	1.6	7.9	1.3	0.26
95% value	16.5	8.1	50	59.0	26.5	0.48

* Total of 5 induced voltages because the recorded voltage shown in Fig. 5.10 did not cross the zero axis and the duration of the second semi-cycle could not be determined.

5.3.4. Type IV

As only two induced voltages were classified as Type IV (about 3% of the total number of cases), it is not possible to perform a statistical analysis of their parameters.

5.4. General Remarks

The maximum absolute voltage value of the recorded lightning-induced voltages varied widely, from about 2 to 69 kV. Based on the log-normal approximation, the median value of the maximum voltage was 12.6 kV, and 95% of the voltage amplitudes were lower than 44.5 kV.

The time parameters $tf_{(10/90)}$, $tf_{(30/90)}$, and *th* of the unipolar induced voltages (Type I), which represented about 67% of the total recorded voltages, were, respectively, 7.3 μs, 6.8 μs, and

19 μs. These values differ significantly from those of the standard lightning impulse voltage ($tf_{(30/90)}$ = 1.2 μs and th = 50 μs).

Regarding the bipolar voltages, the median values of the durations of the first and second semi-cycles were, respectively, 5.5 μs and 13.4 μs. In 5% of the cases, the duration of the first semi-cycle was lower than 1.6 μs and in 95% of the cases it was lower than 18.9 μs. The values corresponding to the second semi-cycle were 2.5 μs (5% of the cases) and 71 μs (95% of the cases.

When the voltages classified as Type II were considered separately, the median of the ratios of the maximum absolute voltage value of the second and first semi-cycles was 0.8; in 5% of the cases the ratio was lower than 0.4, and in 95% of the cases it was lower than 1.5. The median values of the durations of the first and second semi-cycles were, respectively, 8.2 μs and 11.2 μs. In 5% of the cases the duration of the first semi-cycle was shorter than 3.4 μs, and in 95% of the cases it was shorter than 19.9 μs. The values corresponding to the second semi-cycle were 2.9 μs (5% of the cases) and 43.7 μs (95% of the cases).

Regarding the voltages classified as Type III, the median of the ratios of the maximum absolute voltage values of the second and first semi-cycles was 0.3, much lower in comparison with Type II; in 5% of the cases the ratio was lower than 0.26, and in 95% of the cases it was lower than 0.48. The duration of the first semi-cycle was much shorter than that of Type II, while the opposite applies to the duration of the second semi-cycle. The median values of the durations of the first and second semi-cycles were, respectively, 2.3 μs and 22 μs. In 5% of the cases the duration of the first semi-cycle was shorter than 0.9 μs, and in 95% of the cases it was shorter than 8.1 μs. The values corresponding to the second semi-cycle were 7.9 μs (5% of the cases) and 59 μs (95% of the cases).

6. CONCLUSIONS

Lightning overvoltages associated with indirect strokes usually significantly impact the performance of overhead distribution lines. The characterization of such surges is an essential step for a more accurate estimation of the lightning performance and selecting the more efficient protection method for a given line. A better knowledge of the lightning-induced voltages and the statistical distributions of their main parameters is important for the design of power distribution lines with superior performance and power quality indexes.

Despite the large number of theoretical and experimental researches on voltages induced by indirect strokes, a complete characterization of such voltages have not been possible yet. One of the reasons is the lack of a significant amount of experimental data obtained on a matched line with a simple configuration and without equipment such as transformers and surge arresters. This is mainly due to the difficulties in implementing a system for this purpose and the long observation time required to obtain a large volume of data.

It should also be noted that such characterization cannot be based solely on calculations, which usually assume simplifications such as a vertical lightning channel, without branches, and idealized stroke current waveforms. Therefore, experimental results are essential to complement theoretical studies. However, as lightning-induced voltages depend substantially on the line configuration and the features of voltages measured under different conditions cannot be directly compared, it is essential to measure the voltages on a simple matched line.

An investigation with this purpose was initiated by the Lightning and High Voltage Research Center of the University of São Paulo (CENDAT-USP), and a total of 64 lightning-induced voltages with amplitudes higher than 2 kV were recorded on a simple matched experimental line. This is the first time that an amount of data like this was obtained under such conditions. The main objective of this Dissertation was to evaluate the characteristics of the recorded voltages and contribute to a better understanding of their characteristics.

The main results can be summarized as follows:

- the maximum absolute voltage value of the recorded voltages varied widely, from about 2 kV to 69 kV. Based on the log-normal approximation, the median value of the maximum voltage is 12.6 kV, and 95% of the voltage amplitudes are lower than 44.5 kV;

- although, strictly speaking, all the recorded voltages were bipolar, in many cases the initial part of the voltage and the semi-cycles that occur after the maximum absolute value have no significant effects on the behavior of power equipment insulation. Therefore, the induced voltage waveshapes were classified into four categories (Types I, II, III, and IV). Type I is unipolar and Types II, III, and IV are bipolar. The parameters which characterize each voltage type, as well as their statistical distributions, were presented and discussed;

- since the stroke locations and the characteristics of the lightning channels (branches and inclination) and stroke currents were not known, a direct comparison between measured and calculated voltages was not possible. However, a qualitative analysis was made, and the comparisons between measured and calculated results showed that the main features of the recorded voltages could be well reproduced by simulations considering typical conditions. In particular, the occurrence of bipolar induced voltages can be explained based on different combinations between the values of parameters such as the relative position between the line and the stroke location, the current waveform, the ground resistivity, and the observation point;

- about 67% of the induced voltages (43 out of 64 cases) were classified as unipolar (Type I), and, except for one case, all of them had positive polarity. This is coherent with the fact that negative downward flashes, which represent about 90% of the total cloud-to-ground flashes, usually induce either positive or bipolar voltages. The negative induced voltage was most probably induced by a downward positive flash;

- the front times were longer and the times to half-value of the unipolar induced voltages were shorter in comparison with the standard lightning impulse voltage (1.2/50 μs); the median values of the time parameters $tf_{(10/90)}$, $tf_{(30/90)}$, and th were, respectively, 6.1 μs, 5.2 μs, and 15.8 μs. The use of the standard lightning impulse voltage for testing power equipment insulation seems to be on the safe side, since, based on the log-normal approximations, only in 5% of the cases the front time $tf_{(30/90)}$ was shorter than 1.5 μs and in 95% of the cases the time to half-value th was shorter than 45.4 μs;

- it was clearly demonstrated that lightning-induced voltages may present oscillations even in the case of a matched line without surge arresters, shield wire, or neutral conductor. This is certainly not an obvious result. About 33% of the recorded voltages (21 out of 64) were bipolar (Types II, III, or IV);

- about 20% (13 out of 64) of the measured voltages were classified as Type II. When considered separately, the median of the ratios of the maximum absolute voltage values of the second and first semi-cycles was 0.8; in 5% of the cases the ratio was lower than 0.4, and in 95% of the cases it was lower than 1.5. The median values of the durations of the first and second semi-cycles were, respectively, 8.2 μs and 11.2 μs. In 5% of the cases the duration of the first semi-cycle was shorter than 3.4 μs, and in 95% of the cases it was shorter than 19.9 μs. The values corresponding to the second semi-cycle were 2.9 μs (5% of the cases) and 43.7 μs (95% of the cases).

- about 9.3% (6 out of 64) of the recorded voltages were classified as Type III; except for one case, the first semi-cycle had negative polarity, shorter duration, and lower magnitude than the second one. In this specific case, the voltage was most probably induced by a downward positive flash. The median of the ratios of the maximum absolute voltage value of the second and first semi-cycles was 0.3, much lower in comparison with Type II; in 5% of the cases the ratio was lower than 0.26, and in 95% of the cases it was lower than 0.48. The duration of the first semi-cycle was much shorter than that of Type II, while the opposite applies to the duration of the second semi-cycle. The median values of the durations of the first and second semi-cycles were, respectively, 2.3 μs and 22 μs. In 5% of the cases the duration of the first semi-cycle was shorter than 0.9 μs, and in 95% of the cases it was shorter than 8.1 μs. The values corresponding to the second semi-cycle were 7.9 μs (5% of the cases) and 59 μs (95% of the cases);

- only two induced voltages (about 3% of the total) were classified as Type IV, that is, the maximum absolute voltage value occurs in the third semi-cycle, which has negative polarity and the longest duration. Therefore, it was not possible to perform a separate statistical analysis for this specific voltage type;

- considering the three types of bipolar voltages as a whole, the median values of the durations of the first and second semi-cycles were, respectively, 5.5 μs and 13.4 μs. In 5% of the cases, the duration of the first semi-cycle was lower than 1.6 μs and in 95% of the cases it was lower than 18.9 μs. The values corresponding to the second semi-cycle were 2.5 μs (5% of the cases) and 71 μs (95% of the cases).

The main contribution of this research was a better understanding of the features of the lightning-induced voltages on a simple, matched line. The characterization of such surges is an

important step for a more accurate estimation of the lightning performance of overhead distribution lines, as well as for the selection of the more efficient protection methods.

It is important to emphasize, however, that much more data is required for a complete characterization of the lightning-induced voltages. This research may be considered the first step in this direction, but it is absolutely necessary to obtain more data. In this sense, it is relevant to mention that lightning-induced voltages will continue to be collected by the system implemented in Santo Ângelo – RS, a region characterized by a high ground flash density - about 12 flashes/km²/year. Therefore, the database is expected to increase significantly in the next few years.

REFERENCES

[1] E.T.B, Gross and P. Chowdhuri, "Voltage surge induced on overhead lines by lightning strokes," *Proceedings of the Institution of Electrical Engineers*, v. 114, n. 12, p.1899-907, Dec. 1967.

[2] V. Cooray and F. De la Rosa, "Shapes and amplitudes of the initial peaks of lightning-induced voltage in power lines over finitely conducting earth: theory and comparison with experiment," *IEEE Transactions on Antennas and Propagation*, v. 34, n. 1, pp. 88-92, Jan. 1986.

[3] C.A. Nucci, F. Rachidi, M.V. Ianoz, and C. Mazzetti, "Lightning-induced overvoltages on overhead lines," *IEEE Transactions on Electromagnetic Compatibility*, v. 35, n. 1, pp. 75-86, Feb. 1993.

[4] P. F. Obase, A. Piantini, and A.G. Kanashiro, "Overvoltage on LV networks associated with direct strokes on the primary line," in *Proc. International Conference on Lightning Protection (ICLP),* Kanazawa, Japan, v. 1, pp. 479-484, 2006.

[5] A. Piantini, J.M. Janiszewski, A. Borghetti, C.A. Nucci, and M. Paolone, "A Scale Model for the Study of the LEMP Response of Complex Power Distribution Networks," *IEEE Trans. Power Del.*, v. 22, n. 1, p. 710–720, Jan. 2007.

[6] A. Piantini, "Lightning protection of overhead power distribution lines," in *Proc. of the 29th International Conference on Lightning Protection*, pp. 1-29, (invited lecture) Uppsala, Sweden, June 2008.

[7] A. Piantini and J.M. Janiszewski, "The use of shield wires for reducing induced voltages from lightning electromagnetic fields," *Electric Power Systems Research*, p. 46–53, 2013.

[8] F. Rachidi *et al*., "Influence of a lossy ground on lightning-induced voltages on overhead lines," *IEEE Transactions on Electromagnetic Compatibility*, v. 38, n.1996;

[9] S. Yokoyama, K. Miyake, and S. Fukui, "Advanced observations of lightning induced voltage on power distribution lines (II)," *IEEE Trans. Power Del.*, v. 4, n. 4, pp. 2196–2203, Oct. 1989, doi: 10.1109/61.35647.

[10] A. Piantini, A. Borghetti, C.A. Nucci, “Lightning interaction with medium-voltage overhead power distribution systems,” in *Lightning Interaction with Power Systems - Volume 2: Applications*, IET Energy Engineering, 172, A. Piantini, Ed., London, U.K.: The Institution of Engineering and Technology, ch. 4, pp. 113-172, 2020.

[11] C.A. Nucci, “Lightning - induced voltages on distribution systems: influence of ground resistivity and system topology,” in *Proc. VIII Int. Symp. Lightning Protection (SIPDA)*, São Paulo, Brazil, pp. 761-773, Nov. 2005.

[12] A. Piantini and J.M. Janiszewski, “The effectiveness of surge arresters on the mitigation of lightning induced voltages on distribution lines,” *Journal of Lightning Research*, v. 2, pp. 34-52, 2007.

[13] A. Piantini, “Lightning-induced voltages on overhead power distribution lines,” in *Proc. of the World Meeting on Lightning*, Cartagena de Indias, Colombia, 2016.

[14] A. Piantini, “Analysis of the effectiveness of shield wires in mitigating lightning-induced voltages on power distribution lines,” *Electric Power Syst. Res.*, v. 159, pp. 9–16, Jun. 2018, doi: 10.1016/j.epsr.2017.08.022.

[15] M. Paolone, C.A. Nucci, E. Petrache, and F. Rachidi, “Mitigation of lightning-induced overvoltages in medium voltage distribution lines by means of periodical grounding of shielding wires and of surge arresters: Modeling and experimental validation,” *IEEE Trans. Power Del.*, v. 19, n. 1, pp. 423–431, Jan. 2004, doi: 10.1109/TPWRD.2003.820196.

[16] A. Piantini, “Lightning transients in MV power distribution lines,” in *Proc. V Russian Conf. Lightning Protection (RCLP)*, Saint Petersburg, Russia, pp. 1–14 (invited lecture), May 2016.

[17] A. Piantini, “Lightning-induced overvoltages on overhead medium-voltage lines,” in *Proc. IEEE Int. Conf. High Voltage Eng. Appl. (ICHVE)*, Chengdu, China, pp. 1–7 (invited lecture), Sep. 2016.

[18] A. Piantini and J.M. Janiszewski, “Lightning-induced voltages on overhead lines - application of the extended Rusck model,” *IEEE Trans. Electromagn. Compat.*, v. 51, n. 3, pp. 548–558, Jun. 2009, doi:10.1109/TEMC.2009.2023514.

[19] A. Piantini and J.M. Janiszewski, “Lightning induced voltages on distribution transformers: The effects of line laterals and nearby buildings,” in *Proc. VI Int. Symp. Lightning Protection (SIPDA)*, Santos, Brazil, pp. 77–82, Nov. 2001.

[20] A. Andreotti, F. Mottola, A. Pierno *et al.*, “On the statistical characterization of lightning-induced voltages,” *Applied Sciences*, v. 8, n. 4, pp. 1-15, 2018, doi:10.3390/app8040651.

[21] F. Napolitano, F. Tossani, A. Borghetti, C.A. Nucci and G.V. Podporkin, “Statistical Characterization of Lightning Induced Overvoltage Waveforms in Overhead Lines,” in *Proc. IEEE International Conference on Environment and Electrical Engineering and 2019 IEEE Industrial and Commercial Power Systems Europe* (EEEIC / I&CPS Europe), Genova, Italy, pp. 1-6, 2019.

[22] J.O.S. Paulino, I.J.S. Lopes, W.C. Boaventura, G.C. Miranda and C.F. Barbosa, “Waveshapes of lightning induced voltages on an overhead line above lossy ground,” in *Proc. Int. Conf. Lightning Protection (ICLP)*, Shanghai, China, pp. 772-776, 2014.

[23] A.J. Eriksson and D.V. Meal, “Lightning performance and overvoltage surge studies on a rural distribution line,” *IEE Proc. C - Generation, Transmission and Distribution*, v. 129, n. 2, pp. 59-69, doi:10.1049/ip-c.1982.0010, Mar. 1982.

[24] S. Yokoyama, K. Miyake, H. Mitani, and A. Takanishi, “Simultaneous measurement of lightning induced voltages with associated stroke currents,” *IEEE Trans. Power App. Syst.*, v. PAS-102, n. 8, pp. 2420–2429, Aug. 1983, doi: 10.1109/TPAS.1983.317741.

[25] S. Yokoyama, K. Miyake, H. Mitani, and N. Yamazaki, “Advanced observations of lightning induced voltage on power distribution lines,” *IEEE Trans. Power Del.*, v. 1, n. 2, pp. 129–139, Apr. 1986.

[26] M.J. Master, M.A. Uman, W. Beasley, and M. Darveniza, “Lightning induced voltages on power lines: Experiment,” *IEEE Trans. Power App. Syst.*, v. 103, n. 9, pp. 2519–2529, Sep. 1984, doi: 10.1109/TPAS.1984.318406.

[27] V. Cooray and F. De La Rosa, “Shapes and amplitudes of the initial peaks of lightning-induced voltage in power lines over finitely conducting earth: Theory and comparison with experiment,” *IEEE Trans. Antennas Propag.*, v. 34, n. 1, pp. 88–92, Jan. 1986, doi: 10.1109/TAP.1986.1143721.

[28] F. De la Rosa, H. Perez, and A. Galván, “Lightning-induced voltage measurements in an experimental power distribution line in Mexico,” in *Proc. 22nd Int. Conf. Lightning Protection (ICLP)*, Budapest, Hungary, pp. R6b-09/1– R6b-09/6, Sept. 1994.

[29] M. Rubinstein, M.A. Uman, P.J. Medelius, and E.M. Thomson, “Measurements of the voltage induced on an overhead power line 20 m from triggered lightning,” *IEEE Trans. Electromagn. Compat.*, v. 36, n. 2, pp. 134–140, May 1994, doi: 10.1109/15.293277.

[30] K. Michishita, M. Ishii, A. Asakawa, S. Yokoyama, and K. Kami, “Voltage induced on a test distribution line by negative winter lightning strokes to a tall structure,” *IEEE Trans. Electromagn. Compat.*, v. 45, n. 1, pp. 135–140, Feb. 2003, doi: 10.1109/TEMC.2002.808044.

[31] A. Piantini, T.O. de Carvalho, A. Silva Neto, J.M. Janiszewski, R.A.C. Altafim, and A.L.T. Nogueira, “A system for simultaneous measurements of lightning induced voltages on lines with and without arresters,” in *Proc. 27th Int. Conf. Lightning Protection (ICLP)*, Avignon, France, v. 1, pp. 297–302, Sept. 2004.

[32] A. Piantini, T.O. Carvalho, A. Silva Neto *et al*., “A system for lightning induced voltages data acquisition - preliminary results,” in *Proc. VII Int. Symp. Lightning Protection (SIPDA)*, Curitiba, Brazil, pp. 156-161, Nov. 2003

[33] M.N.N. Santos and A. Piantini, “Characteristics of lightning-induced voltages based on experimental data,” *High Voltage*, v. 5, pp. 1-7, Dec. 2020, doi: 10.1049/hve2.12055.

[34] M. N. N. Santos and A. Piantini, “Analysis of Lightning-Induced Voltages on a Matched Experimental Overhead Line,” in IEEE Transactions on Electromagnetic Compatibility, pp. 1-8, Aug. 2021, doi: 10.1109/TEMC.2021.3101488.

[35] P.P. Barker, T.A. Short, A.R. Eybert-Berard, and J.P. Berlandis, “Induced voltage measurements on an experimental distribution line during nearby rocket triggered lightning flashes,” *IEEE Trans. Power Del.*, v. 11, n. 2, pp. 980–995, Apr. 1996, doi: 10.1109/61.489360.

[36] S. Yokoyama, “Calculation of lightning-induced voltages on overhead multiconductor systems,” *IEEE Trans. Power App. Syst.*, v. 103, n. 1, pp. 100–108, Jan. 1984, doi: 10.1109/TPAS.1984.318583.

[37] A. Piantini and J.M. Janiszewski, “An experimental study of lightning induced voltages by means of a scale model,” in *Proc. Int. Conf. Lightning Protection*, Berlin, Germany, pp. 4.08/195–4.08/199, Sep. 1992.

[38] A. Piantini and J.M. Janiszewski, “Lightning induced voltages on overhead lines: the effect of ground wires,” in *Proc. 22nd Int. Conf. Lightning Protection (ICLP)*, Budapest, Hungary, pp. R3b-08/1–R3b-08/5, Sep. 1994.

[39] A. Piantini and J.M. Janiszewski, “Use of surge arresters for protection of overhead lines against nearby lightning,” in *Proc. 10th Int. Symp. High Voltage Eng. (ISH)*, Montréal, QC, Canada, v. 5, pp. 213–216, Aug. 1997.

[40] A. Piantini and J.M. Janiszewski, “Lightning induced voltages on distribution lines close to buildings,” in *Proc. 25th Int. Conf. Lightning Protection (ICLP)*, Rhodes, Greece, v. B, pp. 558–563, Sep. 2000.

[41] M. Ishii, K. Michishita, and Y. Hongo, “Experimental study of lightning induced voltage on an overhead wire over lossy ground,” *IEEE Trans. Electromagn. Compat.*, v. 41, n. 1, pp. 39–45, Feb. 1999, doi: 10.1109/15.748135.

[42] H.K. Hoidalen and F. Dahlslett, “Characterization of lightning induced overvoltages in isolated neutral low-voltage systems,” in *Proc. Int. Conf. Lightning Protection (ICLP)*, Uppsala, Sweden, Jun. 2008.

[43] L. Cai, J. Wang, M. Zhou, S. Chen, and J. Xue, “Observation of natural lightning-induced voltage on overhead power lines,” *IEEE Trans. Power Del.*, v. 27, n. 4, pp. 2350-2359, Oct. 2012, doi:10.1109/TPWRD.2012.2204441

[44] S. Nanayakkara, U. Mendis, M. Fernando, S. Abegunawardana, P. Liyanage, and V. Cooray, “Lightning induced voltages in over head power lines due to cloud to ground flashes in Sri Lanka,” in *Proc. Asia-Pacific Int. Conf. Lightning (APL)*, Nagoya, Japan, Jun. 2015.

[45] D. Aranguren, E. A. Soto, E. Pérez and H. Torres, “Lightning Voltages Measurements on an Energized Distribution Line in Colombia,” in *IEEE Transactions on Electromagnetic Compatibility*, v. 62, n. 4, pp. 1219-1224, Aug. 2020, doi: 10.1109/TEMC.2019.2944618.

[46] S. Wang, et al., “Analysis of Lightning-Induced Overvoltage Waveform Parameters,” in *34th International Conference on Lightning Protection (ICLP)*, pp. 1-5, 2018, doi: 10.1109/ICLP.2018.8503345.

[47] A.E. Lazzaretti, S.L.F. Santos, K.K. Küster, L.F.R.B., Toledo, M.A. Ravaglio, A. Piantini, C.L.S. Pinto, “An integrated monitoring system and automatic data analysis to correlate lightning activity and faults on distribution networks,” *Electr. Power Syst. Res.*, v. 153, pp. 66–72, Dec. 2017.

[48] M.A. Ravaglio, K.K. Küster, S.L.F. Santos, L.F.R.B. Toledo, A. Piantini, A.E. Lazzaretti, L.G. de Mello, C.L.S. Pinto, “Evaluation of lightning-related faults that lead to distribution network outages: An experimental case study,” *Electric Power Systems Research*, v. 174, 2019, ISSN 0378-7796, doi: 10.1016/j.epsr.2019.04.026.

[49] M. Shigihara, A. Piantini, M.C.E.S. Ramos, C.P. Braz, C. Mazzetti, and A. Ancajima, “Evaluation of the performance of different methods for estimating the parameters of the disruptive effect model — Application to 15 kV insulators,” *IEEE Trans. Dielectrics and Electrical Insulation*, v. 23, n. 2, pp. 1030-1037, Apr. 2016, doi:10.1109/TDEI.2015.005433.

[50] A. Rigotti, A. Piantini, D.A. da Silva, and M. Shigihara, “A method for the evaluation of the behavior of a 15-kV insulator under bipolar oscillating impulse voltages,” *Int. Journal Elec. Power & Energy Systems*, v. 109, pp. 307-313, 2019, doi:10.1016/j.ijepes.2019.02.008.

[51] N. Sapumanage, S. Nanayakkara, S. Abegunawardana, M. Fernando, and V. Cooray, “How physical attributes of transient voltages limit the efficiency of SPD array,” in *Proc. 29th Int. Conf. Lightning Protection (ICLP)*, Rzeszow, Poland, pp. 1-7, Sep. 2018.

[52] A. Silva Neto, A. Piantini, M.N.N. Santos *et al*., “A system for experimental studies of lightning currents and overvoltages,” in *Proc. XIV Int. Symp. Lightning Protection (SIPDA)*, Natal, Brazil, Oct. 2017, pp. 370-375, doi:10.1109/SIPDA.2017.8116954.

[53] S. Rusck, “Induced lightning overvoltages on power transmission lines with special reference to the over-voltage protection of low voltage networks,” *Trans. Royal Inst. Technol.*, n. 120, pp. 1–118, 1958.

[54] M. Ishii, K. Michishita, Y. Hongo, S. Oguma, "Lightning-induced voltage on an overhead wire dependent on ground conductivity," *IEEE Trans. Power Deliv.*, v. 9, n. 1, pp. 109–118, Jan. 1994.

[55] A. Borghetti, J.A Gutierrez, C.A. Nucci, M. Paolone, E. Petrache, F. Rachidi, "Lightning-induced voltages on complex distribution systems: models, advanced software tools and experimental validation," in *Journal of Electrostatics*, v. 60, pp. 163-174, Mar. 2004.

[56] A. Piantini, "Extension of the Rusck Model for Calculating Lightning-Induced Voltages on Overhead Lines Considering the Soil Electrical Parameters," in *IEEE Trans. Electromagn. Compat.*, v. 59, n. 1, p. 154-162, Feb. 2017.

[57] A. Andreotti, F. Mottola, A. Pierno, D. Proto, "Statistical features of lightning-induced voltages," *2018 International Symposium on Power Electronics, Electrical Drives, Automation and Motion (SPEEDAM)*, pp. 1037-1042, 2018.

[58] M. Darveniza, A.E. Vlastos, "The generalized integration method for predicting impulse volt-time characteristcs for non-standard wave shapes – a theoretical basis," *IEEE Transactions on Electrical Insulation*, v. 23, n. 3, pp. 373-381, Jun. 1988.

[59] V. A. Rakov, M. A. Uman, "Lightning: physics and effects," Cambridge University Press, Jan. 2007.

[60] A. Piantini, T. O. Carvalho, A. Silva Neto, J. M. Janiszewski, R. A. C. Altafim, and A. L. T. Nogueira, "A full-scale system for lightning data acquisition, with special reference to induced voltages on distribution lines," *Proc. of Int. Conf. on Grounding and Earthing & 3th Brazilian Workshop on Atmospheric Electricity*, Rio de Janeiro, Brazil, pp. 111-116, Nov. 2002.

[61] A. Savitzky and M.J.E. Golay, "Smoothing and differentiation of data by simplified least squares procedures," *Analytical Chemistry*, v. 36, n. 8, pp. 1627-1639, 1964, doi:10.1021/ac60214a047.

[62] M. Rubinstein, M.A. Uman, P.J. Medelius, and E.M. Thomson, "Measurements of the voltage induced on an overhead power line 20 m from triggered lightning," *IEEE Trans. Electromagn. Compat.*, v. 36, n. 2, pp. 134–140, May 1994, doi: 10.1109/15.293277.

[63] A. Piantini and J.M. Janiszewski, “The influence of the upward leader on lightning induced voltages,” in *Proc. 23rd Int. Conf. Lightning Protection*, Florence, Italy, v. 1, pp. 352–357, Sep. 1996.

[64] A. Andreotti, A. Piantini, A. Pierno, and R. Rizzo, “Lightning-Induced Voltages on Complex Power Systems by using CiLIV: The Effects of Channel Tortuosity,” *IEEE Trans. Power Deliv.*, v. PP, n. 99, pp. 1–1, 2017.

[65] V. A. Rakov *et al.*, “Lightning parameters for engineering applications,” in *WG C4.407.*, CIGRE TB 549, p. 118, Aug. 2013.

[66] O. Pinto Jr., K.P. Naccarato, and C. Campinho, “A new methodology to estimate cloud-to-ground lightning flash density in Brazil to support performance analyses of electrical systems,” *Proc. Int. Conf. Grounding and Earthing & 3rd Int. Conf. Lightning physics and Effects*, C5, Nov. 2008.

[67] A. Piantini, “Protective Effect of Shield Wires against Lightning-Induced Overvoltages on Distribution Lines,” in *Proc. VI Russian Conf. Lightning Protection (RCLP)*, Saint Petersburg, Russia, pp. 1–16 (invited lecture), April 2018.

[68] F. Heidler, “Analytische Blitzstromfunktion zur LEMP- Berechnung,” *Proceedings of the 18th International Conference on Lightning Protection (ICLP)*, Munich, pp. 63-66, Sep. 1985.